



3 4456 0022420 0

cy.2

# HEAT TRANSFER IN A GAS-COOLED, HEAT-GENERATING POROUS SOLID

( Thesis )

Robert Pope Rannie

OAK RIDGE NATIONAL LABORATORY  
CENTRAL RESEARCH LIBRARY  
DOCUMENT COLLECTION  
**LIBRARY LOAN COPY**

DO NOT TRANSFER TO ANOTHER PERSON

If you wish someone else to see this  
document, send its name with document  
and the library will arrange a loan.

NON-RECYCLED  
PAPER



## OAK RIDGE NATIONAL LABORATORY

OPERATED BY UNION CARBIDE CORPORATION • FOR THE U.S. ATOMIC ENERGY COMMISSION

Printed in the United States of America. Available from  
National Technical Information Service  
U.S. Department of Commerce  
5285 Port Royal Road, Springfield, Virginia 22151  
Price: Printed Copy \$3.00; Microfiche \$0.95

This report was prepared as an account of work sponsored by the United States Government. Neither the United States nor the United States Atomic Energy Commission, nor any of their employees, nor any of their contractors, subcontractors, or their employees, makes any warranty, express or implied, or assumes any legal liability or responsibility for the accuracy, completeness or usefulness of any information, apparatus, product or process disclosed, or represents that its use would not infringe privately owned rights.

ORNL-4808

UC-38 -- Engineering and Equipment

Contract No. W-7405-eng-26

MATHEMATICS DIVISION

HEAT TRANSFER IN A GAS-COOLED, HEAT-GENERATING POROUS SOLID

Robert Pope Rannie

Submitted as a dissertation to the Graduate School of The  
Pennsylvania State University in partial fulfillment of  
the requirements for the degree of Doctor of Philosophy  
in Chemical Engineering

DECEMBER 1972

OAK RIDGE NATIONAL LABORATORY  
Oak Ridge, Tennessee 37830  
operated by  
UNION CARBIDE CORPORATION  
for the  
U. S. ATOMIC ENERGY COMMISSION



3 4456 0022420 0



## ACKNOWLEDGMENT

To the many persons and organizations which have supported the work on this thesis I should like to express my appreciation, and I would like to single out the following to express special appreciation. I would like to thank my thesis advisor, Dr. Wallis A. Lloyd, for his guidance and particularly for his patience. I am indebted to Jerome Farber for his help and assistance relating to the experimental apparatus which we shared. I would like to express my appreciation to The Department of Chemical Engineering of the Pennsylvania State University and to the Oak Ridge Institute of Nuclear Studies for the awarding of the Scholarships and fellowships which supported the majority of my doctoral studies. I very much appreciate the support I have received from the Oak Ridge National Laboratory in affording me time and facilities to complete this work. A special thanks is due to my colleagues and supervisors in the Mathematics Division of the Oak Ridge National Laboratory. The considerations of J. G. Sullivan in this connection are particularly appreciated. The thesis typing by Mrs. Kathleen A. Christian is gratefully acknowledged.

## ABSTRACT

The use of porous materials in heat transfer has been increasing. The equations which describe heat transfer in porous materials with a fluid flowing through the pores of the material are more complicated than those for heat transfer through solids and into fluids at a plane interface. Calculations of heat transfer in porous materials have been hindered by fairly widespread misconceptions about this type of heat transfer and by the lack of experimental data on the heat transfer related properties of porous materials.

Among articles which have been published that discuss heat transfer in porous materials, there are some which are now acknowledged to contain errors. The erroneous conclusion of these articles, and other reasons, have fostered an assumption that in a fluid cooled porous material the solid and fluid phase temperatures will be nearly identical.

The purpose of this study was to determine if an experimental apparatus could be built that could be used for gas phase chemical reactions in electrically heated porous tungsten and also to measure the heat transfer coefficient in the porous tungsten using nitrogen or helium gas as the coolant. The extent of the alleged similarity between the temperature of the solid and the fluid could thus be determined. It was proposed that the equations for heat transfer in a fluid cooled, heat generating porous solid be derived and used to analyze data from experimental measurements on the porous system. These equations were not to be based on or be restricted by the assumption of the essential equality of the solid and fluid temperature in the porous material.

Appropriate experimental measurements were to be carried out in order to measure four boundary conditions from which the three constants of the equations and the heat transfer coefficient could be determined.

The equations were derived and incorporated into FORTRAN digital computer programs that were used to accomplish the data reduction. The experimental apparatus was successfully built and operated in spite of extensive developmental problems associated with electrical contact resistance at the mounts of the porous tungsten. Due to the lack of data on the effective thermal conductivity of the porous tungsten, a fifth boundary condition was measured from which a conduction correction factor was determined for the porous tungsten.

The heat transfer coefficients that were measured in this study show good agreement with other experimental measurements of heat transfer coefficients. Correlations which had been suggested for heat transfer coefficients and which were not generally based on experimental data gave heat transfer coefficients that were larger than values measured in this study by two or three orders of magnitude.

The assumption of such large heat transfer coefficients could continue to support the idea that the temperature of the solid and fluid are nearly identical. Even at the low Reynolds number of  $10^{-1}$  in this study, solid and fluid temperature differences of hundreds of degrees F were observed.



## TABLE OF CONTENTS

	<u>Page</u>
Acknowledgment . . . . .	iii
Abstract . . . . .	iv
List of Tables . . . . .	ix
List of Figures . . . . .	x
INTRODUCTION . . . . .	1
PURPOSE AND SCOPE . . . . .	9
THEORY	
Heat Transport in Porous Systems . . . . .	11
Basic Heat Transport in the Experimental Porous System . . . . .	18
Special Considerations for the Experimental Porous System . . . . .	21
EXPERIMENTAL WORK	
Experimental Apparatus - General Description . . . . .	35
Electric Power Circuit . . . . .	36
Mechanical Assembly . . . . .	38
Gas System . . . . .	51
Instrumentation . . . . .	53
Experimental Procedure . . . . .	59
DISCUSSION OF RESULTS	
Experimental Developments . . . . .	61
Boundary Conditions and Method of Solution . . . . .	64
Summary of Results . . . . .	74
Nusselt-Reynolds Data Correlation . . . . .	78
Other Non-Experimental Correlations . . . . .	85
Heat Balances and Temperature Profiles . . . . .	90
Conduction Correction Factor . . . . .	94
Analysis of Experimental Errors . . . . .	97
CONCLUSIONS . . . . .	109
FUTURE WORK . . . . .	111
APPENDIX A - Derivation of Equations . . . . .	113
APPENDIX B - Experimental Data: Common Values and Physical Constants . . . . .	121
APPENDIX C - Experimental Data: Individual Run Data . . . . .	125

TABLE OF CONTENTS (continued)

	<u>Page</u>
APPENDIX D - Results of Individual Run Analysis . . . . .	129
TABLE OF NOMENCLATURE . . . . .	133
BIBLIOGRAPHY . . . . .	137

## LIST OF TABLES

<u>Table Number</u>		<u>Page</u>
1	Common Parameters and Physical Constants . . . . .	122
2	Individual Run Data-Optical Pyrometer Temperature and Cylinder Position Pairs . . . . .	126
3	Individual Run Data-Thermometer and Thermocouple Readings . . . . .	127
4	Individual Run Data-Cylinder Specifications, Heat Generation and Fluid Flow . . . . .	128
5	Individual Run Analysis-Heat Balances . . . . .	130
6	Individual Run Analysis-Solid and Gas Temperatures . . . .	131
7	Individual Run Analysis-Heat Transfer Coefficient and Conduction Correction Factor . . . . .	132

## LIST OF FIGURES

<u>Figure Number</u>		<u>Page</u>
1	Heat Flow in a Differential Element of Porous Material . . . . .	16
2	Equivalent Flat Wall Model of the Cylinder . . . . .	22
3	Drilled Channels and Porous Material . . . . .	29
4	Factors Reducing Conductivity in Porous Materials . . . . .	31
5	Rectifier Power Circuit . . . . .	37
6	Photograph of the Experimental Equipment . . . . .	39
7	Photograph of the Mounted Tungsten Cylinder without Marinite Insulation and Instrumentation . . . . .	40
8	Insulated Studs Connecting the Bus Blocks . . . . .	43
9	Stainless Steel Pier and Graphite Washer . . . . .	45
10	Photograph of the Mounted Tungsten Cylinder with Marinite Insulation and Instrumentation . . . . .	47
11	Marinite Insulating Disks . . . . .	49
12	Photograph of the Assembled and Instrumented Tungsten Cylinder Showing the Optical Pyrometer in Position for Viewing . . . . .	50
13	Gas System-Schematic Diagram . . . . .	52
14	Photograph of the Controls and Instrumentation of the Experimental Apparatus . . . . .	54
15	Schematic of the Mounted and Instrumented Tungsten Cylinder . . . . .	56
16	Temperature Profiles and Heat Balances in the Porous Wall . . . . .	76
17	Nusselt Number vs Reynolds Number for Systems of Porous Materials . . . . .	77

## INTRODUCTION

The use and handling of porous materials has been a concern of technology since its beginnings. Beds of granular materials and porous solids have extensive use in chemical and petroleum processing. (4,26,32) While metals have long been available in porous forms, it is only within this century that powder metallurgy has become a significant technology. (19) Powder metallurgy has been used in the fabrication of high melting materials, such as tungsten, and in the preparation of bearing materials which are desirable because of their oil-retaining porous structure.

During the period around the second World War there was an increased interest in heat transfer involving porous materials. The development in this period of the rocket engine with its severe problems in heat transfer led to consideration of film cooling and transpiration cooling. (6,23,30) Transpiration cooling, which has also been referred to as "sweat cooling" and "effusion cooling," is accomplished by the flow of a cooling fluid through a heat conducting material in a direction opposite to the flow of heat in the material. This technique of cooling by countercurrent flow of coolant and heat could in principle be accomplished with coolant passages of any size. Porous materials were used for some of these applications because they offered a large surface-to-volume ratio and the low flow rates generally used did not create excessive pressure drops in the porous material. In addition the porous material had a high degree of homogeneity that could not be achieved by a system of tubes.

The development of nuclear energy in this period led to additional problems in heat transfer. One reason for these problems was that in nuclear reactor cores power densities were now available which were generally larger than those that had existed before the advent of nuclear technology. One technique that has been suggested in connection with the nuclear powered rocket is to use a reactor core that is formed from porous materials so that a large surface area will be available for the transfer of heat to the propellant that is passing through the reactor core. (7)

The general advance of technology has led to systems with higher operating temperatures and more critical problems in heat transfer are now found in well established fields such as the cooling of turbine blades. Another area of interest is in the use of a porous material as a reactor for chemical reactions. When the porous material is heated internally by ohmic or nuclear heat generation it should provide a reactor with a large surface area in a small volume capable of permitting reactions with short contact times. An enhancement to the porous reactor might be obtained by fabricating the reactor from fissionable material and operating it in or near the core of a nuclear reactor where it would be subjected to a high neutron flux. The reacting fluid flowing through the porous reactor could then be subjected to direct fission fragment bombardment which would serve as a catalyst for chemical reactions.

The number of areas which have an interest in heat transfer in porous systems continues to increase as the understanding of this technology has increased and its application has spread.

At the present time there are at least two problems associated with carrying out calculations involving heat transfer in porous systems. The first problem is a misconception regarding the solid-fluid temperature difference in porous materials. The second problem is the shortage of experimental data on heat transfer in porous systems.

The background of the first problem is the following. Many of these new technologies which use porous systems have either come into existence or have received some major new impetus prior to extensive application of the digital computer as a tool for problem solving. This has created the problem of trying to solve the higher order, and sometimes partial, differential equations of porous heat transfer by various simplifying techniques. Accordingly each problem involving porous systems has been simplified by assumptions which were designed to allow relatively easy solution of the equations for the particular case being studied. This procedure has created a variety of approaches to the general problem of heat transfer in porous systems and apparently has fostered certain assumptions about porous systems which are not generally true. In any case, the variety of simplified approaches to the problem has not served to create a uniform set of definitions for porous systems.

The difficulty in solving third order equations does not lie simply in the need for an additional constant to be evaluated by the measurement of a third boundary condition. Rather, the problem occurs because of the coupled nature of the equations for heat transfer in porous systems. In a problem with heat conduction up to a boundary that was cooled by convective heat transfer it was generally possible to separate the solid and fluid phases and treat each as a separate

problem with coupling through the convective heat transfer coefficient. The differential equation for the heat transfer in the solid phase could be solved separately from the differential equation for the heat transfer in the fluid phase. For heat transfer in porous systems the heat transfer coefficient is involved in two different differential equations which are combined to yield the third order heat transfer equations. The phases are now no longer separable in the sense of a fluid contacting a solid wall along a geometric plane. Moreover, the coupling of the phases is not in the algebraic equations which are the solutions of the differential equations. The coupling is now in the differential equations themselves. This prevents the simpler solution of the problem in parts and the combination of the results. In addition the equations for the heat transfer coefficient are transcendental and trial and error solutions are necessary for this parameter.

One early attempt to derive equations for the general problem of heat transfer in porous systems was that of Weinbaum and Wheeler. (34) This work assumed that the porous system could be considered to have pores made up of many small tubes or pipes running through the porous solid in the direction of fluid flow. The heat transfer coefficient assumed in this work was therefore based on the flow of fluids in pipes.

This work had an error of sign in the derivation of the heat transfer equations and the authors erroneously concluded that in a great many systems the fluid would be heated to essentially the solid temperature in a very small percentage of the flow length of the fluid through the porous solid. It has been noted that this error was copied explicitly in at least one other work (17) and several articles have

referenced the article of Weinbaum and Wheeler without taking note of the error in their derivation.

Furthermore, it will be shown that this assumption of essentially equal temperatures in the solid and fluid phases of a porous system has been widely used. While the assumption of equal solid and fluid temperatures might not be directly attributable to the articles cited, those erroneous conclusions may have prompted some authors to make this same assumption in their work. In this connection it is noteworthy that in the chapter in Schneider (28) on porous systems he cites only two references, one of which is Weinbaum and Wheeler, and the other of which is Green (13), who also assumes the equality of the phase temperatures. Schneider notes that the use of the assumption of the equality of the temperature of the two phases greatly simplified the analysis. If equality of phase temperature were true, or rather if this were an assumption that would be sufficiently accurate, then it would be helpful since it effectively reduces the problem from one involving a third order equation to one involving only a second order equation. In the absence of sophisticated computing facilities the desire to use the assumption of phase temperature equality is understandable.

Bussard and DeLauer (7) essentially assume identity of the solid and fluid phase temperatures citing Green as a reference. A more recent article by Weiner and Edwards (35) treats simultaneous conduction, convection, and radiation in a porous bed by initially defining the solid and fluid temperatures to be the same. A still more recent article by Koh and del Casal (21) surprisingly still cites Weinbaum and Wheeler, and Green. While this work initially considers a temperature difference between the solid and the fluid, a significant portion of this work

considers the case where the solid and fluid phase temperatures are assumed to be equal.

The problem of the incorrect sign in the derivation of Weinbaum and Wheeler did not, however, go entirely unnoticed. Bland (2) and Grootenhuis (17) made a correct derivation of the problem. Bland derived equations which coupled the flow equations with those for heat transfer by assuming a correlation for the heat transfer coefficient in the porous material. While this correlation, based on work by Grootenhuis (15) was probably reasonable, it does point out the lack of experimental data on porous systems, a fact which is explicitly noted by Grootenhuis. These two works point up the second shortcoming of the state of this art which was the lack of experimental measurements on porous systems. The difficulties in solving higher order equations which more accurately described the porous system often led to treatment of the porous systems by extrapolation from other models. Among others it was postulated that a porous solid was equivalent to many small tubes or that it resembled a packed bed. (1,34) Some of the concepts of parameters in porous systems will now be considered.

Experimental values for the thermal conductivity of porous materials were generally unknown and Grootenhuis in fact comments on the general lack of experimental data in this area. More recently, Koh and del Casal (21) have reiterated this complaint. The question of the thermal conductivity of porous materials is related to the question of how the area for heat conduction should be defined. Many of the authors (7,28, 34) state that the cross sectional area available for thermal conductivity is based on the geometrical area for conduction. The geometrical area for conduction is generally taken to be an area evaluated by

multiplying the complement of the volumetric porosity by the bulk cross sectional area of the porous material. A notable exception to this assumption is the work of Koh and del Casal (21) on nickel Foametal.

A variety of assumptions are made with regard to the correlation to be assumed for the internal heat transfer coefficient as well as the method to be used to evaluate the area within the pores. Bland evaluates the heat transfer coefficient on the basis that the pores correspond to a system of small tubes. Moreover he relates this to pressure drop during flow measurements in that he calculates the size of a group of small pipes which would produce the observed pressure drop. He then uses these tubes as the basis for both the heat transfer coefficient and the internal area of the porous material.

Grootenhuis has sought to determine an experimental correlation between a volumetric heat transfer coefficient and the flow rate. The volumetric heat transfer coefficient is the product of the classical heat transfer coefficient and the internal area per unit bulk volume of the porous material. Grootenhuis evaluates the internal surface area of any porous solid by assuming that specific surface varies as a linear function of one minus the porosity.

While the case of a heat generating solid phase in a porous system has been considered in some articles (13), there do not appear to be many experimental studies in which this effect occurs. This suggests a need in this area since internal heat generation is the mechanism which would be employed in a porous nuclear reactor core and in a porous chemical reactor. Another difficulty in obtaining a well

defined set of equations for heat transfer in porous systems is due to the desire by some authors to couple the heat transfer problem with the fluid flow problem. This is being done without firm data on the relation of flow rates to the heat transfer coefficients in porous materials. With the large area of uncertainty in porous heat transfer it would probably be better if the problems of heat transfer and fluid flow could be considered separately until better solutions for the individual problems are established.

Studies on heat transfer in porous systems have remained relatively scarce in the sense that there are relatively few articles in this general area which are applicable to the concept as it is examined in this study.

A relatively new area of study involving heat transfer in porous materials is the heat pipe. (9) Present studies on the heat pipe are more concerned with fluid flow through the capillaries of the wick and problems of entrainment during vaporization than they are with problems of heat transfer through the porous wick. This is to be expected because the heat transfer problems are not the most critical problems found in heat pipes at the present time. However, it has been noted (8) that future developments in heat pipes will need to consider problems such as the heat transfer through the fluid and the wick in high performance heat pipes.

## PURPOSE AND SCOPE

One purpose of this study was to build and operate an experimental apparatus that could be used to perform research on porous systems. The apparatus was to be used for studies of the kinetics of gas phase chemical reactions in a heat-generating porous reactor. It was also to be used to measure heat transfer coefficients in heat-generating porous materials.

The development and use of the apparatus for kinetic studies has been described by Farber. (10) The present thesis will describe the development and use of the apparatus for the purpose of experimentally measuring heat transfer coefficients within a gas-cooled, heat-generating porous solid. The method for the determination of the heat transfer coefficient will use only a limited number of assumptions and in particular this method will take into account some factors which, through neglect, omission, or error, appear to have led to certain erroneous assumptions regarding heat transfer in porous systems.

The present study also proposes to examine correlations which have been suggested for porous materials, but which are based on extrapolation from nonporous models, in order to determine the agreement between these proposed correlations and experimental data.

The porous material used in both the kinetic studies of Farber and in this work was porous tungsten in the form of hollow cylinders approximately one and a half inches long,  $3/8$  inch in outside diameter with a wall thickness of  $1/16$  inch. The heat generation within the porous tungsten was obtained from direct current that was supplied from a selenium rectifier of the type used for commercial electroplating

operations. In the present study the heated tungsten was cooled by nitrogen or helium gas which flowed radially outward through the pores of the hollow tungsten cylinder.

Measurements of the porous system were taken when it was in a state of dynamic equilibrium in which heat was being generated within the porous tungsten at the same time that heat was being removed by the heating of the gas that was flowing through the wall of the hollow cylinder. Under these conditions a number of boundary conditions of the porous system were determined. More boundary conditions were measured than were required by the order of the differential equations that describe the porous system and the unknown heat transfer coefficient could then be found from the overdefined system of equations.

Analysis of the experimental data was carried out using third order differential equations to describe the porous system. The use of equations of this order assured that the analysis would not impose any constraint on the heat transfer coefficient such as results when, for example, differential equations of a lower order are used to describe the porous system.

Porous systems have been described by models that consider the porous material to consist of many small pipes or to resemble a packed bed. Correlations obtained from these models will be compared to experimentally measured data.

## THEORY

Heat Transport in Porous Systems

There are many materials which have been described as porous, which literally means that the material contains a number of small openings. This concept of porosity will be retained in this study but additional qualifications will be added. In porous materials, dimensions of the pores are usually small relative to the extensive dimensions of the material. Also the pores are usually uniformly distributed throughout the material. When the term porous is applied to a material, that material is still considered to be uniform but its extensive properties (mass, heat capacity, conductivity, etc.) are now treated as having been reduced by some factor. Oil-bearing strata, a fluidized bed, urethane foam, a car radiator, and turbine blades formed by sintering powdered metal are examples of porous materials.

Porosity is a parameter used to describe porous materials. It specifies the fraction of a particular extensive property that is missing from the porous material. Volume is the extensive property generally referred to when porosity is used. In this sense porosity is a measure of the amount of void in a porous solid. Volume porosity has the dimensions of cubic feet of void volume per cubic feet of bulk volume. These dimensions have been specified for porosity in other references. There are other kinds of porosities such as solid-area-normal-to-conduction per bulk area and solid-length-parallel-to-conduction per bulk length. The first of these porosities is generally assumed to have the same numerical value as one minus the volume porosity while the second is generally assumed to have a numerical value of one.

On this basis, the effective area for conduction through a porous solid would be numerically equal to the bulk area for conduction multiplied by one minus the volume porosity. However, an example will show that all porosities are not the same as the volume porosity. Two materials may have the same volume porosity but the one may be a bed of hard spheres that touch only at the points of contact while the other is a solid block of material that has a number of parallel holes drilled through it. The conductivity through the drilled block parallel to the drilled holes and the conductivity through the bed of hard spheres would certainly be quite different. There would probably also be a difference in the conductivity through the drilled block parallel to the holes and the conductivity through the drilled block perpendicular to the holes.

Porous materials have a certain degree of homogeneity due to the uniformity of their pore structure. However, the ability to analyze porous materials by the method used in this study is dependent on the following considerations. Porous material is clearly heterogeneous when it is examined at a level corresponding to the dimensions of the particulate structure. A rigorous analysis of the heat transfer through a number of such particles would be analogous to an attempt to analyze the heat transfer in the bricks of a regenerator by defining finite difference equations for all of the bricks in the regenerator.

The analysis can be greatly simplified if the porous system can be analyzed on a scale that is at least one or two orders of magnitude larger than the dimensions of the particles of the porous structure. In this case it may now be possible to consider the porous material to be homogeneous and possessed of extensive properties that are reduced in magnitude.

This method for analyzing systems has a clear precedent in the ordinary heat conduction problem in which the problem of defining energy transfer between atoms is avoided by assuming that the conduction problems will consider the material on a scale where the significant dimensions of the conducting material are much larger than the dimensions of the atoms comprising the material. Thus, treating solid material made of atoms, and porous material made of particles as both being homogeneous involves only a quantitative and not a qualitative difference.

A real porous system will be a mixture of solids and voids. A significant number of these voids may be connected to form passages. The voids may contain a fluid. The model of the porous system used in this study treats the porous system as one composed of two phases that occupy the same bulk space but in which each phase is present at a reduced density. The solid phase and the fluid phase are each considered to be homogeneous, continuous, uniformly dispersed through each other, and in contact with each other. In this model the extensive properties of each phase are proportional to the volume fraction of that phase in the porous system.

In order to justify the assumption that a real heterogeneous porous system can be considered to be homogeneous, the Biot number should be determined for the particles in the material. The Biot number is  $hr/k$  where  $h$  is the heat transfer coefficient at the surface of the particle,  $r$  is the radius, or characteristic dimension of the particle, and  $k$  is the thermal conductivity of the solid material comprising the particle. The Biot number is the ratio of the midplane thermal internal resistance to the surface film resistance. (3) The Biot number is exactly the ratio of the conduction temperature gradient over the convection

temperature gradient for the case of a plane of thickness  $r$  with thermal conductivity  $k$  and heat transfer coefficient  $h$  at one surface. The Biot number is twice this ratio for a slab, a cylinder, or a sphere when the solid material is uniformly generating heat. (24) With the exception of the factor of two, the Biot number can be used to determine the ratio of the temperature difference from the center of the particle to the edge of the particle divided by the temperature difference from the edge of the particle to the bulk temperature of the fluid stream.

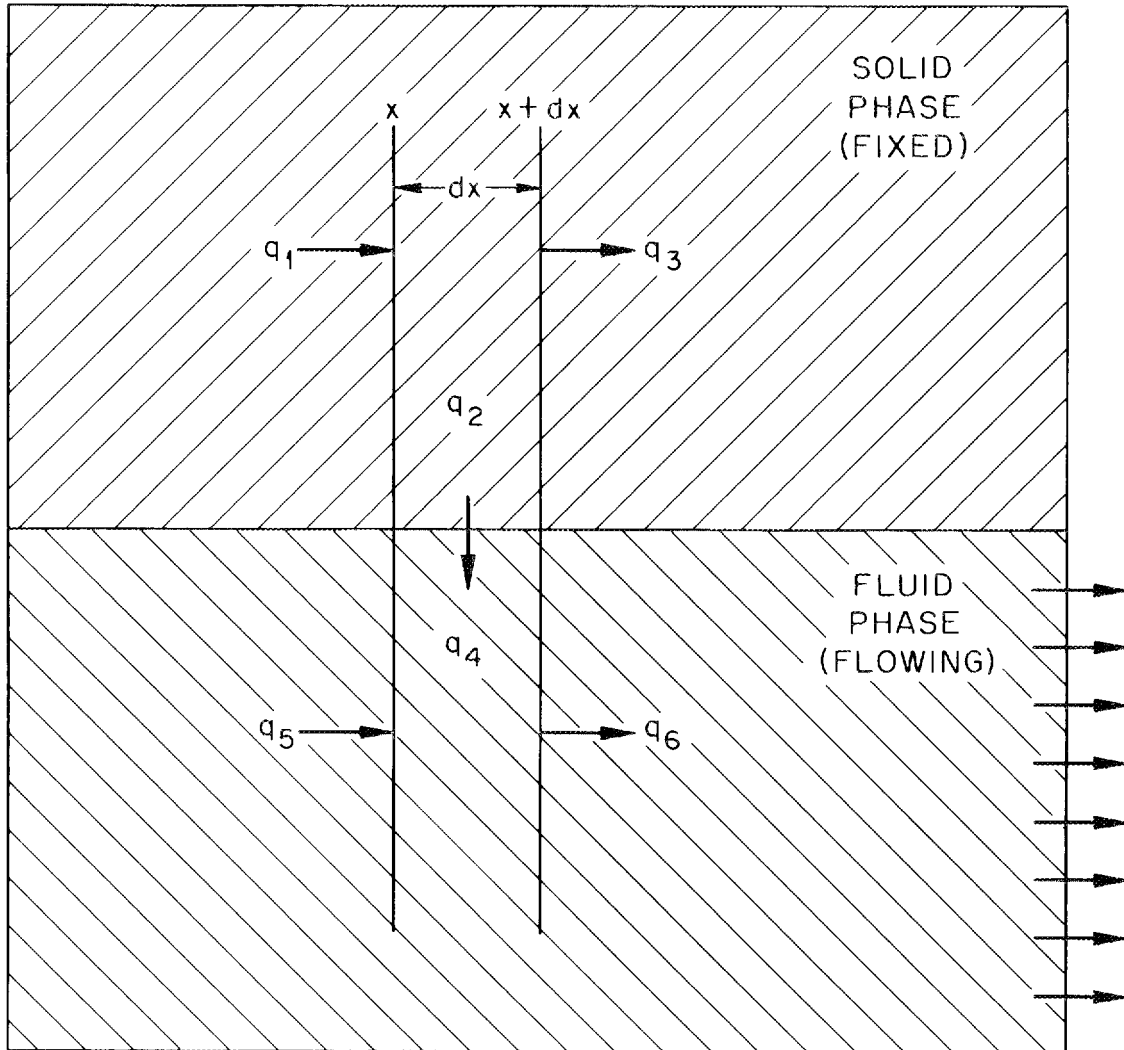
The Biot number for the particles of a porous material may be used to determine the temperature gradients which will be created within the particles by the convective heat transfer coefficient of the system. The assumption has been made that the solid phase temperature varies uniformly across the wall of the porous material. This means that a certain temperature gradient will exist across the width of a single particle of the porous material. In order to justify treating the porous system as if it were homogeneous the central and surface temperatures of the particles should vary less than an amount that could perturb the temperature gradient which may be imposed on the porous material. The temperature change within the particles should also be small enough not to significantly effect any temperature dependent physical parameters of the particle material since they have been assumed to be independent of temperature in this model.

Heat transfer in porous systems, as defined in this study, involves a stationary porous solid phase and a fluid phase that is flowing through the connected pore structure of the porous solid. Heat is being generated within the solid phase material. Three modes of heat transport are involved. Heat is being transferred through the solid phase

by conduction and is being transferred with the fluid phase by mass transport. In addition to these two modes, heat is being exchanged between the solid and fluid phases by convective heat transfer across the solid-fluid interface. This interface is the internal surface area of the porous solid.

The configuration which may be used to study heat transport in heat generating porous systems consists of a generating, conducting, infinite, porous flat plate cooled with a nongenerating, nonconducting fluid flowing through the connected pores in the plate. The flow through the plate is taking place in the one finite dimension. Figure 1 shows the heat flows used to derive the equations for steady state heat transfer in such a system.

The quantities  $q_1$  and  $q_3$  represent respectively the heat conducted into and out of the element  $dx$  of the solid phase of the porous system. Since no conduction through the fluid phase is considered there is no comparable effect in the fluid phase. This assumes the heat transferred by conduction in the fluid is negligible compared to other heat transport effects in the fluid phase. The quantities  $q_5$  and  $q_6$  represent the heat transported into and out of the element  $dx$  of the fluid phase of the porous system by fluid flow. Since there is no movement of the solid phase there is no comparable effect in the solid phase. The quantity  $q_2$  represents the heat generated in the element  $dx$  of the solid phase of the porous system due to ohmic heating. Since there is no ohmic heating of the fluid phase there is no comparable effect in the fluid phase. The quantity  $q_4$  represents the heat transferred by convective heat transfer from the solid phase to the fluid phase. This transfer takes place across the interphase boundary existing in the  $dx$  element.



- $q_1$  = HEAT IN TO SOLID BY SOLID CONDUCTION.  
 $q_2$  = HEAT GENERATED IN SOLID.  
 $q_3$  = HEAT OUT OF SOLID BY SOLID CONDUCTION.  
 $q_4$  = HEAT TRANSFERRED FROM SOLID TO FLUID BY  
 CONVECTIVE HEAT TRANSFER.  
 $q_5$  = HEAT IN TO FLUID BY FLUID TRANSPORT.  
 $q_6$  = HEAT OUT OF FLUID BY FLUID TRANSPORT.

Figure 1

Heat Flow in a Differential Element of Porous Material

Heat balances around the solid and fluid differential elements yield the two related differential equations

$$k\gamma_2(d^2T/dx^2) + \Gamma\gamma_3 = h\epsilon(T - t) \quad (1)$$

and

$$h\epsilon(T - t) = FCp\delta_2(dt/dx). \quad (2)$$

The full derivation is given in Appendix A.

The physical parameters are treated as being independent of temperature, and are therefore handled as constants in the equations. The solution of this system of differential equations gives for the solid and fluid phase temperature distributions

$$T(x) = C_1 e^{r_1 x} + C_2 e^{r_2 x} + C_3 e^{r_3 x} + jx. \quad (3)$$

and

$$t(x) = B_1 e^{r_1 x} + B_2 e^{r_2 x} + B_3 e^{r_3 x} + jx. \quad (4)$$

where the  $r_n$  ( $n = 1, 2, 3$ ) are the roots of the operator equation in  $m$

$$m^3 + bm^2 - cm = 0 \quad (5)$$

and where

$$b = h\epsilon/FCp\delta_2$$

$$c = h\epsilon/k\gamma_2$$

$$j = \Gamma\gamma_3/FCp\delta_2.$$

The  $B_s$  are related to the  $C_s$  by

$$B_n = C_n \left( \frac{b}{r_n + b} \right) \quad (n = 1, 2, 3) \quad (6)$$

Equations (3) and (4) are the form of solution that is characteristic of generating porous systems. The solid phase temperature and the fluid phase temperature are found to depend on a complementary function involving three undetermined coefficients and on a particular integral involving the ohmic heat generation. The three undetermined coefficients arise since third order differential equations are produced in solving the system of two differential equations (1) and (2). The constants of integration ( $C_1$ ,  $C_2$ , and  $C_3$ ) can be found from three boundary conditions involving  $T$ ,  $t$ , or their derivatives with respect to  $x$ . If the various physical parameters involved in formulating (1) and (2) are known, the porous system would now be fully described.

For a porous plate whose  $x$  dimension is  $l$  ft., the simplest boundary conditions, and ones which provide a convenient means for the study of porous heat transfer, are  $t|_{x=0} = t_0$  (specifying the inlet fluid temperature which sets the temperature regime of the system),  $dT/dx|_{x=0} = 0$  and  $dT/dx|_{x=l} = 0$  (adiabatic walls on the porous solid).

Due to the nature of the experimental apparatus used in this study it was not possible to use these simple forms of the heat transfer equations to analyze the experimental system.

#### Basic Heat Transport in the Experimental Porous System

While the infinite flat plate system with the simple boundary conditions just described provides the most ideal model for describing porous heat transfer, systems used for experimental studies are of

necessity less ideal. For this reason it was necessary to consider the experimental system being used and to modify and extend the heat transport equations accordingly.

The porous solid used in this experimental study was tungsten. The porous tungsten was manufactured by sintering tungsten powder at a temperature where physical bonding of the particles occurred without eliminating the porous nature of the compacted powder. The powder used to form the porous tungsten was 20 micron powder. The porosity of the sintered tungsten was approximately one half. The characteristic diameter both of the solid structure and the void space was taken to be that of the powder diameter.

The thermal conductivity of solid tungsten is approximately  $10^2$  B.t.u./hr.-°F-ft. It will be shown the convective heat transfer coefficient at the particle surface in this study is much less than 1.0 B.t.u./hr.-°F-sq.ft. and since 20 microns is approximately  $6 \times 10^{-5}$  ft. the Biot number ( $hr/k$ ) for these particles is approximately  $3 \times 10^{-7}$ . This shows that even with a solid to fluid temperature difference on the order of  $10^3$  °F, as found in this study, intraparticle temperature variation is of the order of  $10^{-4}$  °F and the central and surface particle temperatures are effectively the same. No significant change in temperature dependent physical parameters would take place in this small a temperature difference and this temperature difference is also negligible compared to a gradient of a few degrees of temperature per particle which the temperature gradient across the porous material may impose.

The size of the Biot number indicates that this porous solid is very well suited for consideration as a homogeneous porous solid.

Consideration of the porous tungsten in a homogeneous sense is further enhanced by the fact that the characteristic dimensions of the sintered tungsten (a hollow cylinder) ranged from an axial length of 1.5 in. down to a wall thickness of 0.07 in. Thus, the porous material has dimensions at least two orders of magnitude larger than the characteristic diameter of either the particles or the voids of the porous material.

The fluid flowing through the connected pores of the porous tungsten was either nitrogen or helium gas. The Reynolds number in the pores was approximately  $10^{-1}$  and the Peclet number was therefore of approximately this same order of magnitude.

The system is operating at solid phase temperatures around 1500 °F. Radiative heat transfer considerations involving the fluid phase may be neglected due to the transparency of nitrogen and helium to radiation. Radiative heat transfer at the boundaries of the porous tungsten cylinder are considered but interparticle radiative heat transfer may be neglected since the fine porous structure effectively makes the cylinder a wall consisting of approximately  $10^2$  radiation shields. Further justification for neglecting this effect will be presented later.

In order to define the experimental porous system it is necessary that the parameters used in equations (1) and (2) be known and that three boundary conditions be measured. This would allow evaluation of the Cs, and therefore the Bs, so that the system would be completely defined. However, the volumetric heat transfer coefficient is an unknown parameter in this study. The method of finding this parameter will be to measure four boundary conditions rather than three and then

solve a system of four equations in four unknowns. The four unknowns will be the three coefficients and the volumetric heat transfer coefficient.

### Special Considerations for the Experimental Porous System

#### Coordinate Transformations

The experimental porous system used in this study was a thin-walled, hollow porous tungsten cylinder. Study of this system was facilitated by treating the hollow cylinder as a flat plate. Since the ratio of the radii of the cylinder was approximately 1.5, the error introduced by the use of the arithmetic mean area rather than the logarithmic mean area was less than 2 percent. Additional justification for this simplifying assumption will be found in the discussion of results.

The transformation from cylindrical to rectangular coordinates was performed as shown in Figure 2. The cylinder radius corresponded to the x dimension of the porous system in which temperature was related to x position according to equation (3). The radial wall thickness was taken to be equal to the rectangular wall thickness. The cylinder axis corresponded to the rectangular z dimension. The axial cylinder length was taken to be equal to the rectangular z length.

The cylinder angular dimension corresponded to the y dimension of a rectangular system and due to symmetry no temperature variation in the y dimension was considered. The y dimension of the rectangular model is therefore limited by adiabatic walls. Further, the magnitude of the y dimension was taken to be the quotient of the volume of the hollow cylinder divided by the product of cylinder wall thickness and axial cylinder length. The volume of the porous tungsten, the axial

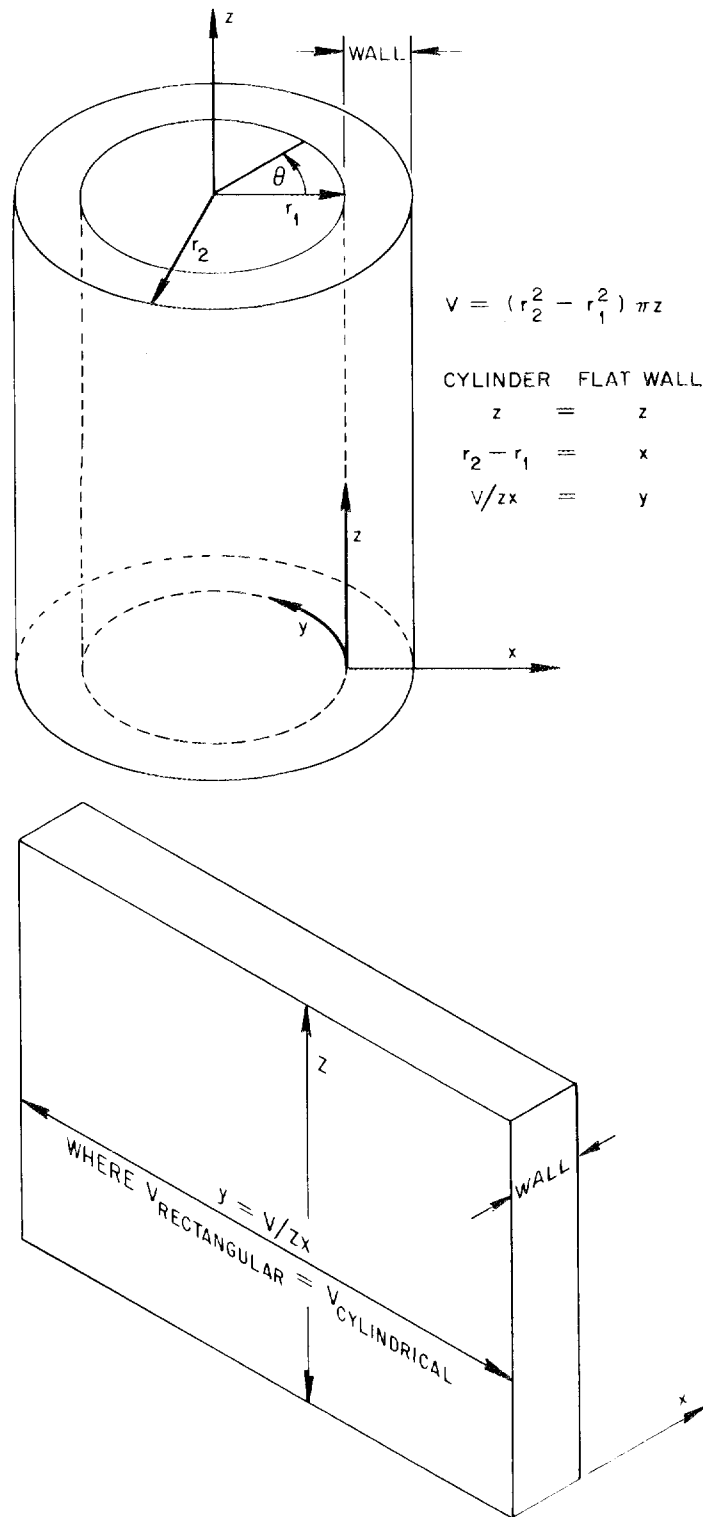


Figure 2

Equivalent Flat Wall Model of the Cylinder

length, and the wall thickness thus remain unchanged across the coordinate transformation.

Cylinder Axis Temperature Gradient

Because of the experimental difficulties in preventing a temperature gradient along the cylinder axis, it was necessary to formulate differential equations that took the axial or z dimension solid phase temperature gradient into account.

The fluid phase z dimension temperature gradient is not considered since fluid phase heat conduction has already been neglected and since no z direction fluid flow is considered. The extension of equations (1) and (2) to the two dimensional cases for the solid phase gives

$$k\gamma_2 \nabla^2 T + \Gamma\gamma_3 = h \epsilon (T - t) = F C_p \delta_2 dt/dx . \quad (7)$$

A solution of equation (7) is obtained by assuming the x and z components of T are separable, i.e.,

$$T(x,z) = X(x) Z(z) \quad (8)$$

and further that

$$\frac{d^2 Z}{dz^2} = -\lambda^2 Z \quad (9)$$

or

$$Z'' = -\lambda^2 Z \quad (10)$$

Equations (9) and (10) are satisfied for the case where the function Z is a Fourier series. The solution of equation (7) gives

$$T = \sum_{i=1}^{\infty} X_i(x) Z_i(z) + jx \quad (11)$$

where

$$X_i(x) = C_{i1} e^{r_{i1}x} + C_{i2} e^{r_{i2}x} + C_{i3} e^{r_{i3}x} \quad (12)$$

and the  $Z_i(z)$  are the terms of the Fourier series.

Experimentally the observation of the outer surface of the tungsten cylinder will be limited to a fixed number of points. These points correspond to the holes in the Marinite disks through which the tungsten surface is viewed with an optical pyrometer. Since there are five holes in the Marinite disks the z axis temperature distribution will be represented by a truncated series using the first five terms of the Fourier series. This should be a very adequate approximation of the axis temperature function in view of the fact that the norm for the z axis temperature gradient is zero and a few terms of the series are typically used to characterize perturbations. Equation (11) therefore becomes

$$T = \sum_{i=1}^5 X_i(x) Z_i(z) + jx . \quad (13)$$

Temperature Dependence of Electrical Resistivity

With one exception, all physical parameters in the porous system were taken to be temperature independent and a parameter value corresponding to the mean temperature of the material was used. The one exception was the electrical resistivity of tungsten. A linear temperature dependence was used to describe this parameter. The volumetric heat generation term  $\Gamma_{\gamma_3}$  was replaced by  $G(T)$  where

$$G(T) = G_0 + \alpha T. \quad (14)$$

The differential equations describing the porous system are now

$$k\gamma_2 \nabla^2 T + G(T) = h \epsilon (T - t) = F C_p \delta_2 dt/dx \quad (15) \text{ and } (16)$$

The solution becomes, using the first 5 terms of the series,

$$T = \sum_{i=1}^5 X_i(x) Z_i(z) - G_0/\alpha. \quad (17)$$

The use of the first five terms appears to give a satisfactory description of the axial temperature profile as will be discussed later.

The volumetric heat generation terms now occur not only in the constant term in equation (17), but also in the operator equation, (5), which now takes the form of

$$m^3 + bm^2 - (c - (\alpha/k\gamma_2) + \lambda^2) m - b (\lambda^2 - (\alpha/k\gamma_2)) = 0 \quad (18)$$

A similar solution exists for  $t$ . The complete derivations are given in Appendix A.

The reason for the use of a temperature dependent physical parameter is to facilitate the computations involved. The necessary calculations could be performed without allowing the temperature dependence. However, introduction of this dependence does not increase the order of the equations involved and thereby makes better use of data available to describe the tungsten. The mean solid temperature is used to evaluate appropriate zero and first order terms for electrical resistivity as used in equation (14).

The computations that involve the electrical resistivity (and thermal conductivity) are performed in order to evaluate the electrical (and by implication the thermal) conductance of the porous tungsten at the operating temperature of the tungsten cylinder. The need for this evaluation will now be considered.

Length Over Area Conduction Correction Factor

A porous material is considered to have intensive properties that have been reduced in proportion to the extent, and the nature, of the porosity. The thermal and electrical conductivity are two such properties of particular interest in this study.

If the pores in a porous material were a series of uniform straight, parallel holes running through the solid in the direction of energy flow (Figure 3a.) then the conductance, which involves the length, area, and conductivity, could be evaluated simply by applying a volumetric porosity correction factor to the area in the form

$$K_{\text{eff}} = k_{\text{bulk}} \frac{A(1-S_3)}{L} \quad (19)$$

where

$K_{\text{eff}}$  = effective conductance

$k_{\text{bulk}}$  = bulk conductivity per unit (area over length)

$L$  = bulk length for conductance

$A$  = bulk area for conductance

$S_3$  = volume porosity, cu. ft. void/cu. ft. bulk

However the real nature of most porous solids, including the ones in this study, is more nearly as shown in Figure 3b. In particular, in the case of sintered materials formed from powders, the channels are in fact formed from the interstices between the powder grains. This implies that the effective length of the conduction path and the effective area of the conduction path can no longer be described by the simple relation shown in equation (19). A new equation is needed to describe the situation, thus

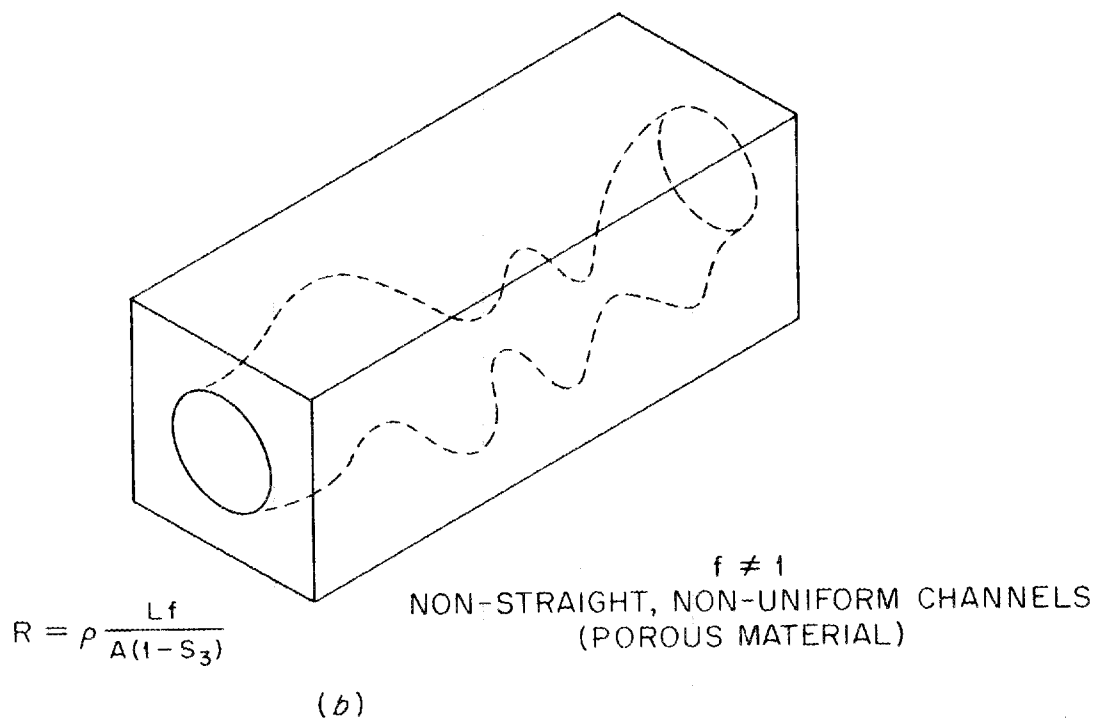
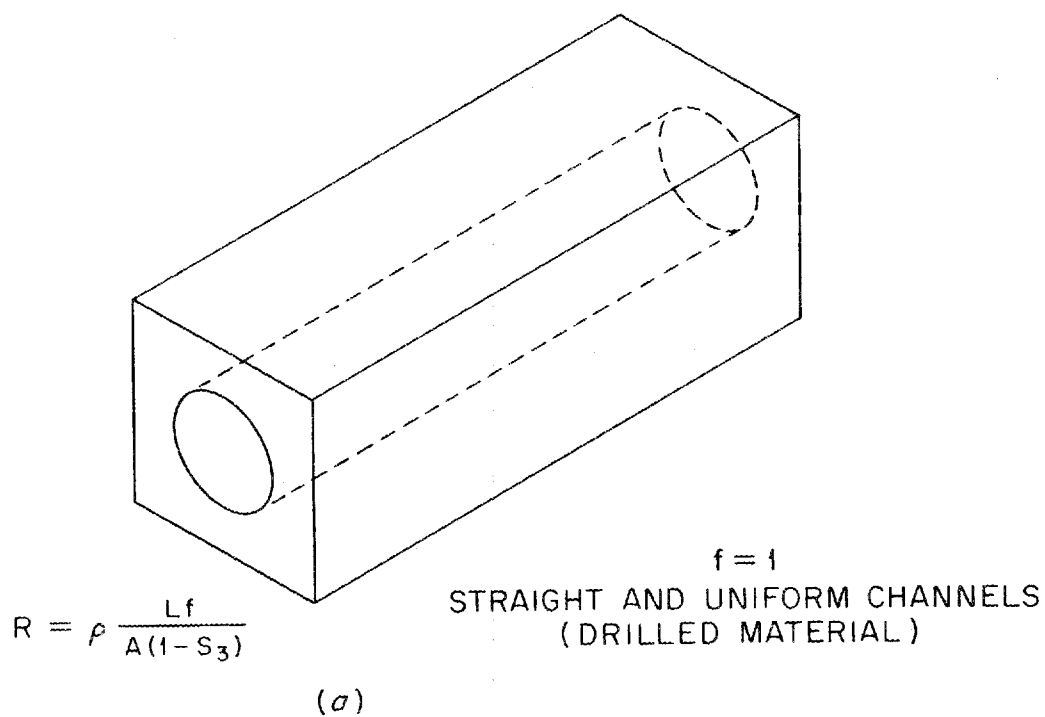


Figure 3

Drilled Channels and Porous Material

$$K_{\text{eff}} = k_{\text{bulk}} \frac{A(1-S_3) f_A}{L f_L} \quad (20)$$

where

$f_L$  = a correction factor to obtain the effective length for conduction.

$f_A$  = a correction factor to obtain the effective area for conduction  
(excluding the volume porosity factor).

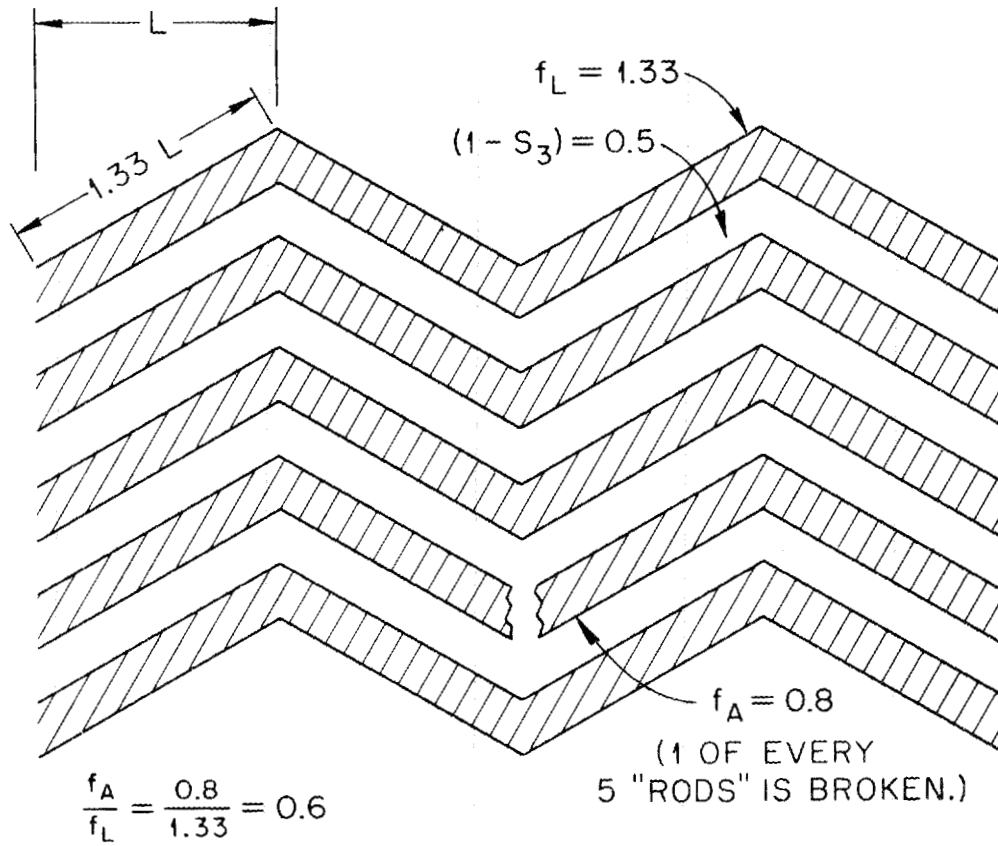
A schematic representation of these factors is shown in Figure 4. This figure shows a hypothetical, idealized, porous solid composed of staggered rods and having a volumetric porosity of one half. The orientation of the rods that comprise the material are not parallel to the direction of conduction. The actual length over which energy travels in moving a distance  $L$  in the direction of conduction is  $1.33L$ . This length factor will reduce the conduction by a factor of 0.75, i.e.

$$f_L = 1.33.$$

The cross sectional area of these rods will be assumed to vary. The area for conduction will "neck down" at points of contact between particles. The simplest example of this effect may be seen by assuming that 1 of every 5 rods has a complete break at some point along its length. Since this removes this rod as a conductor the available area for conduction is reduced by 0.8, i.e.  $f_A = 0.8$ .

Since the effective conduction is proportional to the area and inversely proportional to the length, these two factors combined will reduce the conduction by a factor of 0.6. In combination with the volume porosity factor of 0.5 the overall effective conductivity now becomes 0.3 that of the conductivity of solid material and the porous material may now be considered as a homogeneous material, characterized by extensive properties such as bulk area and bulk length but possessed

VOLUME POROSITY ( $S_3$ ) = 0.5  
 (HALF OF THE VOLUME IS "RODS"  
 HALF OF THE VOLUME IS "VOID")



$$\frac{f_A}{f_L} = \frac{0.8}{1.33} = 0.6$$

$$k_{\text{effective}} = 0.3 k_{\text{bulk}}$$

$$1/\rho_{\text{effective}} = 0.3 (1/\rho_{\text{bulk}})$$

Figure 4

Factors Reducing Conductivity in Porous Materials

of a reduced conductivity. The effect of this factor on the evaluation of the heat transfer coefficient will be considered later.

The volume porosity is readily obtained from measurements of weight and volume of the porous material. While the length and area factors are separable in the example of Figure 4 they may not be as easily separated in real materials. Determination of the combined length-over-area conduction correction factor could be found from experimental steady state measurements of the conductivity of the porous material. In principle the length correction factor could be found from experimental unsteady state (transient) measurements of the conductivity of the porous material. However, since this study deals only with steady state problems, the two factors may be considered together as the length-over-area correction factor,  $f_{L/A}$ , which equals  $f_L/f_A$ .

Information on the effective thermal and electrical conductivity of the porous tungsten used in this study was not available from the manufacturer. Apparatus for independent thermal and electrical conductivity measurements at the operating temperature of 1500°F was not available. Accordingly, the length-over-area conduction correction factor for electrical conduction was determined during each run at the actual operating temperature from experimental data taken during the run.

This type of correction factor is applicable to both the electrical and the thermal conduction problem. It is assumed that the length-over-area correction factor for thermal conduction is equal to that for electrical conduction. This appears to be a valid assumption in view of the direct analogy between the thermal and electrical conduction mechanisms.

The similarity of the mechanisms for thermal and electrical conductivity is not found in similar temperature coefficients for thermal and electrical conductivity. The temperature coefficient of thermal conductivity ( $k$ ) for tungsten is in fact negative while the temperature coefficient of electrical resistance ( $\rho$ ) for tungsten is positive. This behavior is in fact necessary in order that the Lorenz number ( $k\rho/T^\circ\text{K}$ ) remain essentially constant which is known to be the case for metals. (24) The Lorenz number for tungsten varies by only one percent over a range of  $800^\circ\text{K}$  that includes the temperatures found in this study.

The thermal and electrical conductivity are thus related as shown in the Lorenz equation and the agents that are responsible for this relation are the free electrons of the metal. (1)

There have been experimental measurements that tend to verify the assumption that a similar correction factor may be used for thermal and electrical conduction in porous metals. (16) The chapter in Schneider (28) on Experimental Analogic Method gives extensive treatment to electrical analogy in heat conduction problems noting that this analog has a direct mathematical similarity to heat conduction and is the best known and most widely used analog for these types of problems.

#### Fifth Boundary Condition

It was pointed out that the volumetric heat transfer coefficient,  $h_v$ , was to be found along with the three unknown coefficients that resulted from solution of the differential equation. Measurement of four boundary conditions allowed evaluation of  $h_v$ . The combined length-over-area conduction correction factor is a parameter that occurs in the electrical and thermal conduction terms in the original differential

equations describing the porous system. It is treated as a value that is unknown and is to be found from the measurement of a fifth boundary condition. This fifth boundary condition is the average temperature of the solid phase of the porous tungsten cylinder in the region between the two voltage probes ( $\bar{T}_{AB}$ ). Measurement of five boundary conditions will now permit the evaluation of the three unknown coefficients,  $h_c$ , and the length-over-area conduction correction factor.

The length-over-area conduction correction factor becomes another parameter the value of which is initially assumed and which is then used in iterative calculation until the calculated value matches the assumed value.

## EXPERIMENTAL WORK

Experimental Apparatus - General Description

The experimental apparatus consisted of equipment that could generate heat within porous tungsten and that could also remove the heat with gas flowing through the pores of the tungsten. The heat was generated within the porous tungsten by direct current that was supplied by a rectifier. The direct current circuit from the rectifier used copper bus bars of 1 sq.in. cross section to carry the current to the porous tungsten. The heat generating porous tungsten was cooled by passing nitrogen or helium gas through the pores of the tungsten.

The experimental runs were carried out by establishing a heat generation rate and a coolant flow rate. When the apparatus reached a state of dynamic equilibrium, measurements were made of parameters that defined five boundary conditions. The heat transfer coefficient within the porous tungsten and the conduction correction factor for the porous tungsten were calculated from these boundary conditions.

The study was carried out with hollow porous tungsten cylinders fabricated by sintering 20 micron tungsten powder. These tungsten cylinders were obtained from the Kulite Tungsten Co., Ridgefield, New Jersey. The cylinders were approximately 1.5 in. long. They were hollow, having an O.D. of approximately 0.415 in. and an I.D. of approximately 0.275 in. The cylinders had a weight of approximately 18 grams and a volume porosity of approximately 45 percent.

Electric Power Circuit

The electric power used to heat the tungsten cylinder was obtained from a selenium rectifier manufactured by the Rapid Electric Company, Serial Number 68025. The power was direct current flowing in a circuit that passed axially through the tungsten cylinder. All heating effects were due to ohmic (resistance) heating. The electric power circuit is shown in Figure 5.

Input to the rectifier was 230 volt, 60 cycle, 3 phase, alternating current (A.C.). Output from the rectifier ranged from 0 to 12 volts, and from 0 to 6000 amperes, direct current (D.C.). Control of the output voltage on the rectifier, as manufactured, was obtained by means of three, 7-position tap switches. Each of these tap switches controlled the output from the high voltage transformer for one phase of the input alternating current. The direct current output voltage was proportional to the output of the high voltage transformers.

A modification was made to the rectifier circuit in order to obtain continuous, as opposed to stepwise, control of the output voltage. Three 230 volt Variacs were inserted in the rectifier input circuit between the 230 volt laboratory power supply and the three high voltage transformers. The three Variacs were connected along a common axis and were operated in tandem. Continuous output voltage regulation was obtained by using the combination of Variacs and tap switches.

The electric power supply was monitored by means of several instruments. The rectifier had been delivered with a D.C. voltmeter and a D.C. ammeter to monitor the output current. Three A.C. ammeters were connected to the three output lines from the three Variacs in order to

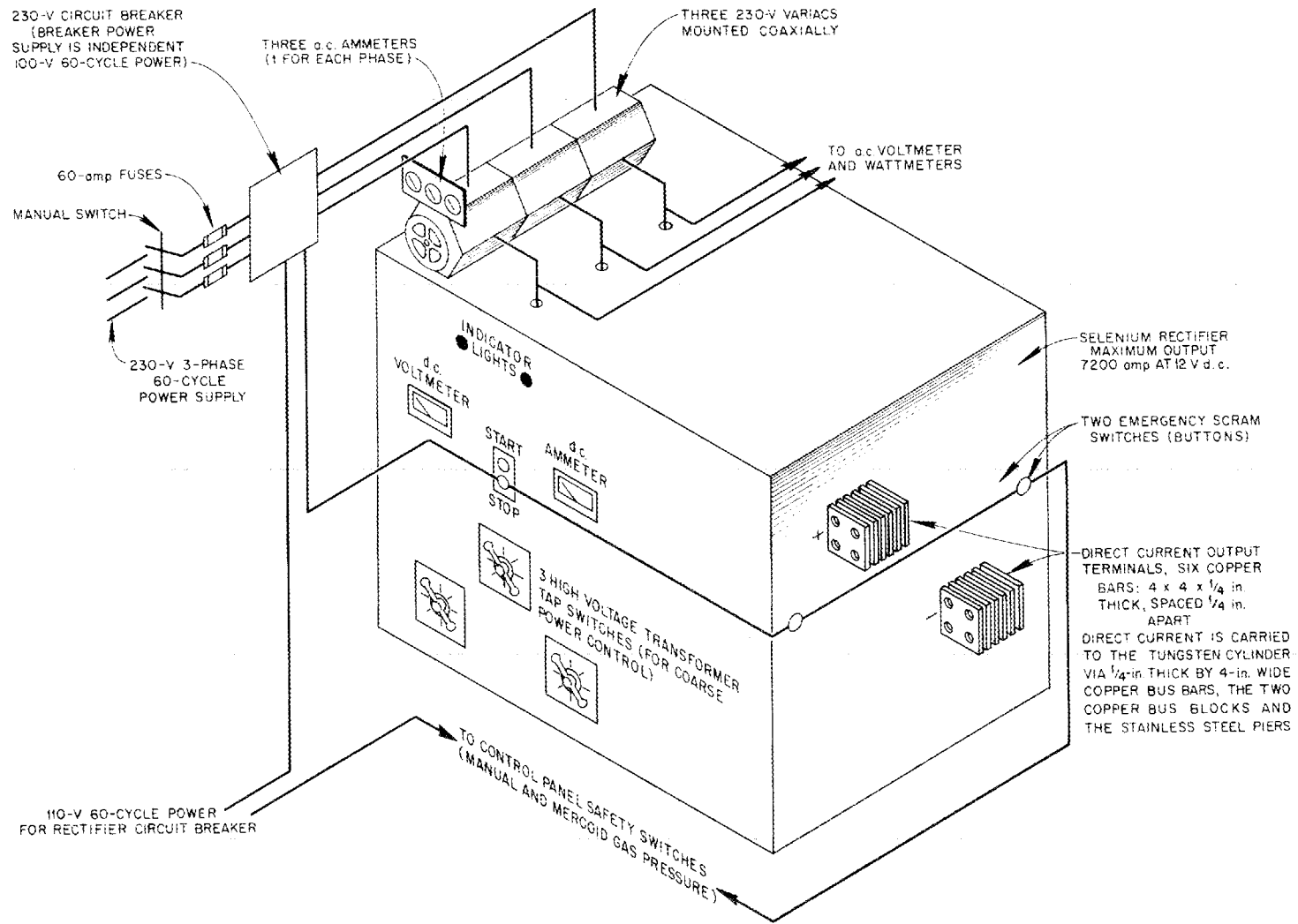


Figure 5  
Rectifier Power Circuit

monitor the current in these circuits. An A.C. voltmeter was set up to selectively monitor the voltage across each pair of A.C. input lines. Two A.C. wattmeters were connected across the three lines supplying power from the Variacs to the high voltage transformer of the rectifier. The wattmeters were equipped with phase reversal switches and were used to monitor the power input to the rectifier. Probes were connected to the direct current circuit at several locations in order to take measurements of voltage at these points in the circuit. The probes attached across the D.C. ammeter shunt were used to measure the D.C. current with high accuracy by means of a high precision potentiometer.

#### Mechanical Assembly

The direct current was carried from the rectifier terminals to the tungsten cylinder through bus bars consisting of several solid copper bars bolted together. The bus bars were  $1/4$  in. thick, 4 in. wide and from  $8-1/2$  in. to 12 in. long. See Figure 6.

A copper bus block was bolted to the terminus of each bus bar. These two bus blocks served as the platforms for the mounting of the tungsten cylinder. These bus blocks were solid copper, 1 in. thick, 4 in. wide, and 5 in. long. See Figure 7. Each bus block had a  $1/8$  in. diameter hole drilled through it at the center of the block. A high pressure fitting was silver soldered into one face of each bus block in a position over the  $1/8$  in. diameter hole in the bus block. The faces of the blocks containing this fitting faced away from the tungsten cylinder and were known as the outside faces of the bus blocks. These high pressure fittings had an I.D. of  $1/8$  in. A hollow stainless steel

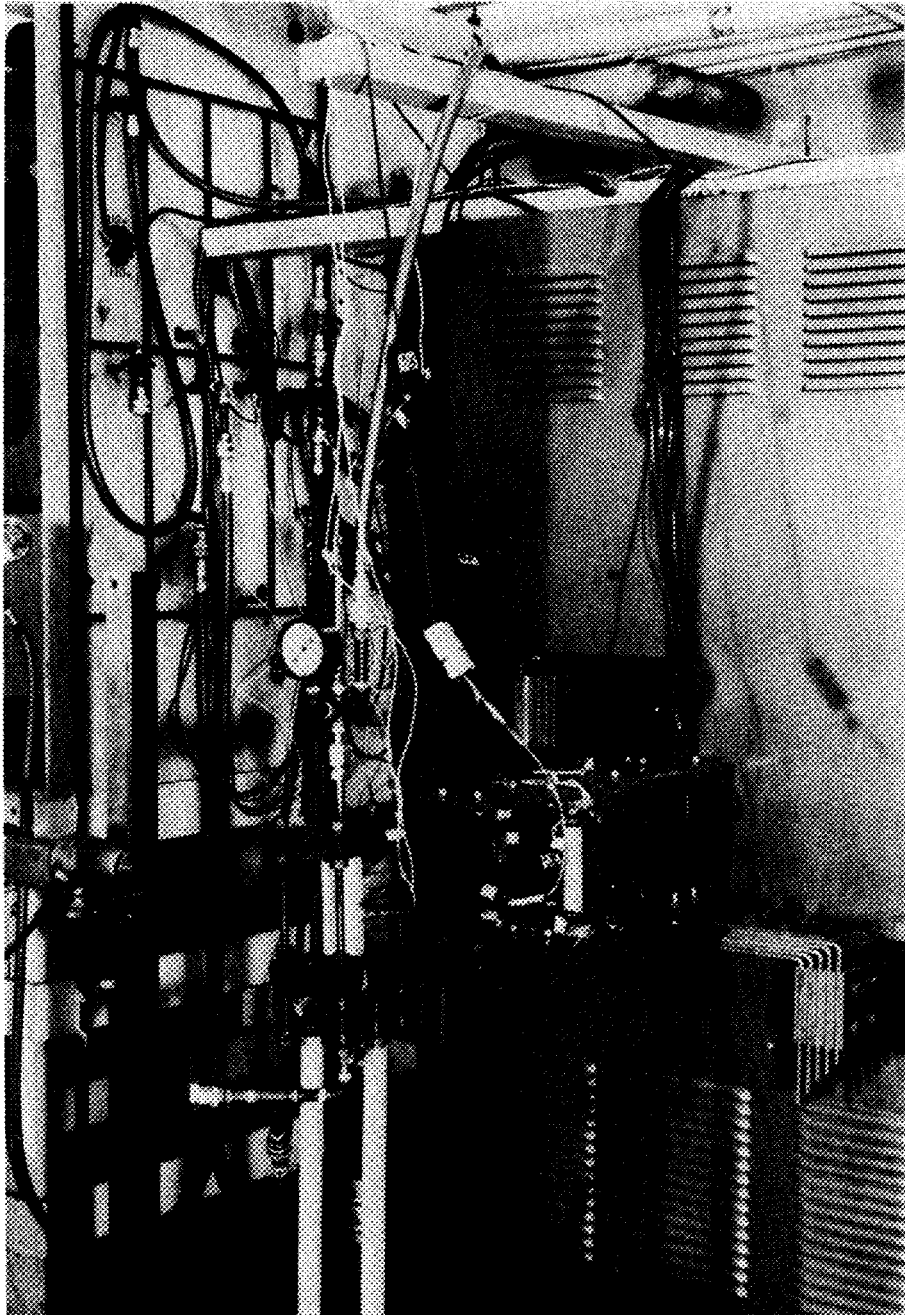


Figure 6

Photograph of the Experimental Equipment

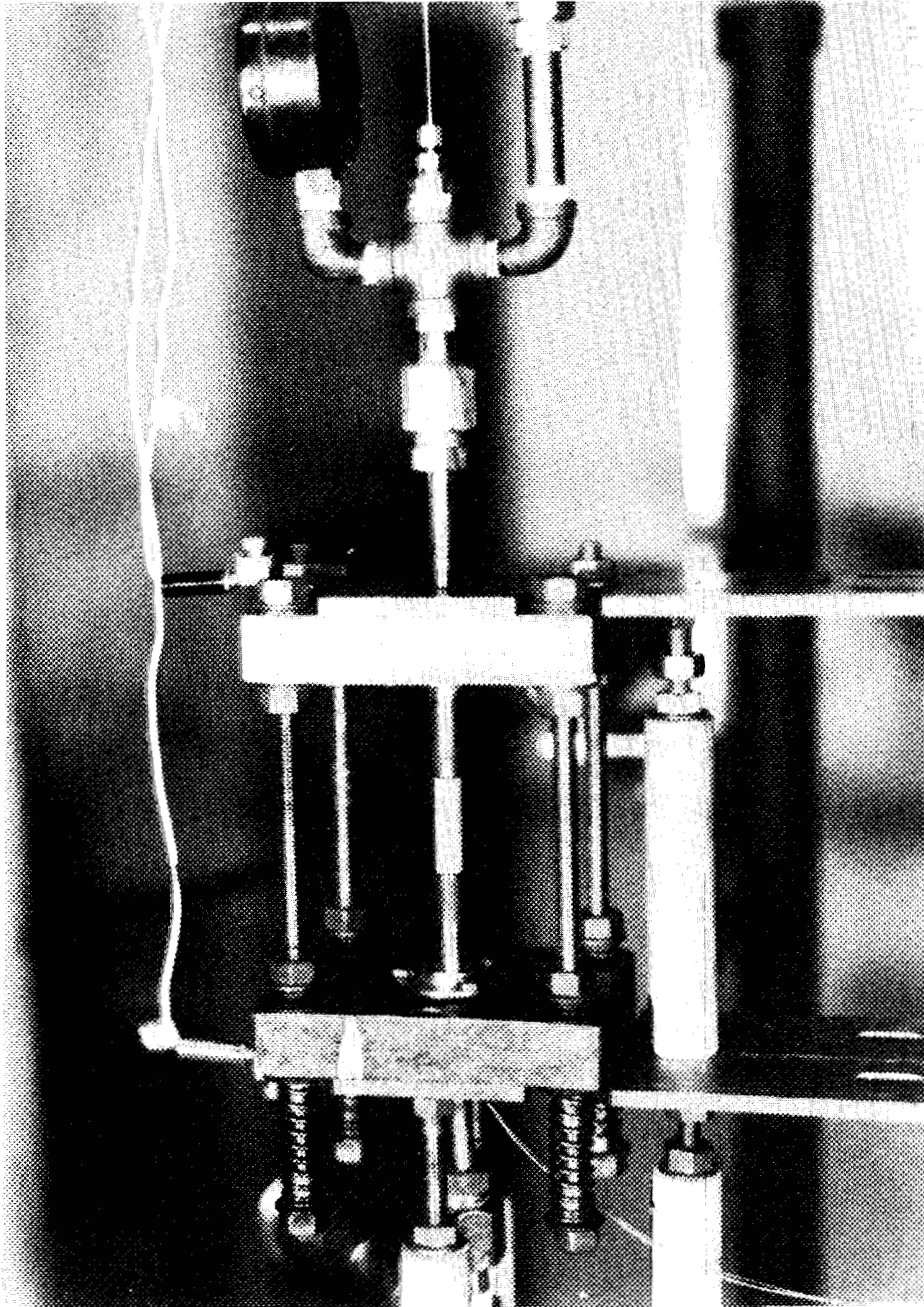


Figure 7

Photograph of the Mounted Tungsten Cylinder Without  
Marinite Insulation and Instrumentation

pier was bolted to the other face of each bus block. The faces of the blocks onto which the piers were bolted face toward the tungsten cylinder and are known as the inside faces of the bus blocks. The I.D. of the piers was  $1/8$  in.

There was a groove in the end of each pier that held a graphite washer. The hollow porous tungsten cylinder rested on the graphite washers. Access to the interior of the tungsten cylinder was through the  $1/8$  in. diameter hole running through the high pressure fitting, the bus block, and the pier. See Figure 7.

The direct current used to heat the tungsten cylinder flowed from the rectifier through the circuit consisting of the copper bus bars, the copper bus block, the stainless steel pier, the graphite washer, the tungsten cylinder, and then back to the rectifier through the other washer, pier, block and bus bars.

The mechanical connection between the two bus blocks was provided by four  $3/8$  by 16 stainless steel studs, each 10 in. long. These studs passed through four matching  $1/2$  in. diameter holes in the four corners of each bus block. These studs were electrically isolated from the bus blocks by means of Mycarta sleeves and washers. A Mycarta sleeve  $1-3/32$  in. long,  $1/2$  in. O.D. and  $3/8$  in. I.D. was placed in each of the four holes in both bus blocks. Each sleeve protruded from either side of the bus block by from  $1/16$  to  $1/32$  in. Mycarta washers,  $1/16$  in. thick,  $1-1/8$  in. O.D. and  $1/2$  in. I.D. were placed on the bus block, around the portion of the Mycarta sleeve that protruded from the surface of the bus block. The insulating Mycarta washers were held in place by steel washers  $5/64$  in. thick,  $7/8$  in. O.D. and  $25/64$  in. I.D. Steel nuts

surmounting the steel washers were used to form a rigid connection between the four stainless steel studs and the upper bus block.

The stainless steel studs were not connected rigidly to the lower bus block. Through a system of compression springs provision was made for small relative movements of the two bus blocks parallel to the common axis of the stainless steel studs. The compression springs were formed from steel wire 0.080 in. in diameter with an axial length of  $2\text{-}\frac{3}{16}$  in. and with an I.D. of  $\frac{1}{2}$  in. Steel washers were modified by the addition of collars  $\frac{1}{2}$  in. O.D. and  $\frac{7}{16}$  in. I.D. These collars were brazed to the steel washers. The compression spring was positioned on the stud with the collar of a collared washer inserted into each end of the spring. This assembly formed the interface between the lower Mycarta washer and the steel nut. See Figure 8. The springs provide the pressure used to hold the tungsten cylinder in place. Since the mounting was spring loaded, it allowed for thermal expansion of the tungsten cylinder and other parts under essentially constant load.

Since there was no rigid connection between the studs and the lower bus block a lightly loaded spring system was used to keep the Mycarta washers in place on top of the lower bus block. These Mycarta hold-down springs were formed from  $\frac{3}{64}$  in. stock, and were  $\frac{5}{16}$  in. long with an I.D. of  $\frac{19}{32}$  in. Additional collared washers were prepared by brazing a collar onto regular steel washers. The collar was  $\frac{19}{32}$  in. O.D.,  $\frac{25}{64}$  in. I.D. and  $\frac{1}{8}$  in. long. The collars with the hold-down springs were positioned on the studs above the lower bus block as shown in Figure 8.

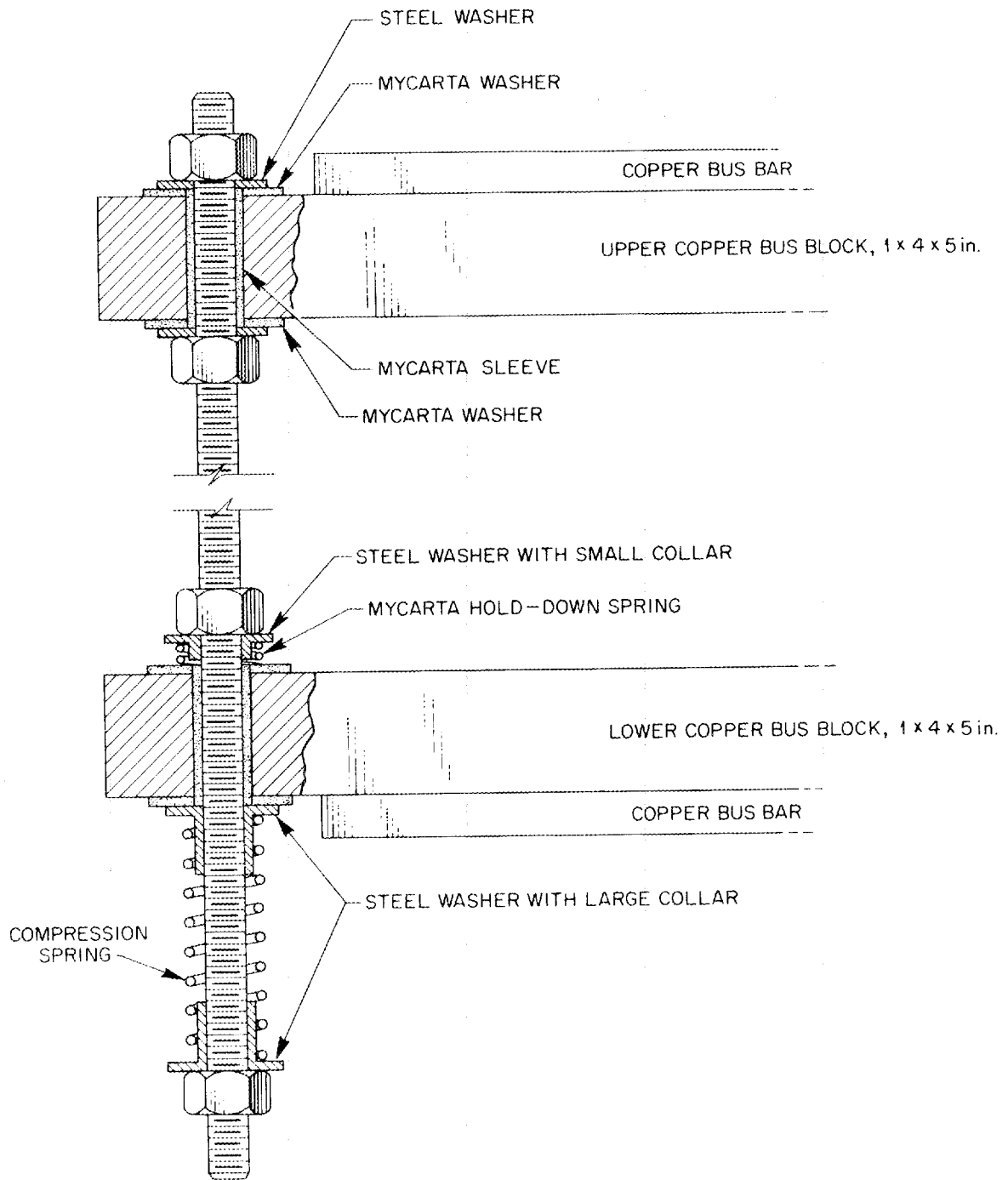


Figure 8

Insulated Studs Connecting the Bus Blocks

Figure 9 shows the stainless steel piers that were used to hold the tungsten cylinder during operation. A neoprene O-ring  $11/32$  in. O.D.,  $13/64$  in. I.D. and  $.070$  in. thick was seated in a spotface at the base of the pier to provide the gas seal between the pier and the bus block. The spotface was created using an  $11/32$  in. drill to a wall depth of  $.012$  in. The lowest step on the pier was  $1-3/4$  in. in diameter,  $1/16$  in. thick, and contained three holes that were used to bolt the stainless steel piers to the bus block by means of three  $5/32 \times 32$  bolts each  $5/16$  in. long. The three holes in this step of the pier were  $11/64$  in. in diameter on a  $1-1/2$  in. bolt circle. The next step of the pier was  $1$  in. in diameter and  $3/16$  in. thick. This step served as the base for the Marinite insulating disks. The major portion of the pier was  $1/2$  in. in diameter and  $1-1/2$  in. long. A  $1/8$  in. diameter hole was drilled through the length of each pier. The top of the pier contained a trench that was used as a seat for the graphite washer. The trench was approximately  $0.264$  in. I.D.,  $0.438$  in. O.D. and  $1/16$  in. deep. The outer wall of the trench was  $1/32$  in. lower than the inner wall. Four thermocouple wells  $1/16$  in. in diameter were drilled along the cylinder axis.

The graphite washers were prepared from Number 2 Graphitar by drilling a  $17/64$  in. ( $\approx 0.265$  in.) hole in a quantity of stock which was then turned to  $0.425$  in. O.D. Washers were cut off from this stock with a thickness of approximately  $1/16$  in. and they were subsequently ground to thickness of from  $0.035$  in. to  $0.060$  in. as needed. Figure 9 shows these washers in position in the trench at the end of the stainless steel pier.

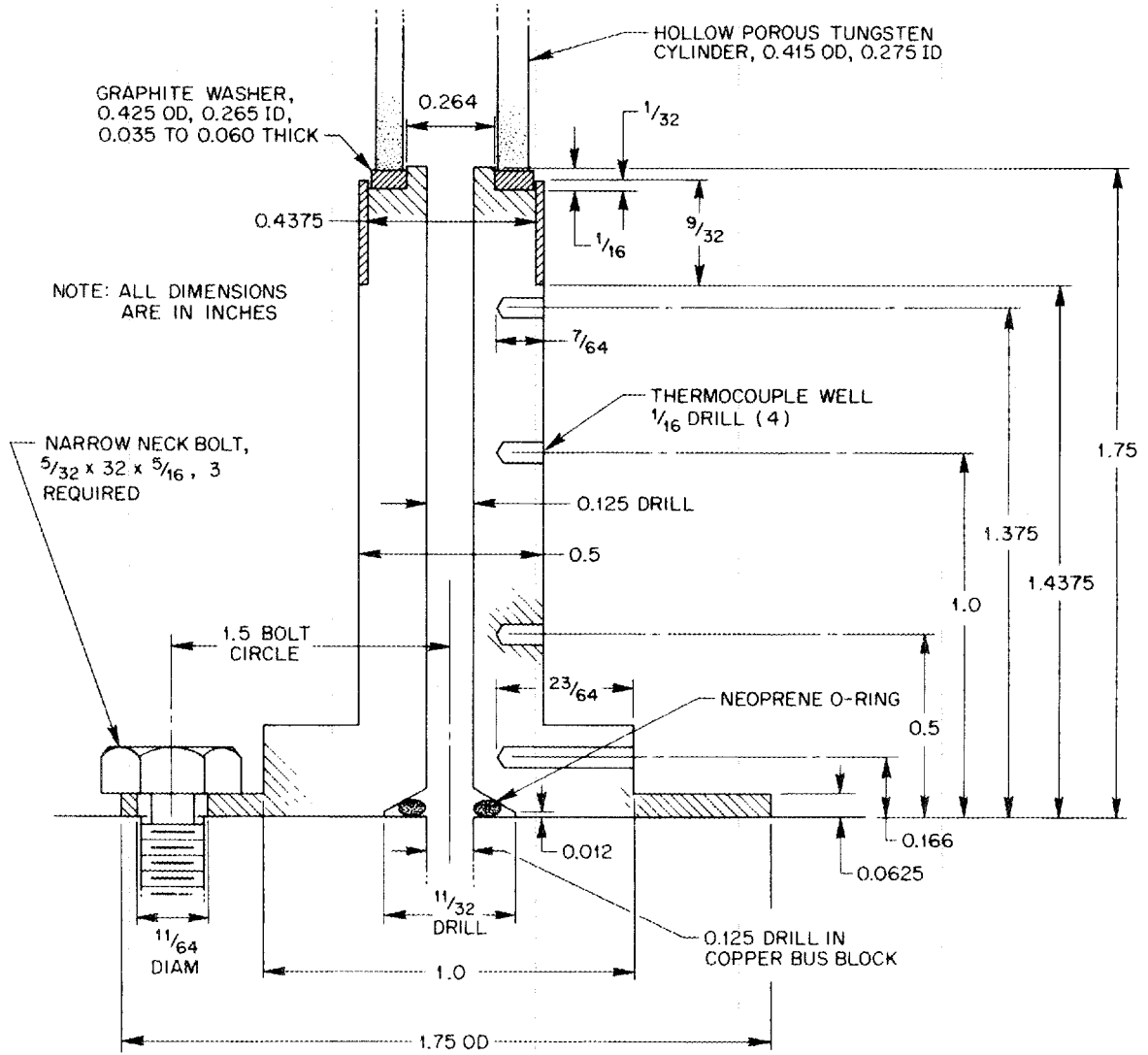


Figure 9

Stainless Steel Pier and Graphite Washer

The weight of the bus blocks is supported by two 1 in. O.D. wooden dowels which rest on the floor and support the lower bus block. The weight of the upper bus bars is supported by a short 1 in. O.D. wooden dowel located between the upper and lower bus bars approximately one-third of the distance from the rectifier terminals to the bus blocks.

Figure 7 shows the tungsten cylinder mounted between the stainless steel piers but without the insulating Marinite disks or various instruments in position. In addition to the two dowels that support the bus blocks, two other dowels may be seen in Figure 7. A wooden dowel below the lower bus bar and the short wooden dowel between the upper and lower bus bars are only used to raise the upper bus bar and bus block during the positioning of the tungsten cylinder. These two dowels are removed during operation of the experimental apparatus. This may be seen by comparing Figure 7 with Figure 6 or with Figure 10.

Figure 10 shows the assembly of the tungsten cylinder with the insulating Marinite disks in position. The Marinite disks are 1-3/4 in. O.D. and 1/2 in. I.D. There are ten disks which are numbered 1 through 10 counting from the bottom up. Disks 1 through 3 and 8 through 10 are each 1/2 in. thick. These disks enclose the lower and upper stainless steel piers. Disks 4 through 7 are each 3/8 in. thick. These disks enclose the tungsten cylinder.

The Marinite disks function in several capacities. They provide thermal insulation around the tungsten cylinder. They keep a blanket of the coolant gas around the tungsten cylinder during operation thereby keeping atmospheric oxygen away from the hot tungsten surface. They provide the mounting to hold the stainless steel hypodermic needles that

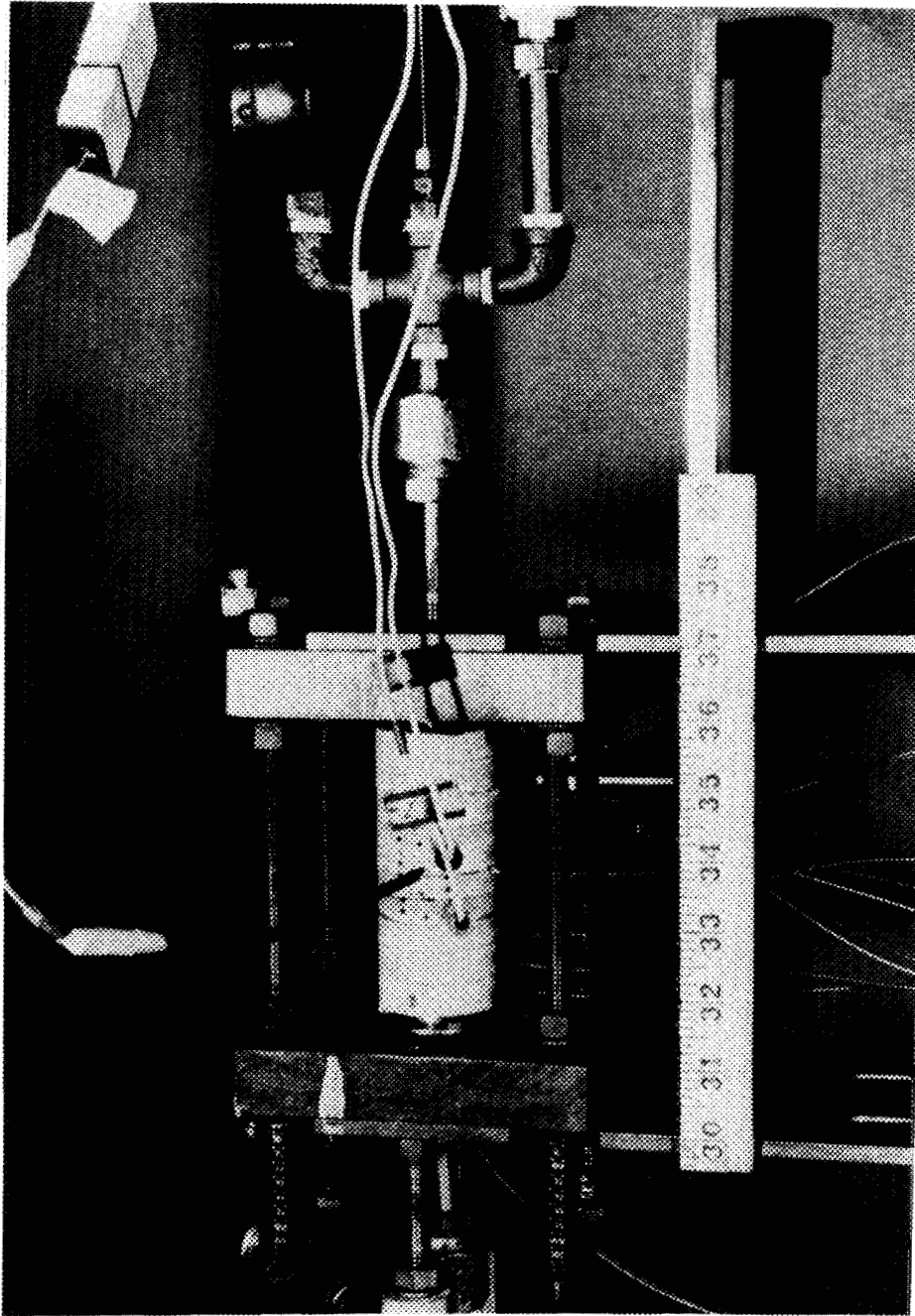


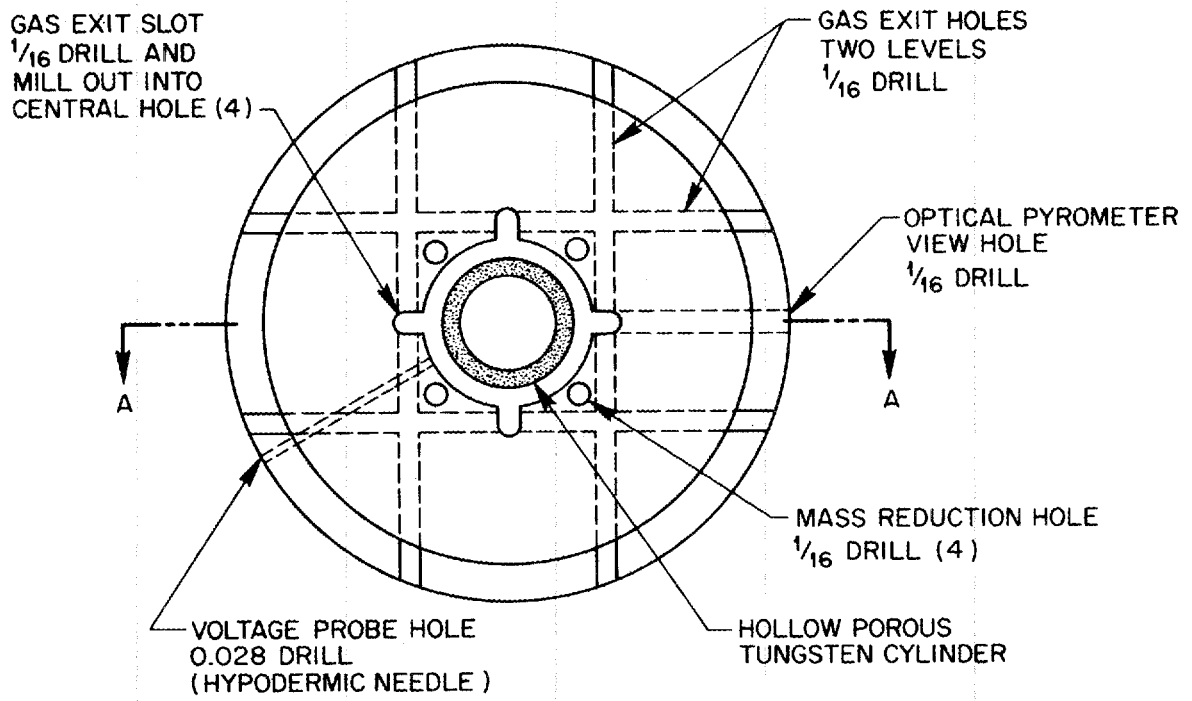
Figure 10

Photograph of the Mounted Tungsten Cylinder with Marinite  
Insulation and Instrumentation

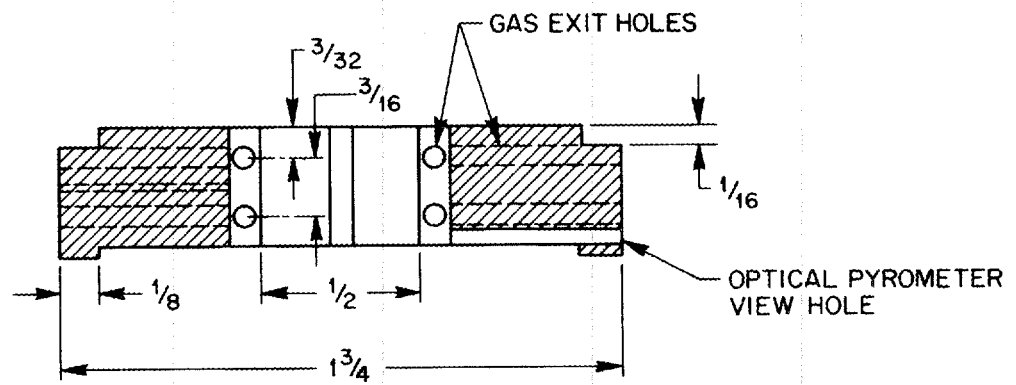
serve to measure the voltage drop across the length of the tungsten cylinder. They provide the mounting to hold the stainless steel sheathed thermocouple number 16 in position against the exterior of the tungsten cylinder.

There are a number of small holes in the disks which serve a variety of purposes. There are  $1/16$  in. diameter holes in disks 1, 2, 3, and 8 which allow thermocouples 2, 3, 4, and 5 to pass through the Marinite disks and be inserted in the  $1/16$  in. diameter thermocouple wells in the stainless steel piers. There are two 0.028 in. diameter holes in Marinite disks 4 and 7 for the stainless steel hypodermic needles and a  $1/16$  in. diameter hole in disk 6 for the stainless steel sheathed thermocouple number 16. Disks 4, 5, 6, and 7 have a series of  $1/16$  in. diameter holes drilled through them in the plane of the disk. These holes are drilled at angles such that they prevent direct radiative heat loss from the tungsten cylinder to the surrounding room. The holes allow the effluent coolant gas to leave the region around the tungsten cylinder. See Figure 11.

There are five  $1/16$  in. diameter holes in disks 4, 5, 6, and 7 (two in disk 7) drilled radially in the plane of the disk. These holes afford the means of observing the surface of the tungsten cylinder with an optical pyrometer. See Figure 12. There are holes in disk number 5 where thermocouples 6 and 7 are positioned at two different radii within the Marinite disk.



TOP VIEW



SECTION A-A

Figure 11

Marinite Insulating Disks

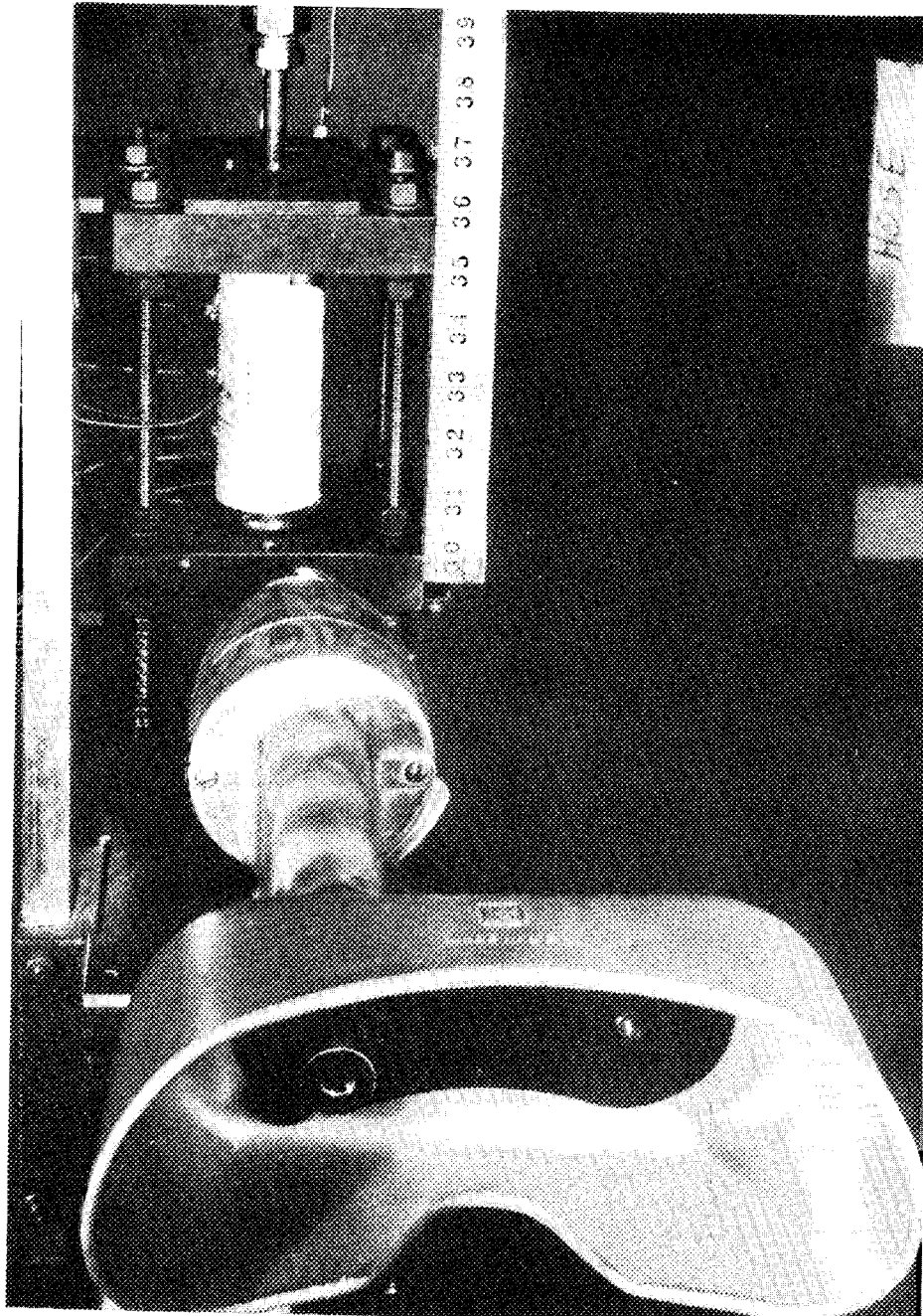


Figure 12

Photograph of the Assembled and Instrumented Tungsten Cylinder  
Showing the Optical Pyrometer in Position for Viewing

### Gas System

The gas used to cool the tungsten cylinder was either high purity nitrogen or helium. The pressure of the gas was regulated and provision was made for measuring the pressure, flow, and temperature of the gas. A pressure sensing switch was included in the system to shut off the electric power to the apparatus in the event of a loss of pressure in the gas system. The layout of the gas system is shown schematically in Figure 13.

Gas was supplied from commercial 2000 lb./sq.in. compressed gas cylinders. From the cylinder the gas passed through a pressure regulator where the gas pressure was reduced to approximately 15 lb./sq.in. gauge. After passing through two control valves, the gas passed through two rotameters in series and from there into the interior of the hollow tungsten cylinder via the high-pressure fitting on the lower bus block.

The connections between the various components of the gas system were made by high-pressure air hose coupled by means of quick-disconnect fittings. Gas pressures were measured by means of Bourdon type pressure gauges on the gas cylinder pressure regulator, a pressure gauge on the output of the first rotameter, and a pressure gauge connected to the hollow tungsten cylinder at the high-pressure fitting on the upper bus block. For precision pressure measurement up to approximately 80 cm. of mercury above atmospheric pressure, a mercury manometer was connected through a valve to the output from the second rotameter. A Mercoid pressure controlled switch was connected to the high-pressure fitting on the upper bus block. The function of this Mercoid switch was to turn off the rectifier power in the event gas pressure was lost within

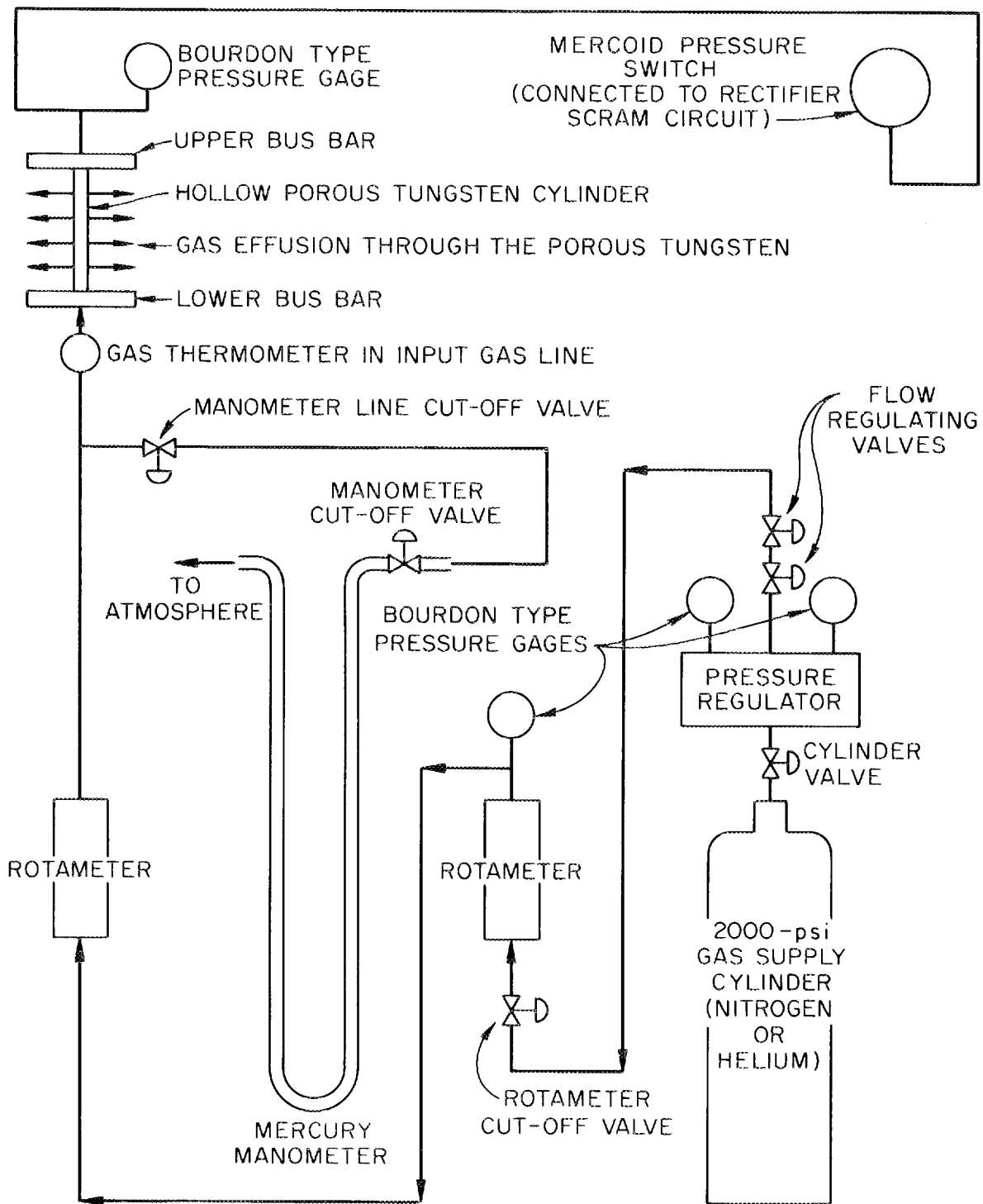


Figure 13

Gas System-Schematic Diagram

the hollow porous tungsten cylinder during an experimental run.

Several components of the gas system can be seen in Figure 14. The gas lines and other parts of the gas system can be seen in Figure 6.

Gas temperature was measured by means of a gas thermometer in the gas inlet line at a point just before the gas entered the lower bus block. See Figure 6. Calibration of the two rotameters used to measure the gas flow was done by means of a wet test meter.

The integrity of the gas system was verified periodically by replacing the hollow porous tungsten cylinder with a hollow cylinder of solid brass and by replacing the graphitar washers with neoprene O-rings. Gas was introduced into the now closed system at a pressure in excess of that used in actual operation. The system was then isolated from the gas supply and observed for pressure loss over a period of several minutes. The absence of pressure loss during this period verified the integrity of the gas system for the purposes of this study.

#### Instrumentation

A number of instruments were used to measure parameters of the experimental system. Temperatures were measured by means of thermocouples, thermometers and an optical pyrometer. Two potentiometers were used to measure the thermocouple voltages and the voltage drop across portions of the direct current heating circuit. Measurements of the gas flow were made by means of rotameters, pressure gauges, and a mercury manometer. Other instruments were used during assembly of the experimental apparatus in preparation for runs and to monitor the operation of the rectifier.

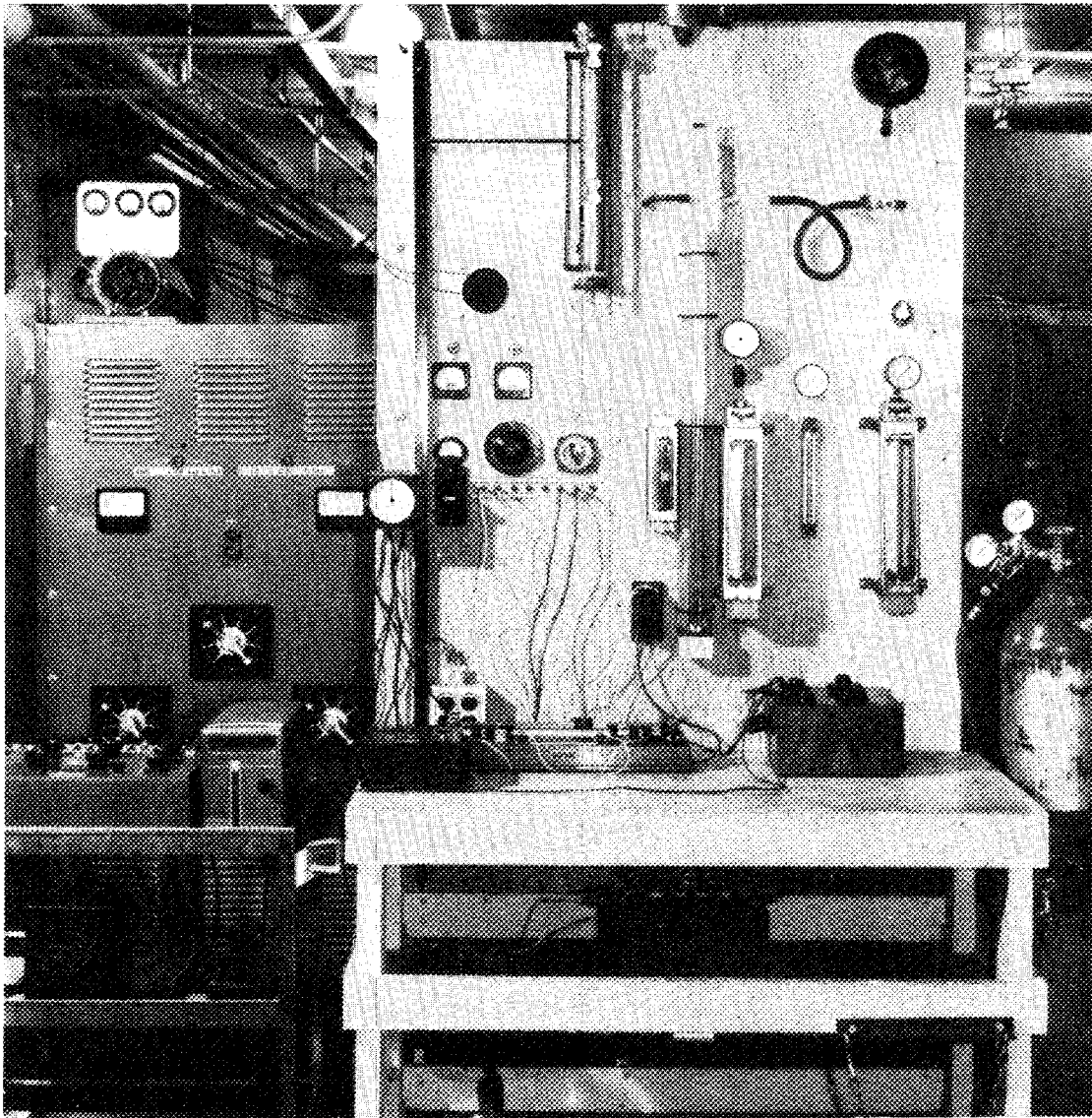


Figure 14

Photograph of the Controls and Instrumentation of the  
Experimental Apparatus

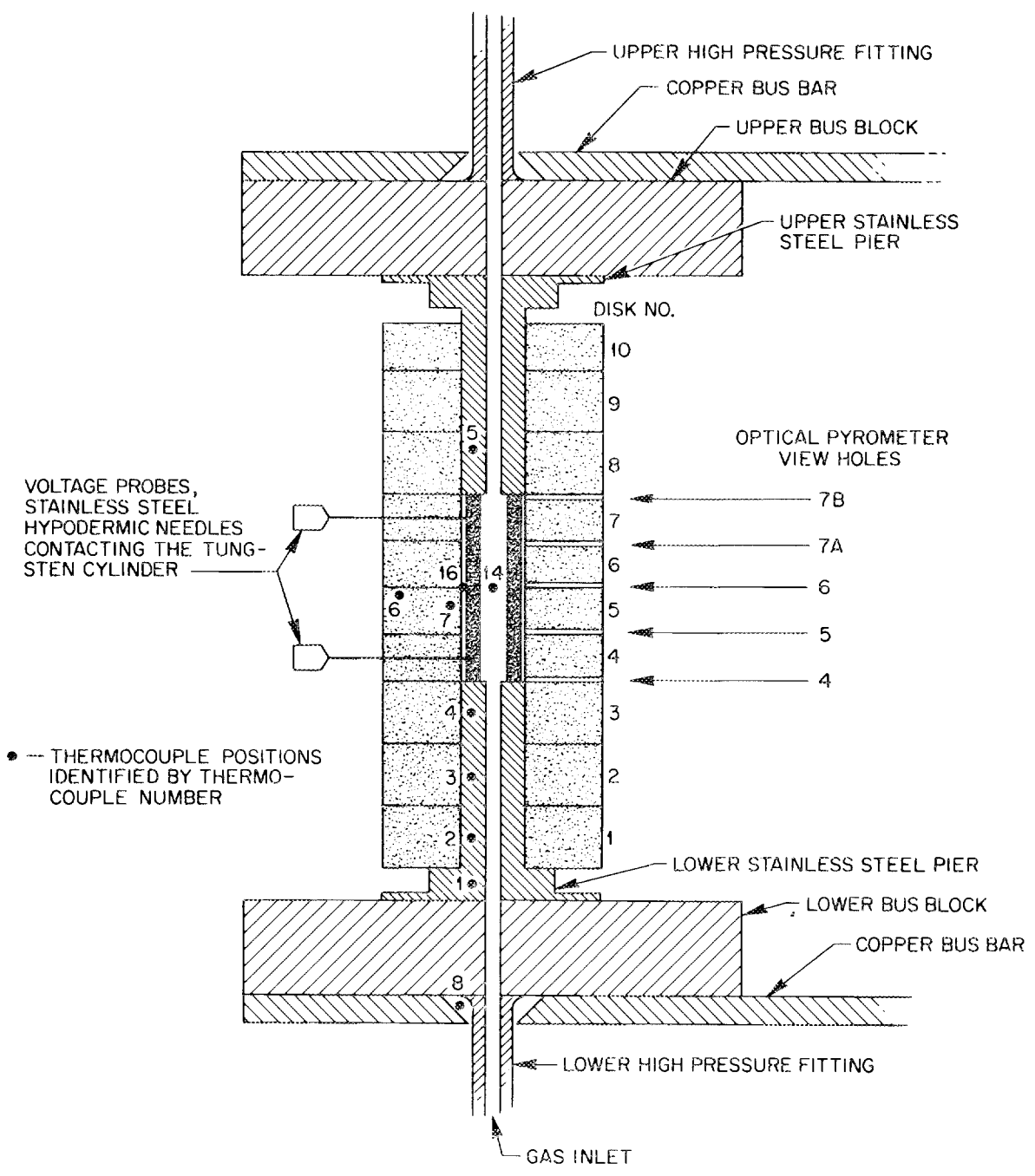
### Thermometers and Thermocouples

Temperatures were measured at several locations within the experimental apparatus. The temperature of the coolant fluid was measured by an immersion thermometer in the gas inlet line just below the lower bus block. See Figures 6 and 13. Chrome-alumel thermocouples with an ice-water reference junction were used to measure temperatures at 11 points within the apparatus. Temperatures were measured at the points designated in Figure 15 as 1 through 8, 14, and 16.

Two potentiometers were used to measure the voltage produced in the thermocouples. A portable, laboratory type potentiometer with self contained batteries, standard cell, and galvanometer was used for rough measurements, and for measurements when the temperature of the system was changing rapidly. When the system was close to dynamic equilibrium a Leeds and Northrup K-3 precision potentiometer was used in conjunction with a Leeds and Northrup ballistic galvanometer for more precise measurements. An external standard cell was used for the calibration of the K-3 potentiometer and an external 2-volt storage battery was used to provide the bridge power supply. A double pole, double throw switch enabled either potentiometer to be connected to the output of a 20 position thermocouple selector switch.

### Optical Pyrometer and Cathetometer

Measurements of the surface temperature of the tungsten cylinder were taken with a Leeds and Northrup potentiometer type optical pyrometer, model number 8621-C. This optical pyrometer was attached to the telescope mount of a cathetometer by means of an especially designed mount. The optical pyrometer mounted on the cathetometer is shown in



THERMOCOUPLES 1-8 ARE BARE CHROME-ALUMEL  
THERMOCOUPLES 14 AND 16 ARE STAINLESS STEEL SHEATHED CHROME-ALUMEL  
THERMOCOUPLE 14 ENTERS THROUGH THE UPPER HIGH PRESSURE FITTING

Figure 15

Schematic of the Mounted and Instrumented Tungsten Cylinder

Figure 6. The lens of the optical pyrometer was 11 in. from the surface of the porous tungsten cylinder. The surface of the tungsten cylinder was observed through five radial holes in the Marinite disks that enclosed the tungsten cylinder. See Figures 11 and 12. These holes were  $1/16$  in. in diameter and  $5/8$  in. long. The relative vertical position of the optical pyrometer at each of the five observation holes was measured in hundredths of cm. from the cathetometer scale. These temperature and position measurements, in conjunction with the relative vertical position of the lower end of the tungsten cylinder, described the tungsten cylinder surface temperature distribution along the cylinder axis.

#### Voltage and Amperage Probes

The ohmic power generation in the tungsten cylinder was determined by measuring the direct current flowing through the tungsten cylinder and the voltage drop over a known fraction of the cylinder length. The two potentiometers used for thermocouple voltage measurements were also used to measure the current flow and voltage drop in the tungsten cylinder. Amperage was determined by measuring the voltage drop across the ammeter shunt provided within the rectifier. The shunt factor of the ammeter was 120. amperes/millivolt.

The voltage drop along the tungsten cylinder was measured using two hypodermic needles as probes. The needles were stainless steel, size B-D 22, which had an O.D. of 0.028 in. The original 2 in. length of the needles was cut down to  $7/8$  in. which also served to blunt the needles. These probes passed through two radial holes in the Marinite disks that had been drilled with a number 70 drill (0.028 in. O.D.).

These holes were in disks 4 and 7. See Figures 10, 11, and 15. The needles touched the tungsten cylinder at two points approximately 1.1 in. apart. This generally represented approximately  $3/4$  of the total cylinder length. The precise separation of the two visible contact points on the tungsten cylinder was measured following a run.

The ohmic power generation in the region of the cylinder between the probes was calculated directly from the current and probe voltage drop. Through the use of other data the ohmic power generation in the entire tungsten cylinder was calculated. A linear extrapolation of the power generation between the probes to that of the entire cylinder was a good first estimate of the total power generation.

#### Other Instrumentation

A Leeds and Northrup Kelvin Bridge, model 4340, that measured resistances on the order of 100 microhms was used to measure the resistance between the two bus blocks measured through the tungsten cylinder and graphite washers. The Kelvin Bridge is shown in Figure 14. These measurements were made during the mounting of a tungsten cylinder in preparation for a run and provided a useful means of determining empirically when the tungsten cylinder and graphite washers were in uniform and stable contact with the piers. Figure 7 shows the tungsten cylinder mounted on graphite washers between the stainless steel piers. The two leads from the Kelvin Bridge are connected to terminals on the upper and lower bus blocks. For a run the leads from the Kelvin bridge are disconnected from the bus block terminals as may be seen in Figure 10. Power for the Kelvin Bridge was supplied by a 12-volt storage battery.

The Kelvin Bridge was not used during runs when the rectifier was in operation.

The portable, laboratory type potentiometer was used in conjunction with the Kelvin Bridge to measure resistance in the circuit formed by the bus blocks, piers, washers, and the tungsten cylinder. Use of the Kelvin Bridge was necessary because the resistance of the circuit made up of the tungsten and graphite was too small to be measured by an ordinary vacuum tube volt-ohm-milliammeter by a factor of from 100 to 1000.

#### Experimental Procedure

The experimental procedure is described below.

1. Prior to the start of a run the ends of the tungsten cylinder were ground flat and perpendicular to the axis of the cylinder, as needed, in order to remove any rough spots that may have resulted from thermal stresses during the shutdown from the previous run. The dimensions of the cylinder were measured and the cylinder was weighted. The flat faces of the graphite washers were ground in order to achieve smoothness as well as to obtain the desired washer thickness.

2. The tungsten cylinder was assembled in the apparatus and an acceptable contact resistance was established using empirical measurements with the Kelvin bridge as a guide.

3. When the tungsten cylinder had been mounted in a configuration which afforded a good probability for a successful run, the final instrumentation was installed on the tungsten cylinder. This included putting into place Marinite insulators, thermocouples, voltage probes, internal and external sheathed thermocouples, and the Marinite disk hold-down springs.

4. The gas flow was started through the cylinder. If no gas leak developed at the ends of the cylinder, electric heating of the cylinder was begun. The heating of the cylinder was allowed to proceed slowly until a heat generation rate and gas flow rate were reached at which measurements of the system were to be made.

5. With the system at or near dynamic equilibrium, measurements were made of those variables necessary to evaluate the heat transfer coefficient. In the event that an adequate approach to equilibrium could not be obtained, due to contact resistance problems, it was then necessary to shut off the electric power, cool the system with the coolant gas, and begin again at step 1 or step 2.

6. When sufficient measurements had been made at one electric power level and gas flow rate the system could be shifted to another equilibrium condition by altering either the electric power level, or the gas flow rate, or both. When the new equilibrium had been obtained, measurements could be resumed at step 5.

7. When the measurements had been finished the system was shut down by turning off the electric power and letting the gas flow until the cylinder temperature had been reduced to near room temperature.

## DISCUSSION OF RESULTS

Experimental Developments

The major difficulty in developing the experimental apparatus which was used in the study by Farber (10) and in this work was obtaining and maintaining uniform mechanical and electrical contact between the porous tungsten cylinder and its mounting. Mechanical contact was needed to obtain a gas seal between the tungsten cylinder and the stainless steel piers. Electrical contact was needed in order to maintain the heat generation within the tungsten cylinder.

Early attempts at mounting the tungsten cylinder between the copper bus blocks using stainless steel disks (approximately 1/4 in. thick) demonstrated a number of problems. The tungsten cylinder tended to weld to the stainless steel. The electrical metal to metal contact resistance was very unpredictable. Gas leakage occurred at the metal to metal interfaces. A significant axial temperature gradient indicated that there was an appreciable heat loss from the cylinder into the stainless disks and the copper bus blocks. The consideration of the axial heat flux introduced a significant increase in the complexity of the analysis needed to evaluate the heat transfer coefficients. While it was not possible to entirely eliminate the consideration of the axial heat flux it was desirable to reduce this effect as much as possible.

All of the preceding problems were alleviated to the degree necessary to obtain successful operation of the experimental apparatus by the introduction of graphite washers between the tungsten cylinder and the stainless steel mounts. The stainless steel mounts were modified from disks to piers and a washer seat was cut in the end of the pier

which served to position the graphite washer. The outer lip of the washer seat was lower than the upper surface of the graphite washer when the washer was in place in the pier. This prevented contact and therefore welding between the tungsten cylinder and the pier along the outside wall of the tungsten cylinder. No major welding problems developed between the interior lip of the graphite washer groove and the inside wall of the tungsten cylinder even though this lip protruded above the upper surface of the graphite washer by approximately 0.015 in.

The relatively soft washer reduced the unpredictability in the contact resistance, and essentially eliminated gas loss at the ends of the cylinder. This was verified by replacing the hollow porous tungsten cylinder with a hollow solid brass cylinder of the same dimensions. The brass cylinder was mounted between the piers using the graphite washers to provide the seal between the cylinder and the piers. The gas system was pressurized to a value above that found within the tungsten cylinder during experimental runs. The gas system was closed and found to show no pressure loss for a test period of several minutes.

The washers also provided a high electrical resistance and therefore served as a heat source at the ends of the tungsten cylinder. This served to flatten the axial temperature gradient by reducing heat loss from the tungsten into the piers. Even with the use of the graphite washers the remaining unpredictability of the contact resistance resulted in significant axial temperature gradients. During the experimental runs the axial heat flux into the ends of the tungsten cylinder ranged from 7 to 108 percent of the heat generated within the cylinder by electric heating.

Since the experimental apparatus was described by third order differential equations the determination of the heat transfer coefficient in the porous tungsten required the evaluation of a total of five boundary conditions. These five boundary conditions allowed evaluation of the five unknown coefficients. These coefficients were the three coefficients of integration of the differential equation, the heat transfer coefficient and the conduction correction factor for thermal and electrical conduction.

## Boundary Conditions and Method of Solution

### First Boundary Condition

In measuring the first boundary condition radial symmetry was assumed for the tungsten cylinder which resulted in no consideration of  $y$  dimensional parameter variation for the flat plate model of the hollow cylinder. The flat plate model was considered to be limited in the  $y$  dimension by adiabatic walls.

The axial surface temperature variation was observed with an optical pyrometer through five 1/16 in. diameter holes in the enclosing Marinite disks. These temperature-position pairs were analyzed to obtain the coefficients of a truncated Fourier series (five terms) that provided a description of the  $z$  dimensional temperature variation. The optical pyrometer holes in the Marinite disks were assumed not to perturb the assumption of radial symmetry. It was also assumed that the small radiation loss from these holes allowed them to be treated as viewing holes for a black body. While this assumption would be strictly true only in the case of a body which has unitary emissivity or from which there was no net heat transfer to the walls of its enclosure, it was believed that the radiative shielding of the Marinite disks, the roughness of the porous tungsten surface, and in particular the slight oxide or nitride coating on the tungsten surface would all combine to justify the assumption of unitary emissivity.

Tables of correction factors for optical pyrometric temperature measurements show that in the temperature range of 800°C to 1000°C the error in the temperature measured is from 5°C to 8°C for a spectral emissivity of 0.9 and from 19°C to 27°C for a spectral emissivity of 0.7.

All radiation considered in this study was assumed to be gray body radiation.

The observations of the outside wall of the tungsten cylinder gave the solid phase temperature as a function of  $z$  position and provided one boundary condition,  $T(z)|_{x=l}$ .

Second Boundary Condition

A network of holes were drilled in Marinite disks number 4 through 7 which surrounded the tungsten cylinder in order to provide an exit for the coolant gas which was emerging from the outer surface of the tungsten cylinder. Thus there was no axial gas flow along the outside wall of the tungsten cylinder and convective heat loss from the cylinder was neglected. In order to evaluate the radiative heat loss from the tungsten to the Marinite, a second series of Fourier coefficients were developed which described the z dimension variation of  $(T^{\circ}R)^4$ . These coefficients were needed in order to obtain a mean value of  $(T^{\circ}R)^4$  that was needed to evaluate the radiative heat transfer. The mean of  $(T^{\circ}R)^4$  is not necessarily equal to the fourth power of the mean of  $T^{\circ}R$ .

The inside wall temperature of the Marinite was determined indirectly by measuring the temperature at other points in the Marinite disks and solving a heat balance involving the heat flow radially outward through the Marinite disks. Thermocouple number 7 was located in a 1/16 in. diameter vertical hole in Marinite disk number 5. This was one of four holes which were drilled in each of the four central disks to reduce the mass of the Marinite disks and improve their insulating properties. The hole containing thermocouple number 7 was separated from the inside wall of the Marinite disk by less than 1/16 in. of Marinite. Thermocouple number 6 was located near the outer edge of Marinite disk number 5.

The heat flow through the Marinite and the inside wall temperature of the Marinite disk was evaluated by two methods. The first method was to solve a conduction heat balance using the temperatures of thermocouples 6 and 7 which were imbedded in the Marinite disk. This was the

simpler method but some mechanical deterioration of the Marinite disks resulted in cracking of the thin web between the inside wall of the Marinite disk and the hole containing thermocouple number 7. This thermocouple was then exposed to some direct radiation from the tungsten cylinder as well as to some of the effluent coolant gas from the tungsten cylinder.

In order to avoid the possible inaccuracies which could result from the exposure of thermocouple number 7 to this variety of temperature sources, a combined radiation and conduction heat balance was solved using the temperature of the tungsten cylinder, the thermal conductivity of the Marinite disks and the temperature at thermocouple number 6 in the Marinite disk. This resulted in a quartic equation which when solved provided the inside wall temperature of the Marinite disk. The radiative heat loss from the tungsten surface could now be evaluated.

Since there was only one pair of thermocouples imbedded in the Marinite disks, the values obtained for the inside wall temperature of the Marinite at the axial position corresponding to the imbedded thermocouples was taken to be the mean temperature for the entire inside wall of the Marinite disks. No axial heat flux in the Marinite was considered. This was probably a good estimate because thermocouple number 6 was located axially near the center of the tungsten cylinder. Also any axial temperature gradient in the Marinite would tend to be flattened by the heating of disks number 3 and 8 due to the heat these two disks received from the region at the tops of each of the stainless steel piers. The graphite washers produced a heat source in this region of the pier which served to reduce conduction heat loss from the tungsten cylinder. This heat was transferred to disks number 3 and 8 which were at the ends of

the four disks which actually enclosed the tungsten cylinder.

Since the heat loss from the tungsten surface to the enclosing Marinite disks could now be calculated, the second boundary condition,  $dT/dx(z)|_{x=l}$ , could now be evaluated.

#### Third Boundary Condition

The third boundary condition was the temperature of the fluid at the point of entry into the porous wall from inside the hollow cylinder,  $t(z)|_{x=0}$ . No z axis variation in the inlet fluid temperature was considered. This temperature corresponded to the use of a single constant term in a Fourier series. It was considered necessary to take into account the heat absorbed by the gas from the time it entered the lower bus block at essentially room temperature until it entered the inside wall of the porous tungsten cylinder.

The passage of the gas into the interior of the hollow cylinder involved two preheating phases. The first occurred as the gas passed up through the relatively cool bus block into the lower pier. One end of the pier was at a temperature comparable to that of the tungsten. The thermocouple wells in the lower pier provided a temperature profile along the entry path of the gas. The temperature of the pier at the end of the pier where the gas left was estimated to be equal to the temperature of the lower end of the tungsten cylinder. This assumption was made in spite of the fact that the graphite washer in the end of the pier probably produced a hot spot in this region but the tungsten end temperature was the only value available.

The calculations for the preheating of the gas were based on the assumption that laminar flow had been established in the 1/8 in.

diameter gas inlet passage in which the Reynolds number was on the order of  $10^{-1}$ . Equations cited by McAdams (24) were used to estimate the value of the heat transfer coefficient in the 1/8 in. entry passage. A series of preheating calculations were carried out assuming a linear variation of the temperature in the bus block and the pier between each of the thermocouple wells. The gas preheating in the pier for nitrogen was found to be from 120 to 230 degrees F. The pier preheating for Helium was from 360 to 740 degrees F.

The other gas preheating consideration was the assumption that after the incoming gas left the pier it would absorb all of the heat transferred to the sheathed stainless steel thermocouple number 14 by radiation from the inside wall of the tungsten cylinder. This was considered the most reasonable assumption since the nature of the flow over this thermocouple was not well known. While the axial flow of the gas entering the cylinder and absorbing heat from the inside cylinder wall and the coaxial sheathed thermocouple could conceivably produce an axial gas temperature profile, this factor was neglected. Since axial flow effects were neglected no consideration was given to any heat loss from the inside wall of the tungsten cylinder directly into the incoming gas. The error analysis at a later point in this work will show that these assumptions are justified.

#### Fourth Boundary Condition

The fourth boundary condition was the temperature gradient in the tungsten at the inside wall of the tungsten cylinder,  $dT/dx(z)|_{x=0}$ . The temperature gradient was evaluated by two methods. The first method was to solve a radiative heat balance between the inside wall of the

tungsten cylinder and the stainless steel sheathed thermocouple number 14. This method required an estimate of the temperature of the inside wall of the tungsten cylinder.

It was found that the tungsten cylinder wall temperature profile was very flat and that the inside wall temperature was within a few degrees of the outside wall temperature at any given position along the cylinder axis. Accordingly the z axis temperature profile at the inside wall of the tungsten cylinder was taken to be the same as that of the outside wall.

Estimates of the radiative transfer from the tungsten wall to the coaxial thermocouple were complicated by the fact that the thermocouple sheath extended into the interior of the tungsten cylinder for only about half of the length of the tungsten cylinder. This problem was circumvented by assuming a pseudo thermocouple in the form of a coaxial cylinder that extended the entire length of the tungsten cylinder. This pseudo thermocouple had the same surface area as the portion of the real thermocouple inside the tungsten cylinder, and the pseudo thermocouple had a correspondingly smaller radius.

The mean of  $(T^{\circ}R)^4$  at the inside wall of the tungsten cylinder was used in the radiative heat transfer calculations. The entire length of the pseudo thermocouple was assumed to be at the temperature of thermocouple number 14. From the rough, oxidized, and blackened condition of the sheathed thermocouple its emissivity was estimated to be 0.95 and unitary emissivity was again assumed for the tungsten.

The second method for evaluating the temperature gradient at the inside wall of the tungsten cylinder was to remove the sheathed thermocouple number 14. This created a radiative black box inside the tungsten

cylinder in which the net temperature gradient at the inside wall of the tungsten cylinder would be zero. However, since there was generally an axial temperature gradient along the outside wall of the tungsten cylinder, and since this gradient was propagated through the tungsten wall, there would generally be the same axial gradient along the inside wall of the tungsten cylinder. The inside wall of the cylinder would not then be strictly adiabatic but it was assumed to be so since the effect of the radiative exchange inside the cylinder would tend to reduce the axial temperature gradients.

The use of this second method for establishing the fourth boundary condition was reasonable and even desirable since it eliminated the need for the radiative heat transfer calculations and also eliminated the need for one of the two gas preheating considerations.

#### Fifth Boundary Condition

The conduction correction factor to be used in the equations for thermal and electrical conduction was not known. In order to evaluate this factor along with the volumetric heat transfer coefficients and the three constants of integration it was necessary to measure a fifth boundary condition. The fifth boundary condition was the amount of heat generated in the length of the tungsten cylinder between the two voltage probes. By assuming that the thermal and electrical conduction correction factors are the same and knowing the temperature dependence of the electrical resistivity, the length-over-area conduction correction factor can be evaluated when the temperature distribution in the tungsten cylinder is known.

### Method of Solution

Since the heat transfer coefficient and the conduction correction factor were contained in transcendental equations the method of solution for the five unknown coefficients was the following. First, an initial estimate was made of the heat transfer coefficient and the conduction correction factor. Then, even though the equations defining the experimental system assume that all parameters except for the electrical resistivity are temperature independent, parameters were used which correspond to those for the mean temperature of the material for which the parameter applies. An initial estimate of the solid phase temperature of the porous tungsten was obtained from an average of the five optical pyrometer temperature readings. An estimate was made of an average fluid temperature during the passage of the fluid through the porous tungsten. Initial values of parameters such as thermal conductivity and heat capacity are estimated. Evaluation of the heat transfer coefficient and the conduction correction factor require that values be chosen for these parameters.

When these values are inserted in the first three boundary conditions a set of equations results which can be solved explicitly for the three constants of integration. The constants of integration are then used along with the assumed heat transfer coefficient and the conduction correction factor to calculate the fourth and fifth boundary conditions. The calculated values of the fourth and fifth boundary conditions are then compared to the experimentally measured boundary conditions. Successive values for the heat transfer coefficient and the conduction correction factor are chosen until sets of assumed values are found which yield calculated boundary conditions that bracket the experimentally determined fourth and fifth boundary conditions.

Successive iterations are then carried out in order to obtain convergence to within a prescribed limit. Convergence to a tolerance of one part in  $10^4$  was facilitated by the use of digital computer programs and by the fact that the conduction correction factor was not particularly sensitive to changes in the heat transfer coefficient. The conduction correction factor was evaluated in the first two to three iterations after which the iterations on the heat transfer coefficient could proceed.

When the computer program obtained a bracket on the heat transfer coefficient the method of false position was used with a quadratic rather than a linear fitting method. Use of this technique usually gave convergence in from two to five iterations. The stability of the conduction correction factor was a result of its essentially singular dependence on the solid phase temperature which defines the electrical power generation equations. It has been noted that the porous tungsten wall had a very flat temperature profile so that the initially observed temperature profile of the outer wall of the cylinder was very nearly the profile for the entire thickness of the tungsten wall.

Summary of Results

The data from 38 experimental runs are tabulated in Tables 2 through 4 which are in Appendix C. Data in these tables represent the values which served as input to the computer programs which calculated the heat transfer coefficient and other parameters for each experimental run. Table 1 tabulates parameters which were common to all runs as well as physical constants. This table is in Appendix B. Tables 5 through 7 contain the heat transfer coefficient and other values calculated from the analysis of the experimental runs. These tables are in Appendix D. All runs are designated by a two digit number ranging from 05 through 82. These numbers were originally related to the date on which the run was made but are used only as reference.

Three different porous tungsten cylinders were used in this study. The four runs 05 through 08 were carried out using cylinder C. The twenty-four runs 14 through 37 and 62 through 82 were carried out using cylinder D. The ten runs 45 through 54 were carried out using cylinder E. All of the cylinders weighed approximately 18 grams at the start of a series of runs. The volume porosity of all the cylinders was approximately one half based on the dimensions of the hollow cylinders, their weight, and the density of solid tungsten.

The coolant gas for the twenty-seven runs 05 through 54 was nitrogen and the coolant gas for the eleven runs 62 through 82 was helium. The nitrogen flow rates varied from approximately 7 to 19 standard cubic feet of gas per hour and the helium flow rates varied from approximately 8 to 30 standard cubic feet of gas per hour.

The stainless steel sheathed thermocouple number 14 was inserted into the interior of the tungsten cylinder for approximately one half of

the length of the tungsten cylinder during 17 of the runs using nitrogen as the coolant. In this configuration heat was transferred from the interior wall of the tungsten cylinder to the thermocouple by radiation where it was absorbed by the incoming coolant gas. The gas was thus preheated by this amount of heat after leaving the end of the pier and before entering the porous wall.

Thermocouple number 14 was withdrawn from the interior of the tungsten cylinder during 10 of the runs using nitrogen as the coolant. In this configuration thermocouple number 14 was not involved in heat exchange in the interior of the tungsten cylinder. The interior wall of the cylinder was assumed to be adiabatic in these runs. All of the runs using helium were made with thermocouple number 14 inserted into the interior of the cylinder.

The evaluation of a heat transfer coefficient in the generating porous tungsten was possible in 30 of the runs. These values are presented in Table 7. A Nusselt number and a Reynolds number are calculated for these runs and presented in Table 7. Figure 16 shows typical solid and fluid temperature profiles within the wall of the porous cylinder. The heat fluxes involved in the evaluation of these profiles are also shown. Figure 17 presents the Nusselt-Reynolds correlation in graphic form. Other experimental data correlations for heat transfer in porous materials are shown in Figure 17. Correlations which have been suggested for heat transfer in porous systems are also shown.

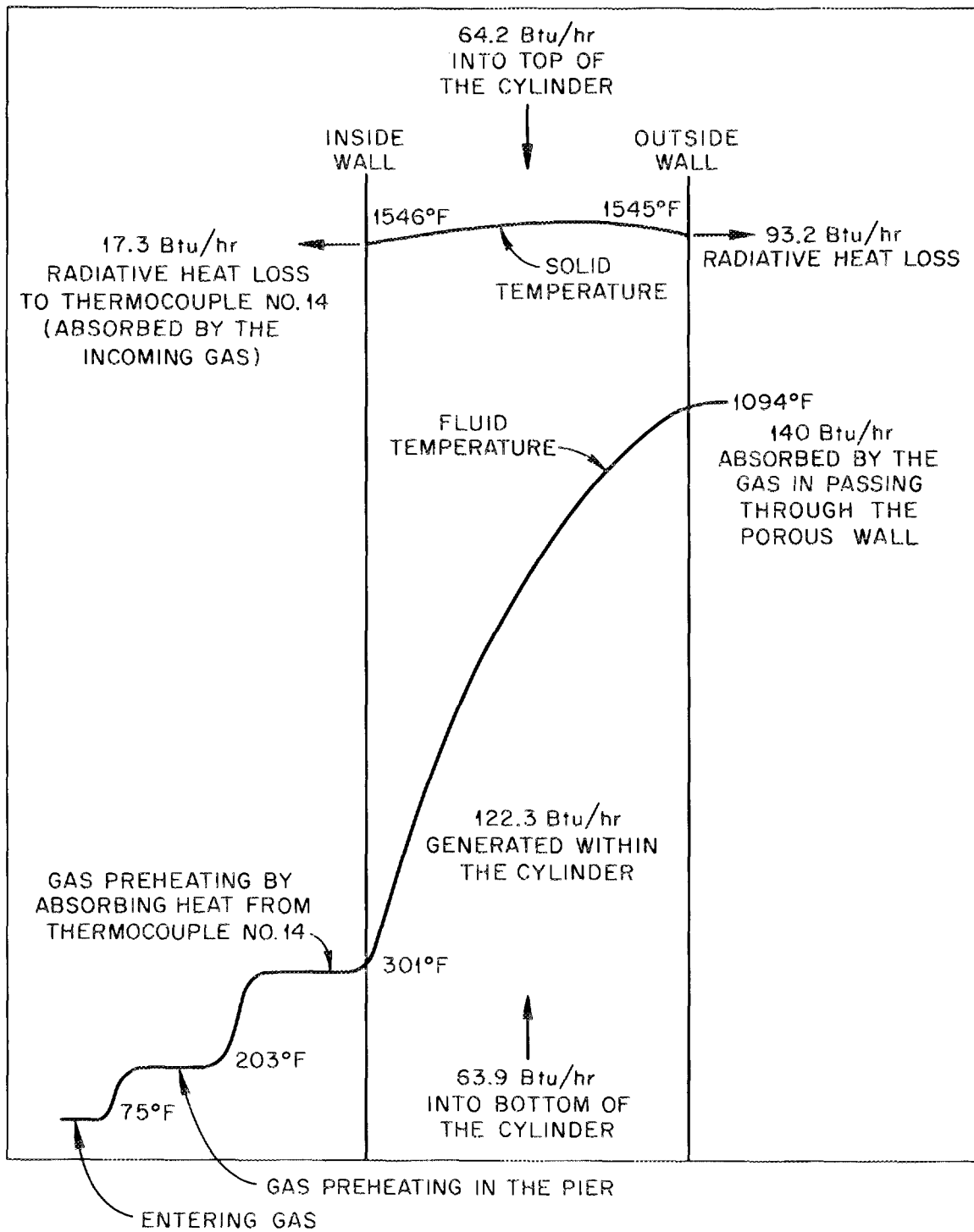


Figure 16

Temperature Profiles and Heat Balances in the Porous Wall

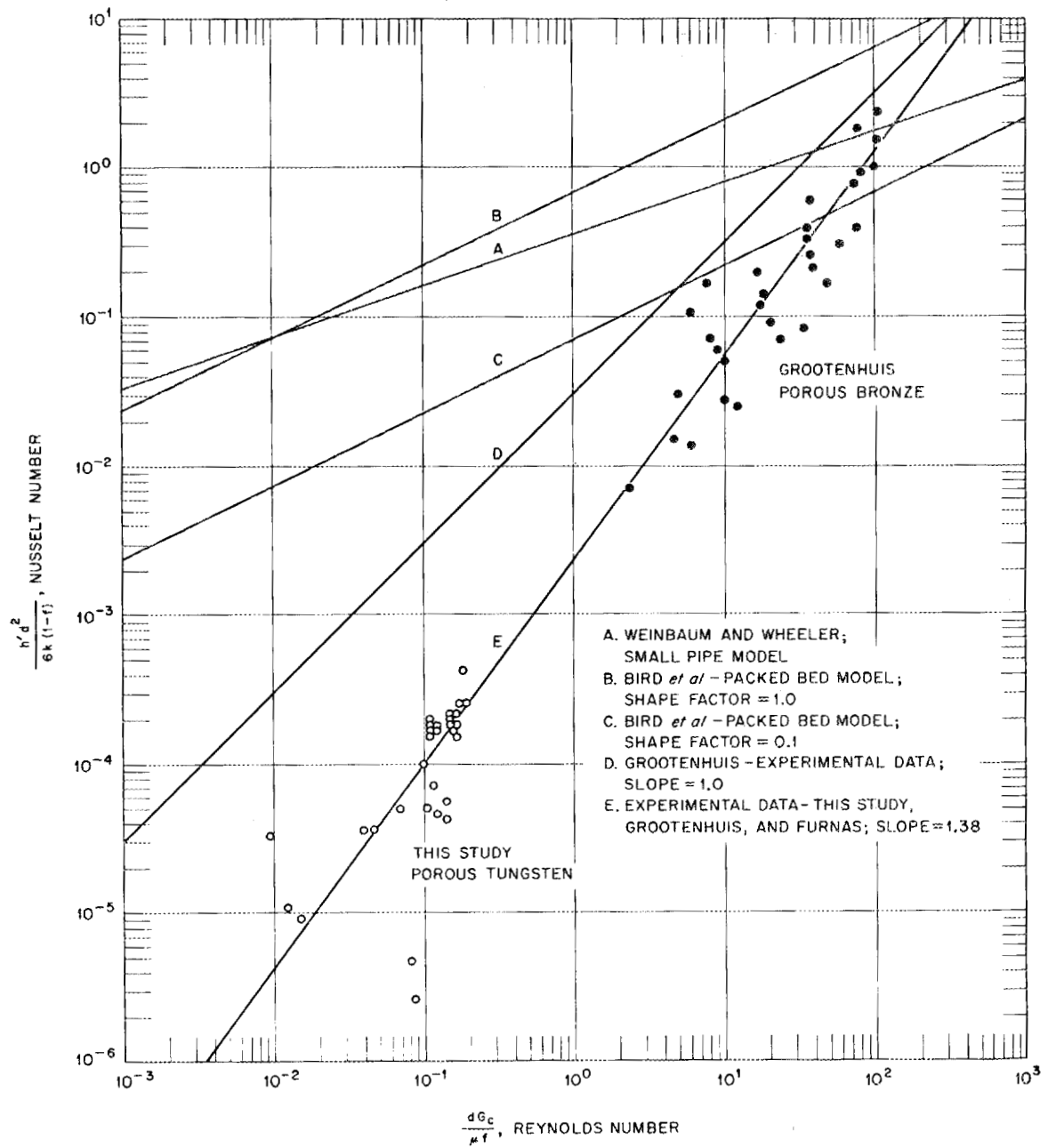


Figure 17

Nusselt Number vs Reynolds Number for Systems of Porous Materials

### Nusselt-Reynolds Data Correlation

Figure 17 is a log-log plot of Nusselt number versus Reynolds number. The Nusselt number in this plot is  $h'd^2/6k(1-f)$  where  $d$  is a measure of the particle size,  $f$  is the porosity of the porous material,  $k$  is the thermal conductivity of the gas passing through the porous material, and  $h'$  is the volumetric heat transfer coefficient in B.t.u./hr.-°F-cu.ft.

The volumetric heat transfer coefficient,  $h'$ , is equal to  $h\epsilon$  where  $h$  is the classical heat transfer coefficient in B.t.u./hr.-sq.ft.-°F and  $\epsilon$  is the surface area within the pores of the material per unit volume measured on a bulk basis. The significance of  $h'$  is that it represents a quantity which can be measured directly, as in this study, without the need to know the internal surface area per unit volume of the porous material. There are a wide variety of techniques for the measurement of the internal surface area of a porous material. Comparisons of heat transfer data using the classical  $h$  can be difficult since the different techniques for the measurement of internal surface area can give different results. The use of mercury porosimetry for example, gives different values depending on the pressure used and the question then becomes which of these values in fact represent the effective area for heat transfer.

The Reynolds number in this plot is  $G_c d/\mu f$  where  $d$  is a measure of the particle size,  $G_c$  is the mass flow rate per unit area of bulk porous material,  $\mu$  is the viscosity of the gas passing through the porous material, and  $f$  is the porosity of the porous material. The measure of particle size,  $d$ , is taken to be the size of the powder used in the manufacture of the porous tungsten. This value is used in both the Reynolds number and

the Nusselt number. The justification for this choice will be presented shortly. The porosity term in the Reynolds number is introduced to give a Reynolds number based more nearly on the true velocity of the fluid in the pores of the porous tungsten. This correction has been made in other studies. (17,11)

Since  $h'$  is a volumetric heat transfer coefficient, the conversion to the area based heat transfer coefficient used in the Nusselt number was accomplished by the use of the term  $6(1-f)/d$  which is taken to be the surface area per unit volume of the porous material.

The particular forms of the Nusselt and Reynolds numbers chosen for Figure 17 are designed to allow comparison of the experimentally determined heat transfer coefficients from this study with other work. The factor  $6(1-f)/d$  does represent the surface area per unit volume for a bed of spheres packed to obtain maximum porosity. It has been assumed from the nature of the factor  $1-f$ , that the surface area per unit volume, based on porosity alone, would vary linearly from  $\pi/d$  at the maximum porosity of approximately 0.476 to  $6/d$  at zero porosity. While this factor is not designed to apply to porosities above 0.476, the porosity of material in this study is close to the limit of this range, and this factor has been used in other work where the porosity was above 0.476.

The use of the factor  $6(1-f)/d$  gives a surface area per unit mass of approximately 0.0078 sq. meters/gr. for the porous tungsten used in this study. This corresponds with the experimentally measured surface area per unit mass of 0.0116 sq. meters/gr. for the porous tungsten. This surface area was determined by nitrogen adsorption. This is a good correspondence in light of the absence of any sphericity considerations which would tend to increase the 0.0078 value. The agreement

might be considered very good if the sphericity-porosity correlation in Brown (4) is used. The sphericity value of 0.6 to 0.7 for packed beds at a porosity of 0.5 would bring the value of 0.0078 into close agreement with the measured value.

The thermal conductivity, viscosity, and heat capacity used in the Nusselt and Reynolds numbers were evaluated at the mean fluid temperature during the passage of the fluid through the porous tungsten. The Reynolds numbers studied in this work are on the order of  $10^{-1}$ . The Nusselt numbers corresponding to this order of Reynolds number are on the order of  $10^{-4}$ . The use of the measured surface area per unit mass of 0.0116 sq. meters/gr. gives heat transfer coefficients on the order of 0.1 B.t.u./hr.-sq.ft.-°F.

#### Agreement with Other Experimental Data

Figure 17 shows the results of this study along with other experimentally measured heat transfer coefficients. The data of Grootenhuis (17) for heat transfer from porous bronze to air is shown. This group of data have Reynolds numbers on the order of  $10^0$  to  $10^2$ . The results found in this work give a correlation that agrees with the data of Grootenhuis. A line through the data from this study and the data of Grootenhuis has a slope slightly greater than one. This is curve E in Figure 17. This line would also correlate well with other reported experimental data cited by Grootenhuis and in particular with the data of Furnas<sup>1</sup> on heat transfer from beds of iron and iron ore to air. These latter points have Nusselt numbers on the order of  $10^2$  and Reynolds

---

<sup>1</sup>Cited by Grootenhuis (15).

numbers on the order of  $10^3$  and  $10^4$ .

The correlation line through the data of this study, the data of Grootenhuis, and the data of Furnas has the equation

$$\text{Nu} = 2.0 \times 10^{-3} (\text{Re})^{1.38}, \quad (21)$$

where the Nusselt and Reynolds number are those described previously. Grootenhuis suggests that a correlation line should not have a slope greater than one which is presumably based on the Graetz analysis. Equation (21) is not a violation of this principle since the Graetz analysis is not particularly applicable to these porous systems as will be shown. In any event, equation (21) should be considered an empirical correlation.

It is difficult to describe the flow regime in porous materials. Friction factor data on porous systems do not show a distinct transition from laminar to turbulent flow. It has been suggested that the rough nature of the flow channels in porous material leads to a gradual increase in the number of channels which are in turbulent flow. The fact that the data on packed beds have a transition at a Reynolds number of 50 (1) suggests that a different type of flow regime has been acknowledged. It has been suggested that there are multiple transitions at Reynolds numbers around 42 and 1200 (11) for other data on packed beds.

The laminar portion of tube or pipe friction factor curves are dependent on  $L/D$ . It has been found (22) that for  $L/D$  around 5 the laminar friction factor curve joins the turbulent friction factor curve with only a small transition. This same characteristic is seen in the continuous friction factor curve for porous materials. A porous

material might therefore be considered to have a small value of  $L/D$ , possibly as small as one.

Thus, to whatever extent the flow in porous materials is laminar, the use of the Graetz analysis would still call for a uniform wall temperature, undistorted laminar flow, no viscosity dependence on temperature, and some value for  $L/D$  in a porous system.

Since it would probably be hard to meet these requirements, it would seem that a correlation with the Graetz analysis should not necessarily be the basis for accepting or rejecting a correlation line of slope greater than one.

In general the points in Figure 17 lie further below a line of slope one as the Reynolds number decreases. The particle diameter of the bronze particles is on the order of  $10^{-3}$  to  $10^{-4}$  ft. The particle diameter of the tungsten particle is approximately  $6.5 \times 10^{-5}$  ft. It has been suggested that the correlation line is actually of slope one but that the loss of surface area, during the forming of porous materials, is greater for particles of smaller diameters. Thus, the factor  $6(1-f)/d$  is an overestimate of the actual surface area with a resulting lowering of the Nusselt number values.

The bronze data vary in particle diameter over one order of magnitude and they do show an indication of this dependence on particle size. The iron ore data of Furnas have particle sizes on the order of  $10^{-1}$  ft. The Nusselt values for the data of the present study do fall further below a correlation line of slope one than do data based on larger particle diameters. Curve D in Figure 17 is a line of slope one that was used as a reference by Grootenhuis since it gave a good correlation with data of Furnas and others at Reynolds numbers of  $10^2$  and

Nusselt numbers of  $10^3$  to  $10^4$ .

It should also be noted that the ratio of wall and bulk viscosities has not been included in the evaluation of the ordinate in Figure 17 or in equation (21). The effect of this term as a multiplier of the Nusselt number would be to move the data points in this study closer to the correlation line of slope one, curve D.

An evaluation of the wall viscosity in the porous tungsten was made at the average solid phase temperature. The viscosity correction factor,  $(\mu_w/\mu_b)^{0.14}$  has been used for both laminar and turbulent flow. The correction which would be introduced by the ratio of the wall and bulk viscosities to the 0.14 power is on the order of 1.05 to 1.1.

If, following Bird (1), the diameter to be used in the Reynolds number was evaluated as four times the hydraulic radius of the porous material the diameter would be approximately 13 percent smaller than the diameter used in the Reynolds number which was assumed to be the particle size of 20 microns. Also if the diameter used in the Nusselt number were evaluated as  $6/a_v$  where  $a_v$  is the specific surface of the porous material, the diameter would be approximately 33 percent larger than the particle size diameter of 20 microns which was used in the Nusselt number. These corrections would lower the value of the Reynolds number and raise the value of the Nusselt number. Both of these effects would move the data points observed in this study toward the correlation line of slope one in Figure 17.

These evaluations were not made because their use would not effect the evaluation of the heat transfer coefficients and because there was no specific surface data available for the porous bronze and the iron ore. In addition, the use of a hydraulic radius is questionable for

laminar flow and the Reynolds numbers in this study are in the laminar region.

Regarding the flow regime, the correlation line of equation (21) or even a correlation line in the vicinity of slope one offers some indication that the nature of the flow in porous materials may be different from that found in pipes at Reynolds numbers of  $10^{-1}$ . A correlation line with a slope around one would be expected for high Reynolds numbers, turbulent flow, and a large relative roughness speaking in the sense of flow in pipes. Porous materials show friction factor correlations which correspond to low if not unitary  $L/D$  as the transition region is approached from the laminar region. Correspondingly, porous materials act in the turbulent region as if they were a pipe with a large relative roughness. Some friction factor correlations show relative roughnesses in the vicinity of 0.05. A porous material may well have a relative roughness as large as the order of one.

The effect of the nature of porous materials on the friction factor correlation is to lower the Reynolds number at which the flow in a porous material begins to take on the aspects of turbulent flow. This should also be true to some extent and possibly even to a greater extent for heat transfer. This fact in conjunction with the correlation presented in Figure 17 suggests that flow in porous materials may contain elements of turbulent flow and that Nusselt-Reynolds correlations with a slope of one are more reasonable than correlations based on laminar flow which postulate correlation lines with a slope of from  $1/3$  to  $1/2$ .

Other Non-Experimental Correlations

Figure 17 also shows curves which have been suggested as correlations that might be used to determine heat transfer coefficients in porous materials.

Curve A in Figure 17 is a Nusselt-Reynolds correlation based on the small pipe model for porous materials used by Weinbaum and Wheeler. (34) This curve was evaluated using values for parameters typical of those found in this study. The characteristic diameter of both the particles and the flow passages was 20 microns. The wall thickness or the equivalent pipe length was 1/16 in. and the Prandlt number was 0.705. This curve was calculated by assuming, as did Weinbaum and Wheeler, that the wall-bulk viscosity correction could be neglected.

The equation used in the correlation of Weinbaum and Wheeler was the empirical modification of the Graetz theoretical temperature solution for fully developed laminar flow with constant wall temperature. Weinbaum and Wheeler reference McAdams (24) for their source of this equation. The slope of this correlation line is 1/3. Figure 17 shows that this small pipe model does not describe the slope of heat transfer correlation determined in this study. It also overestimates the heat transfer coefficient by approximately three orders of magnitude at Reynolds numbers of  $10^{-1}$ . The use of the correlation of curve A for heat transfer in porous materials would not be recommended.

As has been noted previously, the use of the Graetz analysis is questionable in the case of porous materials since it is by no means clear that the nature of the flow in the pores satisfies the Graetz conditions. It is unclear how a value of L/D would be evaluated for a

porous system in the sense in which it is used in this analysis.

The Graetz correlation was not designed for the low range of Reynolds numbers encountered in this study. McAdams notes in his commentary on the use of this correlation that there are large deviations associated with the use of this correlation even in the cases being described. These cases include asphalt at temperatures of  $300^{\circ}\text{F}$  flowing in 1 in. tubes at 2 ft./sec. with heat transfer coefficients of 30 B.t.u./hr.-sq.ft.- $^{\circ}\text{F}$ . Bird et al., (1) points out that there are significant uncertainties in the use of this correlation at values of the Graetz number less than 10.

The use of the correlation of Weinbaum and Wheeler could help to propagate the idea that porous materials have essentially equal solid and fluid phase temperatures since the use of the much overestimated heat transfer coefficients obtained from this correlation could indeed predict that the fluid temperature quickly reaches the temperature of the solid phase.

Curves B and C in Figure 17 are based on a packed bed model of a porous system that is described by Bird, et al., (1). Bird's correlation was based on heat and mass transfer data for packed beds and it was correlated in terms of the Colburn  $j_H$  factor versus Reynolds number. This correlation involved a particle shape factor, 1.0 for spheres and less for other shapes. Curve B is based on a shape factor of 1.0 and Curve C is based on a shape factor of 0.1. In both cases a Prandlt number of 0.69 was assumed.

The slope of curves B and C on the Nusselt-Reynolds plot are 0.49 in a range of Reynolds number less than 50. Curves B and C have been chosen for comparison to the experimental data cited in this study

because they suggest one of the largest slopes proposed for the Nusselt-Reynolds correlation line in materials of a porous nature.

From Figure 17 it can be seen that these two curves do not describe the data points found in this study. Further, the slope of this correlation is still too low to describe the data observed in this work and by Grootenhuis and Furnas. Use of this correlation would also overestimate the heat transfer coefficient by two to three orders of magnitude at Reynolds numbers of  $10^{-1}$ .

The correlation is presented in Bird et al. as being based on large amounts of experimental data on both heat and mass transfer in packed beds. The primary reference to this data is described as a private communication but the authors give a secondary reference to charts by Hougen et al.<sup>1</sup> The charts give no indication as to how small a value of Reynolds number could be described by their correlation. However, the particle diameters explicitly discussed on the charts extend down only to the order of  $8.0 \times 10^{-4}$  ft. which is still an order of magnitude above the particle size in this study.

The fact that this correlation was designed for a wide range of data and was seeking a correlation for not only heat transfer but also for mass transfer suggests that it would not be applicable to the small particle diameter and low Reynolds numbers found in this study.

Green (12) presents a correlation of heat and mass transfer data in terms of a plot of j-factor versus Reynolds number. The slope of this curve is on the order of -0.45 which would give a slope of 0.55 when presented on a Nusselt-Reynolds plot. The inadequacies of this

---

<sup>1</sup>Cited by Bird et al. (1)

correlation in describing data cited in this work are essentially those of the correlation from Bird et al.

Green does note that transient methods are generally used to measure heat transfer coefficients in porous systems because of what he describes as the difficulty of measuring the heat transfer coefficient in the porous material directly. He does note that there are frequently discussed errors in the use of the transient method of evaluating the heat transfer coefficient. Green cites, but does not use the data from Grootenhuis in establishing his heat transfer correlation. The method of Grootenhuis had been to continuously supply radiant heat at one surface of a porous plate and thereby achieve a steady state system for the measurement of the heat transfer coefficient in his apparatus. Green does however use the concept of the volumetric heat transfer coefficient in his calculations which was used by Grootenhuis.

A study by Han<sup>1</sup> was considered by Green in establishing his heat transfer correlation. It is interesting that Green rejected the data in this study on the basis that it predicted heat transfer coefficients which he considered abnormally low by about two orders of magnitude.

The results of this present work suggest that the heat transfer coefficient at low Reynolds numbers should be much lower than those predicted by correlations of the type used by Weinbaum and Wheeler, Bird et al., and Green.

As noted, curve D in Figure 17 is a line of slope one which was used by Grootenhuis to include the data of Furnas and to serve as a suggested correlation line for the Nusselt-Reynolds correlation of data

---

<sup>1</sup>Cited by Green (12).

on heat transfer in porous materials.

Grootenhuis notes that his experimental data on heat transfer to porous bronze have fallen below this line. It is this line toward which he suggests his data could be moved if the loss of heat transfer surface during fabrication of the porous bronze could be taken into consideration.

The effect of small corrections to the data of the present study would also tend to move the data points as presently reported in the direction of curve D. These corrections have been cited and include the effect of a viscosity correction, the evaluation of a more precise hydraulic radius for use in the Reynolds number, and a more precise average particle diameter for use in the Nusselt number.

### Heat Balances and Temperature Profiles

Figure 16 presents typical heat balances around the porous wall of the tungsten cylinder. At any given axial position, the solid phase temperature profile through the wall of the cylinder is quite flat because of the high thermal conductivity of the tungsten and the low heat transfer coefficient. The solid phase temperature curve has a slight slope or is zero at the inside wall depending on whether or not the sheathed thermocouple is inserted into the interior of the tungsten cylinder. The slope of the temperature curve at the outside wall provides the heat lost by radiation to the enclosing Marinite disks.

A significant amount of heating of the fluid flowing through the porous wall does take place within the porous wall but because of the low value of the heat transfer coefficient, the fluid phase temperature profile does not show the near step function of fluid heating proposed by Weinbaum and Wheeler. It can be seen from Figure 16 that the assumption that the temperature of the solid and fluid phases are nearly identical would be in error for the porous system used in this study.

The low value for the heat transfer coefficients found in this study and correlated with other experimental studies on heat transfer in porous systems suggest that errors, which may be as large as two orders of magnitude at Reynolds numbers of  $10^{-1}$ , may result from the use of porous heat transfer correlations using Nusselt-Reynolds correlations with slopes of  $1/3$  to  $1/2$ .

There is an additional experimental verification of the fact that the gas exiting from the outside wall of the tungsten cylinder has not been heated to the temperature of the tungsten wall. The stainless steel

sheathed thermocouple number 16 was positioned at the axial position of the optical pyrometer hole in Marinite disk number 6 on the opposite side of the tungsten cylinder from the optical pyrometer and in contact with the outside wall of the tungsten cylinder. The thermocouple was in this position during the experimental runs. The temperatures recorded by this thermocouple were generally found to be intermediate between that of the tungsten wall with which it was in contact, and that of the calculated temperature of the gas leaving the tungsten surface. In addition the temperature of the Marinite wall through which the thermocouple was inserted was generally above that of thermocouple number 16 so that the existence of an exiting fluid below the wall temperature would be needed to explain these temperatures.

The effect of fluid phase heat conduction which has been neglected in this study was examined and found to contribute only about 7 percent of the heat transferred by fluid transport even at the low Reynolds numbers of this study. Neglecting this effect at higher flow rates would seem justified but studies at lower flow rates will need to take this effect into account.

In order to justify the exclusion of the fluid conduction term, differential equation (2) for the fluid phase heat transfer was modified to include fluid conduction terms. The result was a fourth order differential equation. The resulting equations for the solid and fluid temperature distributions now included four constants of integration and the operator equation now included the fluid conduction terms. The small magnitude of the fluid conduction terms could be ignored in the operator equation where they were added to the existing terms. However, since the operator equation was now of the fourth order, it was uncertain whether

or not the four roots resulting from the solution of the fourth order polynomial equation would describe the same temperature profiles obtained with the third order operator equations. During the analysis of each run, the roots of the fourth order operator equation were evaluated and compared to those of the third order equation. For two of the roots that were found to be essentially common between the third and fourth order operator equations, the differences were negligible. While this suggested that the temperature profiles described by the fourth order equations might not differ significantly from those described by the third order equations, the best verification of this fact through the use of the differential equations would be to solve the system of fourth order equations and use an additional boundary condition to obtain results which could be compared to the results of the solution of the third order equation. The equations involving fluid conduction are derived in Appendix A.

To avoid the difficulties associated with this problem an estimate of the magnitude of the heat flux from fluid conduction was made during the evaluation of the data from each run. A check had always been run on the heat balance at the points  $x = 0, z = 0$  and  $x = l, z = 0$ . This check calculated the heat flux in B.t.u./hr. at these points for each of the heat transfer mechanisms of conduction in the tungsten, heat transport in the fluid, heat generation in the solid, and heat transfer from solid to fluid. The evaluation of the heat flux due to conduction in the fluid was added to these existing checks and the magnitude of this effect provided the most realistic measure of the justification for leaving the fluid conduction effect out of the present calculations.

The conclusion reached in this study, that there is a large difference between the solid and fluid phase temperatures, should not be construed to be a conclusion that would be applicable to all porous systems. There are probably many porous systems in which the solid phase temperature is approached quite closely by the fluid phase temperature and it is this effect in those systems that gives added weight to the idea that this will be the case in all porous systems. Data for these systems are usually at much larger Reynolds numbers than those considered in this study. An example of this would be the work of Koh and del Casal (21) with Reynolds numbers above 60.

### Conduction Correction Factor

The length-over-area conduction correction factor was found to vary from approximately 0.45 for a new porous tungsten cylinder to approximately 0.22 for a used porous tungsten cylinder. These values are presented in Table 7.

It has been widely assumed that the conductivity, both electrical and thermal, of a porous material would be less than that of the solid material. The factor most commonly used to evaluate this reduction is the complement of the volumetric porosity. Grootenhuis uses this concept and shows that points describing the thermal conductivity of porous bronze lie on a straight line running from the conductivity of solid bronze at zero porosity to zero thermal conductivity at a porosity of 0.476. However he does point out that certain data for porous stainless steels do not conform to this type of correlation and that another correlation would have to be expected for these stainless steels and other materials.

The conductance used in this work has been assumed to consist of the conductivity, the bulk area for conduction, one correction factor in the form of the complement of the volumetric porosity, and another correction factor which is the length-over-area conduction correction factor described earlier in this work. Since the thermal conductivity of the porous tungsten could not be measured while the equipment was running at the operating temperature, the electrical conductivity of the porous tungsten was measured under operating conditions and the conduction correction factor for the electrical conductivity was assumed to apply to thermal conduction.

As has been noted, this should be a good assumption because the electrical and thermal conductivity are known to be related through the Lorenz number. This relation has been verified experimentally for some porous metals by Grootenhuis.

The electrical resistivity of the portion of the tungsten cylinder between the voltage probes is proportional to the average solid phase temperature over that region,  $\bar{T}_{AB}$ . Since the electrical resistivity of the tungsten is described as a polynomial in temperature, the resistance of this section of the tungsten cylinder can be found once the average temperature of that section has been evaluated. As has been noted, the iteration to determine this value is carried out in the early stages of the determination of the heat transfer coefficient.

Tungsten cylinder C showed conduction correction factors of approximately 0.44. This cylinder had been in use for development for some time when these data runs were made. Tungsten cylinder D, after being used for some development work, gave a conduction correction factor of approximately 0.42 to 0.38. Later, after being used at high temperatures and showing evidence of physical deformation and a definite oxide or nitride coating, this cylinder was found to have a conduction correction factor of approximately 0.22. Cylinder E was used in essentially a brand new condition and initially showed a conduction correction factor of approximately 0.45 but this value fell during the runs to approximately 0.41.

Koh and del Casal (21) take specific notice of the fact that the experimentally measured thermal conductivity of porous nickel Foametal is less than the value predicted by the use of the porosity correction

factor (one minus the porosity) by a factor of about six. The conduction correction factor reported by Koh and del Casal for the nickel Foametal matrices range from a value of 0.242 at a porosity of 0.42 to a value of 0.151 at a porosity of 0.735.

## Analysis of Experimental Errors

### Divergent Data

Two of the data points from this study which are shown in Figure 17 lie well below the main group of experimental data. There are also eight data runs which are tabulated in Appendix C which did not converge. That is, no value of the heat transfer coefficients was found from which a fourth boundary condition could be calculated corresponding to the measured fourth boundary condition. The reasons for the scattered data points and the lack of convergence of the other data runs are understood and are symptoms of the major experimental difficulty encountered in this study.

The uncertainties in this study stem from problems associated with obtaining equilibrium conditions under which to take measurements of the system. The instability of the experimental system was due, in turn, largely to fluctuation in the electrical contact resistance at the interfaces between the tungsten, the graphite washers, and the piers.

The experimental system could be characterized as metastable. If the system was initially stable with fairly uniform contact between the tungsten, graphite, and piers, the tungsten would heat fairly uniformly and a very good gas seal was obtained between the tungsten cylinder and the piers. However, as the run proceeded it is reasonable to assume that various thermal stresses developed throughout the experimental apparatus as its components were heated by the power being generated in the apparatus. Some stresses were handled by the system of spring loaded stainless steel studs used to maintain pressure on the tungsten and the graphite. However, the metastable nature of the system appeared when any noncoaxial load changed the pressure and therefore the contact

resistance around the circumference of one face of a graphite washer. The increased pressure and the resulting reduced electrical resistance at the pressure point would generate more heat at this point because power generation at constant voltage is inversely proportional to resistance. Thermal expansion at this point would then increase the magnitude of the hot spot. Gas leakage at points other than the hot spot would in turn selectively cool the balance of the circumference.

This pattern of operation was generally observed. In order to gather experimental data it was necessary to bring the system from a cold state into one operating near the desired conditions in a period on the order of several minutes. During the fairly short stable period of the apparatus it was necessary to take measurements, often while the system was still fluctuating. The experimental run was invariably terminated by the onset of the unstable conditions described previously. It was very difficult to shift the experiment to a region of a different gas flow rate or heat generation rate because this attempted shift generally terminated the run by initiating the onset of instability.

The two data points which lie approximately one order of magnitude below the main group of data points at a Reynolds number of approximately  $10^{-1}$  are data points taken during the start of a series of runs when the experimental system had not yet approached very close to equilibrium.

In addition to the scattered data points there were two runs using nitrogen as the coolant which did not converge. One of these runs was made at a point in time adjacent to one of the runs which had produced the scattered data point. The same reasons would seem to explain why this run failed to converge. The second run using nitrogen which failed to converge was being made as the power and the temperature

in the system were falling rapidly just before termination of the series of runs. There were six runs using helium gas as the coolant which failed to converge. Four of these runs were at very low gas flow rates of approximately 3 standard cubic feet per hour. These four runs were the start-up runs for a series of runs and the system may not yet have been in equilibrium. The effect of gas conduction would have needed to have been considered in these runs since the run using helium at a flow rate of 8 standard cubic feet per hour showed gas conduction effects comparable to the effect of heat transfer by fluid transport. The lowest flow rate in helium runs which did converge was approximately 8 standard cubic feet per hour which corresponded to a Reynolds number of approximately  $10^{-2}$ . The other two runs using helium which failed to converge had gas flow rates of approximately 30 standard cubic feet per hours. Since this series of runs was terminated just after these two runs due to the instability of the system described above, there is a strong suspicion that the high flow rates of these two runs represent the onset of leakage around the ends of the tungsten cylinder.

#### Miscellaneous Justifications

It has been noted that interparticle radiative heat transfer effects within the porous tungsten have been neglected due to the fact that the porous material forms a wall composed of a large number of radiation shields. The neglect of the radiative contribution to thermal conductivity is further justified by evaluating a correlation of Dankohler<sup>1</sup> that estimates the radiative contribution to thermal

---

<sup>1</sup>Cited by McAdams (24).

conductivity in a packed bed of known porosity and particle diameter at a given temperature. The radiative contribution to thermal conduction in this study would be 1.5 to 2 orders of magnitude smaller than the thermal conductivity of tungsten. Even by considering the thermal conductivity of the porous tungsten when reduced by the volumetric porosity factor and the conduction correction factor, the radiative contribution to thermal conductivity would still be approximately an order of magnitude smaller than the residual thermal conductivity.

The temperature profile through the cylinder wall is quite flat. This fact contributes to the validity of the assumption that the coordinate transform from cylindrical to rectangular coordinates is justified. It has been previously noted that the hollow cylinder was sufficiently thin walled so that the difference between the mean areas for cylindrical and rectangular conduction did not differ by two percent. The flat temperature profile through the wall suggests that there would not be any radial dependence on temperature in the solid phase.

The Reynolds number will drop as the gas flows radially outward through the cylinder wall because the cross sectional area for flow at any given radius is increasing. The question then becomes whether or not the use of a mean value for the Reynolds number is a satisfactory method for determining the heat transfer coefficient.

While the heat transfer coefficient will decrease as the gas flows outward through the wall, the volume of porous material available for heat transfer at any given radius will increase. The heat transferred by convective heat transfer at any radius will be proportional to the product of the heat transfer coefficient and the volume of the cylinder

at that radius since the heat transfer coefficient is a volumetric heat transfer coefficient. For a slope of one on the Nusselt-Reynolds correlation, the reduction in the heat transfer coefficient is offset by the increase in the volume with a resulting uniformity in the heat transfer at any given radius. Since the slope of the Nusselt-Reynolds correlation is close to one, the flux across the cylinder wall should have nearly the uniformity of a flat wall.

The thinness of the cylinder wall, the flat wall temperature profile, and the nature of the volumetric heat transfer coefficient should all combine to justify the assumption that the cylinder wall can be replaced by an equivalent flat wall.

The axial temperature profile was approximated by the first five terms of a Fourier series. The use of this number of terms would seem to be justified after examining the magnitude of the coefficients for each of the five terms of the Fourier series.

The fifth term of the series was found to be contributing only a few percent of the sum represented by the terms of the series. This would generally indicate that the major components of the series had been described by the first four terms and that no major change in the series would be expected by the inclusion of additional terms.

#### Effect of Errors in Selected Variables

In order to determine the effect of experimental uncertainties on the results of this study, various components of the input data for one run were altered by 10 to 50 percent in order to represent the effect of experimental errors. The effect of these changes on the calculated heat transfer coefficient are considered.

The temperature of thermocouple number 14 which was located inside the hollow tungsten cylinder was decreased by 10 percent which corresponded to a temperature reduction of approximately  $109^{\circ}\text{F}$ . The effect of this change on the heat transfer coefficient was negligible. The value of the heat transfer coefficient was only reduced by 1 percent. This error of  $109^{\circ}\text{F}$  represents a much larger error than would be expected for the stainless steel sheathed thermocouple. However, it can be seen that even for errors of this magnitude the effect on the heat transfer coefficient is quite small.

The temperature of this thermocouple does not appear to be critical because the heat loss to this thermocouple from the tungsten cylinder is relatively small in the overall heat balance, only about 7 percent of the heat flux from the tungsten cylinder. The small significance of thermocouple number 14 should justify the runs in which this thermocouple was removed from the inside of the tungsten cylinder and an adiabatic inside wall was assumed for the cylinder.

The temperature of thermocouple number 6 which was located near the outer edge of the Marinite disks was decreased by 20 percent which corresponded to a temperature reduction of approximately  $123^{\circ}\text{F}$ . The effect of this change was to reduce the heat transfer coefficient by approximately 14 percent. An error of  $123^{\circ}\text{F}$  would be a large error, even for a bare thermocouple pair. The significant effect of this parameter on the value of the heat transfer coefficient would seem to be due to the fact that this temperature is used in the evaluation of the heat balance through the Marinite disks which is in turn related to the radiative heat loss from the outside wall of the tungsten cylinder.

Since the radiative heat loss from the outer tungsten wall is approximately 37 percent of the heat flux from the tungsten cylinder, the parameters which play a part in the calculation of this heat flux could have a significant role in the determination of the heat transfer coefficient.

The average value used for the heat capacity of the gas during its passage through the porous tungsten was increased by 10 percent. The effect of this change was to reduce the calculated value of the heat transfer coefficient by approximately 7 percent. This is not a particularly critical parameter since its value as a function of temperature is well known and it should be possible to construct models in which the temperature dependence of the heat capacity of the gas was taken into account.

The thermal conductivity of the tungsten was reduced by 10 percent. This resulted in a reduction in the calculated value of the heat transfer coefficient of approximately 15 percent. The sensitivity of the heat transfer coefficient to the thermal conductivity might seem strange in view of the very flat temperature profile within the wall of the tungsten cylinder. However, the thermal conductivity is directly involved in the determination of the temperature gradient at the walls of the tungsten cylinder. This does point up the need for more nearly adiabatic walls on the porous material in order to reduce the dependency of the heat transfer coefficient on this value. In addition to the involvement of the thermal conductivity in boundary conditions at the inside and outside walls of the tungsten cylinder, in this particular run there is a heat flux into the cylinder from both piers which amounts to half of the heat flux from the tungsten cylinder.

Accordingly the thermal conductivity is directly involved with the flow of this heat into the cylinder. Again, the point can be made that axial heat flows such as these should be held to a minimum in order to reduce the need for consideration of such effects.

Since the length-over-area conduction correction factor is always found in conjunction with the thermal conductivity the previous observations regarding thermal conductivity are equally applicable to the conduction correction factor. The sensitivity of the heat transfer coefficient to these parameters should further support the observations made in this study and cited elsewhere that there is a need for experimental data for the determination of what values should be used for conduction in porous materials.

It should be noted that the values of thermal conductivity used in this study, while taken as a constant value for the entire tungsten cylinder, were evaluated as a function of temperature based on the average temperature of the tungsten cylinder.

The amount of preheating that the incoming gas underwent in the lower stainless steel pier was increased by 50 percent based on the present pier exit temperature in °F. This increase in preheating of the gas amounted to approximately 96°F. The effect of this change was to raise the calculated value of the heat transfer coefficient by approximately 16 percent. The preheating normally experienced in the pier had been calculated to be approximately 128°F.

The incoming gas passed through a 1/8 in. diameter pipe in its passage into the interior of the tungsten cylinder. This 1/8 in. diameter pipe was approximately 5 to 6 inches long and consisted of the

inside of the high pressure fitting on the lower bus block, one inch of passage through the bus block, and 1-3/4 in. of the inside of the lower stainless steel pier. The Reynolds numbers for the flow through this pipe were on the order of  $10^{-1}$ .

While it would be difficult to say what the effect on the flow would be of the various junctions in the 1/8 in. inlet passage it was assumed that they would be negligible. Thus, the preheating considerations were based on the temperature profile of the last three inches of the 1/8 in. pipe assuming that laminar flow had been developed in the first few inches of the pipe. The last three inches of the pipe were used for the preheating calculation because there was no significant heating of the high pressure fitting which extended below the lower bus block. The heated three inches were assumed to start just as the gas entered the lower bus block.

The heat transfer coefficients under these conditions are described by McAdams and the values of  $hD/k$  which are cited for the various modes of flow do not vary by more than a factor of two. The effect of the calculation using an increased preheating value of  $96^{\circ}\text{F}$  may therefore be indicative of the effect that variation in the heat transfer coefficient might produce in the gas preheating.

The change in the heat transfer coefficient due to gas preheating effects is also indicative of the effect that gas absorption of the heat from thermocouple number 14 would have on the heat transfer coefficient. The increase in the temperature of the gas due to the absorption of the heat radiated to thermocouple number 14 is approximately  $98^{\circ}\text{F}$ . This further suggests that the absence of thermocouple number 14 is not only a justified but a desirable condition.

The effects of the changed heat transfer coefficient due to the increased gas preheating also slightly reduces the Reynolds number for the flow (due to the higher viscosity during the passage through the porous tungsten) and increases the Nusselt number. One result of such an adjustment would be to move the data points from this study toward alignment with curve D of slope one in Figure 17. However, such changes would not change the order of magnitude of the heat transfer coefficient and in the case of the helium runs, even with several hundred degrees of preheat, the heat transfer coefficients remain quite small. In these cases the effect of large preheating effects does not appear to be altering the primary correlation between Nusselt number and Reynolds number that was found in this study.

The five optical pyrometer temperatures were increased by 10 percent which amounted to approximately 145°F. The result of this change was that the calculated value of the heat transfer coefficient was decreased by approximately 20 percent. A large change such as this would be expected since nearly all parameters in this study are dependent on the temperature of the tungsten. In addition, these temperatures control the radiative heat loss at the outside wall of the tungsten cylinder and it has been noted that this is a significant portion of the heat flux from the tungsten cylinder.

However, an optical pyrometer temperature error of this magnitude would require that the spectral emissivity of the porous tungsten be much smaller than could be reasonably expected from a rough, oxidized surface.

The effect of introducing simulated experimental errors into the calculations for this study show that the evaluation of the heat transfer coefficient was subject to various uncertainties that could introduce errors that may be estimated to be on the order of 15 to 20 percent. However none of these experimental errors would alter the magnitude of the heat transfer coefficients which have been found in this study. The position of the data in the Nusselt-Reynolds correlation shown in Figure 17 would be essentially unchanged by errors that might reasonably be associated with this study.

#### Maximum Overall Error Estimates

A "worst case" error calculation was carried out by combining five of the individual errors into one case where all of these errors combined to raise the calculated heat transfer coefficient. The effect of raising the calculated heat transfer coefficient was chosen because a major assertion of this study is that heat transfer coefficients in porous systems are (at low Reynolds numbers) significantly lower than would be predicted by other correlations in the literature. Thus, this "worst case" analysis would give some indication of the extent to which the conclusions of this study are dependent on experimental errors.

The following changes were made for the "worst case" analysis. The temperature of thermocouple number 14 was increased by 10 percent. The temperature of thermocouple number 6 was increased by 20 percent. The average value of the fluid heat capacity during its passage through the porous tungsten was decreased by 10 percent. The thermal conductivity of tungsten was increased by 10 percent. The amount of gas preheating in the stainless steel pier was increased by 50 percent.

No change was made in the five observed optical pyrometer temperatures for the "worst case" analysis for the following reason. The five parameters that were perturbed for this analysis might reasonably be suspected of errors which could vary symmetrically about the true value, i.e., errors might be either positive or negative. The possible errors in the optical pyrometer temperatures would, however, be markedly asymmetrical since the observed optical pyrometer temperatures represent a lower limit from which the true value could only vary upward. It would be extremely unlikely for the true surface temperature of the tungsten to be less than the observed value. Therefore, due to the nature of the optical pyrometer temperature measurements and the fact that increasing the observed optical pyrometer temperatures would, in fact, decrease the calculated heat transfer coefficient, the least decrease in the calculated heat transfer coefficient can be obtained by not changing the observed optical pyrometer temperatures for the "worst case" analysis.

The result of the "worst case" was to raise the calculated heat transfer coefficient by a factor of approximately 2.5.

Thus, as was observed for the individual errors, the results of the "worst case" error would still not change the magnitude of the heat transfer coefficients calculated in this study nor would it change the general nature of the heat transfer correlation for porous material that was determined in this study.

## CONCLUSIONS

It was possible to build and operate a simple experimental apparatus for studies involving heat generating porous materials using porous tungsten heated by direct current. The major problem in the use of this apparatus was that of obtaining uniform and reproducible contact resistances at the tungsten-graphite stainless steel interfaces. This disadvantage was offset by the advantage of being able to use less expensive individual components for experimental studies. The use of separate tungsten, graphite, and pier components allowed great flexibility. This would not have been possible if the porous tungsten had been welded or otherwise mechanically attached to the piers. In particular, the reduction of the axial temperature gradient by the use of the graphite washers as combination heat sources and thermal conductivity insulators would not have been possible.

The equations for heat transfer in a heat generating, fluid cooled, flat porous plate were derived. These equations were successfully extended to describe the hollow porous tungsten cylinder used in this study.

The heat transfer coefficients found in this study show good agreement with other experimental measurements of heat transfer in porous materials. The data for the porous materials examined in this study show that heat transfer coefficients on the order of  $10^{-1}$  (for Nusselt numbers on the order of  $10^{-4}$ ) are found at Reynolds numbers on the order of  $10^{-1}$ . In comparison with other correlations for heat transfer in porous materials which are extrapolated from heat transfer data in small tubes or in beds of granular material, the results of this study

found heat transfer coefficients two or three orders of magnitude lower than those predicted by these correlations. The use of correlations which predict high values of heat transfer coefficients can continue to foster the basically incorrect idea that the temperature of the solid and fluid phase are essentially identical in porous materials. Differences of several hundred degrees F between the solid and fluid temperature were computed for the porous tungsten in this study.

The effects of fluid phase heat conduction which were neglected in the study were found to account for only a small percentage of the fluid heat transport effect in the majority of the cases studied.

It was possible to evaluate a length-over-area conduction correction factor in this study and to apply it to the determination of the heat transfer coefficient in porous tungsten. The conduction correction factor that was computed indicates that the effective conduction of porous tungsten should be reduced by a factor of from 0.25 to 0.4 over and above corrections based on the volumetric porosity of the tungsten.

## FUTURE WORK

Future studies should consider eliminating the graphite washers from the experimental system. The graphite washer did serve a useful purpose in providing a mechanical seal and serving as a thermal barrier at the ends of the tungsten cylinder. However, the problems of fluctuating contact resistances at these washers suggest that future studies should use large porous specimens which can be welded or otherwise mechanically attached to a supporting pier. Larger porous specimens would be desirable since the welding process would modify the porous structure adjacent to the weld and this modified region should occupy only a small percentage of the porous specimen. Other techniques for obtaining a flat axial temperature profile, such as separate electrical heating circuits for the piers, should be considered.

The measurement of the surface temperature of porous materials by the use of optical pyrometry has eliminated any possibility that the nature of the porous medium was altered at the point of temperature measurement. However, in order to eliminate problems which are associated with the operation of a porous system at high temperature, consideration should be given to the use of temperature measuring devices which could be attached to the surface of the porous material and allow operation at a lower temperature.

If there is a need for operation of the porous system at high temperatures, the use of two color optical pyrometers would eliminate the need for extensive emissivity corrections in temperature measurement and provide better values for use in radiative heat transfer calculations.

Direct measurement of the conduction correction factors for electrical and thermal conduction in porous specimens should be carried out prior to utilizing them in experiments. This information would be particularly useful if the apparatus was to be operated at temperatures which corresponded to that at which the correction factor was measured.

The use of heat generating porous materials as a device for the measurement of the heat transfer coefficient should be continued and extended as this apparatus eliminates the problems associated with the measurement of heat transfer coefficients by transient means.

APPENDIX A  
Derivation of Equations

All parameters are independent of  $T$ ,  $t$ ,  $x$ , and  $z$ . The solid and fluid temperatures are a function of  $x$  and  $z$ .

$$T = T(x, z) \quad (22)$$

$$t = t(x, z) \quad (23)$$

At steady state with no accumulation of heat the heat balance for the solid phase of the  $dx$  element in Figure 1 is heat in = heat out. Net heat in by conduction =  $k\gamma_2 \nabla^2 T$ . Heat in by generation =  $\Gamma\gamma_3$ . Heat out by convective heat transfer =  $h\epsilon(T-t)$ .

$$k\gamma_2 \nabla^2 T + \Gamma\gamma_3 = h\epsilon(T-t) \quad (24)$$

At steady state with no accumulation of heat the heat balance for the fluid phase of the  $dx$  element in Figure 1 is heat in = heat out. Heat in by convective heat transfer =  $h\epsilon(T-t)$ . Net heat out by fluid transport =  $F C_p \delta_2 dt/dx$ .

$$h\epsilon(T-t) = F C_p \delta_2 dt/dx \quad (25)$$

The volumetric heat generation rate is expressed as a linear function of solid phase temperature.

$$\Gamma\gamma_3 = G = G(T) = G_0 + \alpha T(x, z) \quad (26)$$

The volumetric heat generation rate is therefore a function of  $x$  and  $z$ . These functions are assumed to be separable.

$$G = G(x, z) = X(x) Z(z) \quad (27)$$

The following relations may be derived:

$$T = G/\alpha - G_0/\alpha \quad (28)$$

$$\nabla^2 T = \nabla^2 G / \alpha \quad (29)$$

$$\nabla^2 G = X''Z + XZ'' \quad (30)$$

Equation (24) now becomes

$$k\gamma_2 \nabla^2 G + G\alpha = h\epsilon(G - G_0 - \alpha t) \quad (31)$$

and equation (25) becomes

$$h\epsilon(G - G_0 - \alpha t) = \alpha F C p \delta_2 dt/dx \quad (32)$$

Differentiation of equation (31) with respect to x and the substitution of the X and Z components of G gives

$$k\gamma_2 (X'''Z + X'Z'') + \alpha X'Z = h\epsilon (X'Z - \alpha dt/dx) \quad (33)$$

Solution of equation (33) for dt/dx gives

$$dt/dx = \left( \frac{1}{\alpha} - \frac{1}{h\epsilon} \right) X'Z - \frac{k\gamma_2}{\alpha h\epsilon} (X'''Z + X'Z'') \quad (34)$$

Substitution of dt/dx from equation (34) into equation (32) gives upon rearrangement

$$X'''Z + bX''Z - (c - a) X'Z + X'Z'' + baXZ + bXZ'' = 0 \quad (35)$$

where

$$a = \alpha/k\gamma_2 \quad (36)$$

$$b = h\epsilon/F C p \delta_2 \quad (37)$$

and

$$c = h\epsilon/k\gamma_2 \quad (38)$$

In order to separate the Z function from equation (35) a form of Z function is chosen which will satisfy the condition:

$$Z'' = -\lambda^2 Z \quad (39)$$

The Fourier series satisfies this condition. Substitution of equation (39) in equation (35) gives, after canceling Z,

$$X''' + bX'' - (c - a + \lambda^2) X' - b(-a + \lambda^2)X = 0 \quad (40)$$

The solution of equation (40) is

$$X = C_1 e^{r_1 x} + C_2 e^{r_2 x} + C_3 e^{r_3 x} \quad (41)$$

where the  $r_n$  are the roots of the operator equation

$$m^3 + bm^2 - (c - a + \lambda^2) m - b(-a + \lambda^2) = 0 \quad (42)$$

The Cs are the constants of integration.

One solution for G in equation (27) is now

$$G = X(x) Z(z) = (C_1 e^{r_1 x} + C_2 e^{r_2 x} + C_3 e^{r_3 x}) Z(z) \quad (43)$$

or

$$G = \left( \sum_{n=1}^3 C_n e^{r_n x} \right) Z(z) \quad (44)$$

Having found one of an infinity of solutions the general solution for G is

$$G = \sum_{i=1}^{\infty} \left( \sum_{n=1}^3 C_{in} e^{r_{in} x} \right) Z_i(z) \quad (45)$$

where the  $r_{in}$  are the  $n$  roots of the  $i$ th operator equation using  $\lambda_i$

where the first five  $\lambda$ s are:

$$\lambda_1 = 0 \quad \lambda_2 = \lambda_3 = \pi/L \quad \lambda_4 = \lambda_5 = 2\pi/L \quad (46)$$

where  $L$  is the  $z$  length of the cylinder (wall) and where the first five  $Z_i$  are:

$$\begin{aligned} Z_1 &= 1 \\ Z_2 &= \cos \lambda_2 z \\ Z_3 &= \sin \lambda_3 z \\ Z_4 &= \cos \lambda_4 z \\ Z_5 &= \sin \lambda_5 z \end{aligned} \quad (47)$$

Converting back to  $T$  and approximating the Fourier series by the first five terms.

$$T = \sum_{i=1}^5 \left( \sum_{n=1}^3 c_{in} e^{r_{in} x} \right) Z_i(z) - G_0/\alpha \quad (48)$$

By a similar process a solution for  $t$  is found to be

$$t = \sum_{i=1}^5 (X_i^* Z_i) - G_0/\alpha \quad (49)$$

where

$$X_i^* = B_{i1} e^{r_{i1} x} + B_{i2} e^{r_{i2} x} + B_{i3} e^{r_{i3} x} \quad (50)$$

The relation between the coefficients of the  $t$  equation and the  $T$  equation is found by substituting the solution of the  $T$  equation back into equation (24). This shows that

$$B_{in} = C_{in} (c - a + \lambda_i^2 - r_{in}^2)/c \quad (51)$$

or that

$$B_{in} = C_{in} b/(r_{in} + b) \quad (52)$$

Equation (49) thus becomes

$$t = \sum_{i=1}^5 \left( \sum_{n=1}^3 \left( \frac{b}{r_{in} + b} \right) C_{in} e^{r_{in} x} \right) Z_i(z) - G_0/\alpha \quad (53)$$

The evaluation of the conduction correction factor,  $f_{L/A}$ , is based on the following analysis. The volumetric heat generation rate is expressed in the following:

$$G = JIv = JI^2 R \quad (54)$$

and

$$G = JI^2 \left( \frac{\rho_0 L f_{L/A}}{A(1-S_3)} + \frac{\alpha' L f_{L/A} \bar{T}}{A(1-S_3)} \right) \quad (55)$$

Solution of equation (26) in connection with equation (55) shows that

$$\alpha = \frac{\alpha' J I^2 L f_{L/A}}{A(1-S_3)} \quad (56)$$

Since

$$\alpha = \frac{G}{\frac{G_0}{\alpha} + T} = \frac{JIV_{AB}}{\frac{\rho_0}{\alpha'} + \bar{T}_{AB}} \quad (57)$$

The value of  $f_{L/A}$  can be found from equation (57) once the average value of the solid phase temperature between voltage probes A and B can be found.

When thermal conduction effects in the fluid are included, equation (25) becomes

$$h\epsilon(T - t) = F C_p dt/dx - k_{\text{fluid}} \delta_2 d^2t/dx^2 \quad (58)$$

Equation (40) then becomes

$$\begin{aligned} (b/c')X'''' + X''' + b(1 + (c - a + \lambda^2)/c')X'' \\ - (c - a + \lambda^2)X' - b(-a + \lambda^2)X = 0 \end{aligned} \quad (59)$$

where

$$c' = h\epsilon/k_{\text{fluid}} \delta_2 \quad (60)$$

This equation differs from equation (40) only in those terms which involve  $c'$  and in the fact that this is now a fourth order equation.



APPENDIX B

Experimental Data  
Common Values and Physical Constants

Table 1

Common Parameters and Physical Constants

Rectifier Current Shunt Factor	120. amperes/millivolt
Stefan-Boltzmann constant	$0.1712 \times 10^{-8}$ B.t.u./sq.ft.-hr.- $^{\circ}\text{R}^4$
Total Emissivity of Thermocouple number 14	0.95
Total Emissivity of tungsten	1.0
Total Emissivity of Marinite	0.8
Spectral Emissivity of tungsten at 0.65 micron wave length	1.0
Spectral Emissivity of Marinite at 0.65 micron wave length	0.8
Marinite Disks:	
Thermal Conductivity B.t.u./hr.-ft.- $^{\circ}\text{F}$	$0.12 + 5.0 \times 10^{-5} T^{\circ}\text{F}$
Inside Diameter	0.5 in.
Outside Diameter	1.75 in.
Thermocouple number 7 - radius position	0.302 in.
Thermocouple number 6 - radius position	0.750 in.
Tungsten:	
Density of Solid Tungsten	19.3 gr./cu.cm.
Coefficient of thermal expansion	$4.45 \times 10^{-6}/^{\circ}\text{F}$
Electrical resistivity (ohm-ft.)	$0.1479 + 4.378 \times 10^{-4} T^{\circ}\text{F} + 3.725 \times 10^{-8} T^{\circ}\text{F}^2 - 2.094 \times 10^{-12} T^{\circ}\text{F}^3$
Thermal Conductivity (B.t.u./hr.-ft.- $^{\circ}\text{F}$ )	
$T^{\circ}\text{K}$	
1100	78.52 - .0099 ( $T^{\circ}\text{K}$ )
1200	76.96 - .0086 ( $T^{\circ}\text{K}$ )
1300	77.87 - .0093 ( $T^{\circ}\text{K}$ )
1400	77.73 - .0092 ( $T^{\circ}\text{K}$ )
1500	78.81 - .0099 ( $T^{\circ}\text{K}$ )
1600	

Table 1 (Continued)

## Porous Tungsten:

Measured internal area by gas adsorption 0.0116 sq. meters/gr.

Original Powder Size 20 micron =  $6.56 \times 10^{-5}$  ft.

0.06726 lb.-mass/Standard Cubic Foot - Nitrogen

0.01034 lb.-mass/Standard Cubic Foot - Helium

## Viscosity:

$$\mu_{N_2} (\text{lb.-mass/ft.-hr.}) = 0.04017((t^\circ\text{F}/491.7) + 0.9349)^{0.756}$$

$$\mu_{He} (\text{lb.-mass/ft.-hr.}) = 0.04525((t^\circ\text{F}/491.7) + 0.9349)^{0.647}$$

## Heat Capacity(B.t.u./SCF-°F at Constant Pressure)

$$C_p (\text{nitrogen}) = 1.513 \times 10^{-2} + 2.426 \times 10^{-6} t^\circ\text{R} - 2.557 \times 10^{-10} t^\circ\text{R}^2$$

$$C_p (\text{helium}) = 1.289 \times 10^{-2}$$

Thermal Conductivity - at  $t^\circ\text{F}$ :

$$k_{N_2} (\text{B.t.u./hr.-ft.-}^\circ\text{F}) = \frac{k_{N_2}(620^\circ\text{F}) C_{p_{N_2}}(t^\circ\text{F}) \mu_{N_2}(t^\circ\text{F})}{C_{p_{N_2}}(620^\circ\text{F}) \mu_{N_2}(620^\circ\text{F})}$$

$$k_{He} (\text{B.t.u./hr.-ft.-}^\circ\text{F}) = \frac{k_{He}(620^\circ\text{F}) \mu_{He}(t^\circ\text{F})}{\mu_{He}(620^\circ\text{F})}$$



APPENDIX C

Experimental Data  
Individual Run Data

TABLE 2

INDIVIDUAL RUN DATA  
OPTICAL PYROMETER TEMPERATURES AND CYLINDER POSITION PAIRS

POSITION ON TUNGSTEN CYLINDER IN CM.

OPTICAL PYROMETER TEMPERATURES -- DEGREES C

RUN IDENTIFICATION	CYLINDER TOP BOTTOM		HOLE 7B		HOLE 7A		HOLE 6		HOLE 5		HOLE 4	
	CM.	CM.	CM.	T(C)	CM.	T(C)	CM.	T(C)	CM.	T(C)	CM.	T(C)
05	64.29	60.67	64.30	913.0	63.55	808.0	62.62	776.0	61.70	824.0	60.76	926.0
06	64.29	60.67	64.30	889.0	63.56	811.0	62.61	794.0	61.68	846.0	60.76	954.0
07	64.29	60.67	64.30	991.0	63.55	929.0	62.61	930.0	61.69	991.0	60.77	1074.0
08	64.29	60.67	64.30	1171.0	63.55	1166.0	62.62	1189.0	61.71	1273.0	60.78	1256.0
14	64.47	60.69	64.21	961.0	63.45	962.0	62.54	971.0	61.61	1038.0	60.73	1032.0
15	64.47	60.69	64.21	941.0	63.45	933.0	62.54	912.0	61.61	971.0	60.73	992.0
16	64.47	60.69	64.21	981.0	63.45	956.0	62.54	937.0	61.61	1000.0	60.73	1001.0
24	64.51	60.72	64.24	770.0	63.48	825.0	62.57	870.0	61.64	915.0	60.76	936.0
25	64.51	60.72	64.24	820.0	63.48	809.0	62.57	804.0	61.64	863.0	60.76	909.0
26	64.51	60.72	64.24	836.0	63.48	840.0	62.57	848.0	61.64	895.0	60.76	931.0
31	64.23	60.58	64.13	844.0	63.38	867.0	62.46	857.0	61.54	901.0	60.65	904.0
32	64.23	60.58	64.13	856.0	63.38	881.0	62.46	869.0	61.54	912.0	60.65	915.0
33	64.23	60.58	64.13	862.0	63.38	870.0	62.46	855.0	61.54	907.0	60.65	927.0
34	64.23	60.58	64.13	854.0	63.38	858.0	62.46	835.0	61.54	898.0	60.65	922.0
35	64.23	60.58	64.13	891.0	63.38	881.0	62.46	850.0	61.54	915.0	60.65	945.0
36	64.23	60.58	64.13	910.0	63.38	887.0	62.46	836.0	61.54	909.0	60.65	972.0
37	64.23	60.58	64.13	920.0	63.38	904.0	62.46	862.0	61.54	929.0	60.65	976.0
45	64.19	60.39	63.98	1040.0	63.22	870.0	62.29	758.0	61.37	840.0	60.47	1040.0
46	64.19	60.39	63.98	1097.0	63.22	971.0	62.29	860.0	61.37	919.0	60.47	1095.0
47	64.19	60.39	63.98	1128.0	63.22	1072.0	62.29	991.0	61.37	1009.0	60.47	1123.0
48	64.19	60.39	63.98	1105.0	63.22	1085.0	62.29	1051.0	61.37	1053.0	60.47	1096.0
49	64.19	60.39	63.98	1111.0	63.22	1069.0	62.29	1010.0	61.37	1010.0	60.47	1072.0
50	64.19	60.39	63.98	1064.0	63.22	1002.0	62.29	914.0	61.37	903.0	60.47	992.0
51	64.19	60.39	63.98	1060.0	63.22	983.0	62.29	888.0	61.37	879.0	60.47	964.0
52	64.19	60.39	63.98	1029.0	63.22	953.0	62.29	856.0	61.37	841.0	60.47	935.0
53	64.19	60.39	63.98	932.0	63.22	864.0	62.29	787.0	61.37	775.0	60.47	863.0
54	64.19	60.39	63.98	956.0	63.22	896.0	62.29	815.0	61.37	800.0	60.47	875.0
62	64.09	60.44	64.02	758.0	63.25	818.0	62.34	886.0	61.42	928.0	60.51	897.0
64	64.09	60.44	64.02	758.0	63.25	818.0	62.34	886.0	61.42	928.0	60.51	897.0
66	64.09	60.44	64.02	759.0	63.25	795.0	62.34	845.0	61.42	886.0	60.51	871.0
68	64.09	60.44	64.02	759.0	63.25	795.0	62.34	845.0	61.42	886.0	60.51	871.0
70	64.09	60.44	64.02	868.0	63.25	919.0	62.34	940.0	61.42	956.0	60.51	900.0
72	64.09	60.44	64.02	855.0	63.25	938.0	62.34	943.0	61.42	951.0	60.51	884.0
74	64.09	60.44	64.02	882.0	63.25	923.0	62.34	923.0	61.42	935.0	60.51	873.0
76	64.09	60.44	64.02	882.0	63.25	923.0	62.34	923.0	61.42	935.0	60.51	873.0
78	64.09	60.44	64.02	882.0	63.25	923.0	62.34	923.0	61.42	935.0	60.51	873.0
80	64.09	60.44	64.02	935.0	63.25	911.0	62.34	876.0	61.42	969.0	60.51	943.0
82	64.09	60.44	64.02	948.0	63.25	916.0	62.34	887.0	61.42	980.0	60.51	948.0

TABLE 3

 INDIVIDUAL RUN DATA  
 THERMOMETER AND THERMOCOUPLE READINGS

ALL TEMPERATURES IN DEGREES F

RUN IDENTIFICATION	ROOM TEMPERATURE	INLET GAS TEMPERATURE	THERMOCOUPLES--- LOWER PIER TEMPERATURES				MARINITE		LOWER BUS BLOCK NO. 8	INSIDE TUNGSTEN CYLINDER NO. 14	OUTSIDE TUNGSTEN CYLINDER NO. 16	AREA OF THERMOCOUPLE NUMBER 14 (SQ. FT.)
			NO. 1	NO. 2	NO. 3	NO. 4	OUTER NO. 6	INTER NO. 7				
05	86.4	75.0	250.	387.	685.0	956.0	613.	1123.	112.	1088.	1210.	.001023
06	86.4	75.	262.	406.	718.	1001.	617.	1133.	115.	1090.	1211.	.001023
07	85.8	74.	320.	498.	887.	1254.	743.	1438.	127.	1361.	1545.	.001023
08	82.4	72.	407.	613.	1095.	1550.	899.	1819.	145.	1735.	2008.	.001023
14	78.4	73.	323.	603.	1079.	1345.	765.	1539.	146.	1316.	1600.	.001023
15	77.7	73.	268.	482.	869.	1090.	650.	1161.	139.	933.	1229.	.001023
16	77.	73.	312.	580.	1038.	1299.	749.	1455.	142.	1167.	1482.	.001023
24	86.	80.9	313.	555.	945.	1198.	561.	1165.	125.	1451.	1291.	.001023
25	83.7	76.9	274.	475.	808.	994.	602.	1117.	120.	1045.	1260.	.001023
26	83.3	76.4	285.	487.	825.	1007.	594.	1143.	126.	1165.	1305.	.001023
31	78.8	74.5	308.	526.	898.	1129.	644.	1271.	130.	1135.	1358.	.001023
32	78.8	74.5	308.	526.	898.	1129.	644.	1271.	130.	1135.	1358.	.001023
33	78.8	74.	324.	546.	922.	1162.	705.	1295.	138.	936.	1333.	.001023
34	78.8	74.	324.	546.	922.	1162.	705.	1295.	138.	936.	1333.	.001023
35	80.6	76.5	336.	565.	950.	1195.	748.	1336.	143.	840.	1350.	.001023
36	82.4	78.5	355.	600.	1008.	1269.	819.	1420.	148.	857.	1420.	.001023
37	82.4	78.5	355.	600.	1008.	1269.	819.	1420.	148.	857.	1420.	.001023
45	84.4	82.	370.	620.	963.	1385.	967.	1547.	145.	1920.	1574.	0.
46	84.4	82.	370.	620.	963.	1385.	967.	1547.	145.	1920.	1574.	0.
47	84.6	82.5	395.	644.	991.	1409.	1007.	1710.	156.	1914.	1777.	0.
48	84.4	82.5	379.	627.	958.	1342.	943.	1645.	161.	1834.	1752.	0.
49	84.2	82.5	367.	604.	922.	1313.	878.	1541.	161.	1829.	1662.	0.
50	84.2	82.	334.	555.	839.	1190.	819.	1390.	157.	1754.	1494.	0.
51	84.2	82.	334.	555.	839.	1190.	819.	1390.	157.	1754.	1494.	0.
52	84.2	82.	322.	526.	794.	1126.	783.	1300.	152.	1706.	1430.	0.
53	83.8	82.	295.	478.	692.	1025.	671.	1161.	140.	1555.	1288.	0.
54	83.8	81.5	295.	478.	692.	1025.	671.	1161.	140.	1555.	1288.	0.
62	86.4	79.	309.	565.	988.	1262.	669.	1295.	134.	1716.	1370.	.001023
64	86.4	79.	309.	565.	988.	1262.	669.	1295.	134.	1716.	1370.	.001023
66	86.4	79.5	309.	565.	988.	1262.	669.	1295.	134.	1734.	1361.	.001023
68	86.4	79.5	309.	565.	988.	1262.	669.	1295.	134.	1734.	1361.	.001023
70	86.4	80.	286.	536.	937.	1231.	769.	1428.	131.	1601.	1461.	.001023
72	86.4	80.	286.	536.	937.	1231.	779.	1435.	131.	1540.	1465.	.001023
74	86.4	80.	280.	523.	915.	1214.	783.	1449.	130.	1484.	1460.	.001023
76	86.4	80.	280.	523.	915.	1214.	783.	1449.	130.	1484.	1460.	.001023
78	86.4	80.	274.	512.	900.	1194.	783.	1449.	129.	1484.	1460.	.001023
80	86.	79.	282.	528.	934.	1256.	874.	1501.	130.	1186.	1460.	.001023
82	86.	79.	282.	528.	934.	1256.	881.	1520.	130.	1196.	1490.	.001023

TABLE 4

INDIVIDUAL RUN DATA  
CYLINDER SPECIFICATIONS, HEAT GENERATION AND FLUID FLOW

CYLINDER IDENTIFICATION	RUN NUMBER	CYLINDER SPECIFICATIONS				HEAT GENERATION		VOLTAGE PROBE		FLOW-STANDARD CU. FT./HR.
		LENGTH (IN.)	MASS (GR.)	O.D. (IN.)	I.D. (IN.)	AMMETER SHUNT MILLIVOLT DROP	CYLINDER PROBE VOLTAGE DROP	Z-POSITION A	B	
C	05	1.431	17.643	.416	.276	1.686	.1455	.0483	-.0475	10.72 N2
C	06	1.431	17.643	.416	.276	1.648	.1423	.0483	-.0475	10.56 N2
C	07	1.431	17.643	.416	.276	2.150	.2285	.0483	-.0475	11.61 N2
C	08	1.431	17.643	.416	.276	2.876	.3686	.0483	-.0475	13.6 N2
D	14	1.492	18.304	.416	.276	2.19	.2369	.0483	-.0475	7.22 N2
D	15	1.492	18.304	.416	.276	2.286	.2335	.0483	-.0475	12.62 N2
D	16	1.492	18.304	.416	.276	1.949	.1803	.0483	-.0475	12.11 N2
D	24	1.487	17.511	.411	.276	1.503	.1557	.0483	-.0475	6.72 N2
D	25	1.487	17.511	.411	.276	1.752	.1711	.0483	-.0475	10.7 N2
D	26	1.487	17.511	.411	.276	1.722	.1788	.0483	-.0475	11.59 N2
D	31	1.434	15.784	.405	.277	1.763	.2062	.0483	-.0475	6.67 N2
D	32	1.434	15.784	.405	.277	1.763	.2062	.0483	-.0475	6.67 N2
D	33	1.434	15.784	.405	.277	1.884	.2242	.0483	-.0475	8.94 N2
D	34	1.434	15.784	.405	.277	1.884	.2242	.0483	-.0475	8.94 N2
D	35	1.434	15.784	.405	.277	2.049	.2289	.0483	-.0475	10.27 N2
D	36	1.434	15.784	.405	.277	2.266	.263	.0483	-.0475	14.28 N2
D	37	1.434	15.784	.405	.277	2.346	.2807	.0483	-.0475	14.28 N2
E	45	1.504	18.400	.416	.275	2.411	.2045	.0483	-.0475	19. N2
E	46	1.504	18.400	.416	.275	2.411	.2172	.0483	-.0475	19. N2
E	47	1.504	18.400	.416	.275	2.887	.2508	.0483	-.0475	18. N2
E	48	1.504	18.400	.416	.275	2.383	.2749	.0483	-.0475	12. N2
E	49	1.504	18.400	.416	.275	2.396	.2705	.0483	-.0475	13. N2
E	50	1.504	18.400	.416	.275	2.353	.2425	.0483	-.0475	15. N2
E	51	1.504	18.400	.416	.275	2.353	.2425	.0483	-.0475	15. N2
E	52	1.504	18.400	.416	.275	2.289	.2265	.0483	-.0475	16. N2
E	53	1.504	18.400	.416	.275	2.103	.1780	.0483	-.0475	15. N2
E	54	1.504	18.400	.416	.275	2.116	.1952	.0483	-.0475	15. N2
D	62	1.434	15.784	.405	.277	1.285	.2382	.0459	-.048	3. HE
D	64	1.434	15.784	.405	.277	1.246	.2166	.0459	-.048	3. HE
D	66	1.434	15.784	.405	.277	1.209	.2072	.0459	-.048	3. HE
D	68	1.434	15.784	.405	.277	1.209	.2133	.0459	-.048	3. HE
D	70	1.434	15.784	.405	.277	1.411	.2980	.0459	-.048	8. HE
D	72	1.434	15.784	.405	.277	1.341	.3031	.0459	-.048	9.5 HE
D	74	1.434	15.784	.405	.277	1.213	.3085	.0459	-.048	11.25 HE
D	76	1.434	15.784	.405	.277	1.18	.1425	.0459	-.048	11.25 HE
D	78	1.434	15.784	.405	.277	1.196	.2255	.0459	-.048	11.25 HE
D	80	1.434	15.784	.405	.277	1.813	.3779	.0459	-.048	30. HE
D	82	1.434	15.784	.405	.277	1.821	.3777	.0459	-.048	27. HE

APPENDIX D

Results of Individual Run Analysis

TABLE 5  
INDIVIDUAL RUN ANALYSIS  
HEAT BALANCES

ALL HEAT FLUXES(Q) IN B.T.U./HR.

Q GENERATED IN CYLINDER + Q INTO CYLINDER (TOP AND BOTTOM)  
- Q OUT AT CYLINDER WALLS (INSIDE AND OUTSIDE) = C ABSORBED IN GAS.

RUN IDENTIFICATION	Q(GENERATED)	Q(IN TOP)	Q(IN BOTTOM)	Q(CUT X=L)	Q(OUT X=0)	Q(ABS. IN GAS)
05	128.1	78.2	60.8	100.6	16.1	150.3
06	122.2	64.2	63.9	93.2	17.3	140.0
07	254.8	47.8	37.5	108.5	23.5	208.2
08	543.9	-9.1	-57.8	152.4	47.2	277.1
14	277.8	-32.2	-39.9	110.1	28.2	67.3
15	286.8	-37.4	-25.6	116.9	32.4	74.3
24	124.1	-30.6	-4.8	79.1	6.0	2.7
25	160.9	-10.9	0.7	86.2	17.8	46.9
26	164.6	-10.6	1.9	92.6	17.8	45.5
31	186.7	-34.4	-30.0	97.6	19.8	4.9
33	217.6	-25.0	-21.6	92.6	25.0	53.8
34	217.9	-28.3	-26.4	89.9	23.7	49.9
35	242.5	-23.7	-25.3	93.4	27.5	73.1
36	309.5	-20.0	-12.1	85.8	27.5	164.2
37	341.1	-21.3	-17.1	90.6	29.5	182.7
45	278.2	95.8	103.5	87.5	-0.0	390.4
46	292.2	57.0	89.7	105.7	0.0	333.1
47	397.0	14.0	68.5	117.5	-0.0	362.3
48	355.0	2.8	21.3	126.5	0.0	252.8
49	352.8	10.0	31.4	134.8	-0.0	259.1
50	312.2	19.3	52.2	129.3	-0.0	254.1
51	312.8	25.5	47.7	128.8	-0.0	257.0
52	284.4	28.8	57.9	124.8	-0.0	246.3
53	205.2	37.1	63.6	112.3	-0.0	193.8
54	225.8	21.6	47.8	120.3	0.0	174.8
70	218.0	-22.2	-26.5	99.2	6.4	64.0
72	210.7	-25.7	-29.6	104.0	10.3	40.8
74	194.3	-19.8	-25.0	101.5	11.4	37.0
80	360.6	-17.2	-41.3	97.0	24.2	180.9
82	361.8	-13.0	-41.6	99.5	24.9	182.7

TABLE 6  
INDIVIDUAL RUN ANALYSIS  
SOLID AND GAS TEMPERATURES

RUN IDENTIFICATION	ALL TEMPERATURES ARE IN DEGREES F --						
	TUNGSTEN WALL AT THERMO. NO. 16	THERMOCOUPLE NUMBER 16	INSIDE WALL MARINITE	EXIT GAS AT THERMO. NO. 16	INLET GAS BELCW PIER	GAS AFTER PREHEATING IN PIER	GAS AFTER HEAT ABSORBED FROM THERMO. NO. 14
05	1429.	1210.	1356.	1061.	75.	196.	286.
06	1461.	1211.	1306.	1041.	75.	203.	301.
07	1706.	1545.	1545.	1335.	74.	220.	338.
08	2172.	2008.	2025.	1526.	72.	226.	420.
14	1780.	1600.	1578.	1039.	73.	292.	518.
15	1674.	1229.	1514.	686.	73.	197.	350.
24	1598.	1291.	1145.	392.	81.	308.	368.
25	1475.	1260.	1239.	612.	77.	265.	364.
26	1558.	1305.	1279.	522.	76.	203.	294.
31	1575.	1358.	1365.	513.	75.	296.	471.
33	1571.	1333.	1389.	759.	74.	253.	419.
34	1535.	1333.	1370.	722.	74.	253.	410.
35	1562.	1350.	1438.	793.	77.	240.	398.
36	1537.	1420.	1453.	944.	79.	206.	320.
37	1584.	1420.	1489.	1032.	79.	206.	328.
45	1396.	1574.	1613.	1187.	82.	166.	166.
46	1580.	1574.	1748.	1074.	82.	167.	167.
47	1816.	1777.	1875.	1273.	83.	179.	179.
48	1924.	1752.	1877.	1430.	83.	239.	239.
49	1850.	1662.	1874.	1339.	83.	224.	224.
50	1677.	1494.	1774.	1136.	82.	195.	195.
51	1630.	1494.	1770.	1153.	82.	210.	210.
52	1573.	1430.	1705.	1033.	82.	183.	183.
53	1449.	1288.	1501.	901.	82.	177.	177.
54	1499.	1288.	1560.	834.	82.	177.	177.
70	1724.	1461.	1502.	1644.	80.	943.	1005.
72	1729.	1465.	1547.	1327.	80.	901.	985.
74	1693.	1460.	1533.	1156.	80.	820.	898.
80	1609.	1460.	1591.	935.	79.	442.	504.
82	1629.	1490.	1616.	1030.	79.	474.	545.

TABLE 7  
INDIVIDUAL RUN ANALYSIS  
HEAT TRANSFER COEFFICIENTS AND CONDUCTION CORRECTION FACTOR

RUN IDENTIFICATION	REYNOLDS NUMBER	NUSSLET NUMBER	HEAT TRANSFER COEFFICIENTS B.T.U./HR.-F---		
			VOLUMETRIC --- CU.FT.	CLASSICAL --- SQ.FT.	CORRECTION FACTOR FOR CONDUCTION
05	.1112	.0001678	3189.	.0947	.4445
06	.1101	.0001487	2809.	.0835	.4511
07	.1095	.0001898	4054.	.1202	.4191
08	.1225	.0001632	3800.	.1123	.4338
14	.0693	.0000490	1000.	.0294	.4201
15	.1435	.0000561	926.	.0272	.4245
24	.0864	.0000024	35.	.0010	.4121
25	.1250	.0000451	717.	.0213	.4193
26	.1451	.0000417	611.	.0181	.4090
31	.0823	.0000047	75.	.0022	.3870
33	.1021	.0000522	919.	.0270	.3816
34	.1037	.0000493	851.	.0250	.3765
35	.1163	.0000702	1248.	.0367	.4088
36	.1562	.0001633	3023.	.0889	.3921
37	.1514	.0001800	3458.	.1017	.3881
45	.1832	.0004193	8506.	.2484	.4525
46	.1938	.0002589	4918.	.1435	.4678
47	.1744	.0002503	5063.	.1475	.5343
48	.1104	.0001744	3754.	.1094	.4153
49	.1228	.0001801	3756.	.1094	.4127
50	.1518	.0001977	3792.	.1106	.4167
51	.1498	.0002107	4104.	.1198	.4078
52	.1681	.0002066	3786.	.1105	.4110
53	.1662	.0001825	3135.	.0916	.4444
54	.1710	.0001536	2553.	.0746	.4198
70	.0096	.0000320	3922.	.1153	.2234
72	.0122	.0000113	1301.	.0382	.2096
74	.0152	.0000090	985.	.0289	.1834
80	.0468	.0000350	3318.	.0976	.2230
82	.0406	.0000364	3580.	.1052	.2260

## TABLE OF NOMENCLATURE

A	=	Cross sectional area for conduction - sq. ft. bulk
a	=	$\alpha/k\gamma_2$
B <sub>n</sub>	=	Nth constant of integration in the fluid phase temperature equation
b	=	$h\epsilon/FCp\delta_2$
C <sub>n</sub>	=	Nth constant of integration in the solid phase temperature equation
C <sub>p</sub>	=	Heat capacity of fluid - B.t.u./lb.mass.-°F
c	=	$h\epsilon/k\gamma_2$
D	=	Characteristic diameter in laminar flow - ft.
d	=	Particle diameter - ft. Pore diameter - ft. Derivative
e	=	Exponential function
F	=	Fluid flow rate - lb.mass./hr.
f	=	Porosity - cu.ft.void/cu.ft. bulk
f <sub>A</sub>	=	Conduction correction factor to obtain effective conduction area from bulk conduction area (excluding the volume porosity correction factor)
f <sub>L</sub>	=	Conduction correction factor to obtain effective conduction length from bulk conduction length
f <sub>L/A</sub>	=	Ratio of the factors - $f_L/f_A$
G	=	Volumetric heat generation rate - B.t.u./hr.-cu.ft. bulk
Go	=	Constant term in the temperature dependent expression for G - B.t.u./hr.-cu.ft. bulk
G <sub>c</sub>	=	Mass flow rate - lb.mass./hr.-sq.ft.
h	=	Heat transfer coefficient - B.t.u./hr.-sq.-ft.°F
h'	=	Volumetric heat transfer coefficient h <sub>e</sub> B.t.u./hr.-cu.ft.-°F

I	=	Current - amperes
J	=	Conversion factor - 3.41276 B.t.u./hr.-watt
j	=	$\Gamma_{\gamma_3}/FCp\delta_2$
K	=	Conductance - B.t.u./hr.-°F
k	=	Thermal conductivity of solid or fluid material (nonporous form) - B.t.u./hr.-ft.-°F
L	=	Characteristic length in laminar flow - ft. Axial cylinder length - ft. Length for conductance - ft.
l	=	Thickness of porous wall - ft.
m	=	Variable of the operator equation
q	=	Heat flux - B.t.u./hr.
R	=	Resistance - ohms
r	=	Particle radius - ft.
$r_n$	=	Nth root of the operator equation - ft. <sup>-1</sup>
$S_3$	=	Volumetric porosity - cu.ft. solid/cu.ft. bulk
T	=	Solid phase temperature - °F
t	=	Fluid phase temperature - °F
V	=	Bulk volume - cu.ft.
v	=	Voltage - volts
X	=	The x dependent component of T(x,z) or G(x,z)
x	=	Dimension - ft. Distance - ft. Variable
y	=	Dimension - ft. Distance - ft.
Z	=	The z dependent component of T(x,z) or G(x,z)
z	=	Dimension - ft. Distance - ft. Variable

Subscripts

- AB = Variable measured over the range between the voltage probes A and B
- b = Bulk fluid temperature
- i = Designates parameters associated with the  $i$ th term of the Fourier Series
- n = Designates parameters associated with the  $n$ th root of the operator equation
- w = Wall temperature

Superscripts

- ' = Designates the derivative with respect to the single variable of the function
- = Indicates an average value of the function

Greek Letters

- $\alpha$  = Coefficient of temperature dependence in  $G$   
B.t.u./hr.-cu.ft. $^{\circ}$ F
- $\alpha'$  = Coefficient of temperature dependence in  $\rho$  - ohms/ft.- $^{\circ}$ F
- $\Gamma$  = Volumetric heat generation rate  
B.t.u./hr.-cu.ft. solid
- $\gamma_2$  = Effective area for solid phase heat and electric conduction - sq. ft. solid/sq.ft. bulk
- $\gamma_3$  = Effective volume for heat generation - cu.ft. solid/cu.ft. bulk
- $\delta_2$  = Effective area for fluid flow - sq. ft. flow area/sq.ft. bulk
- $\epsilon$  = Internal surface area of porous material  
sq. ft. area/cu.ft. bulk
- $\lambda_n$  = Coefficient in the argument of the Fourier series -  $n\pi/L$
- $\mu$  = Gas viscosity - lb.mass./ft.-hr.

$\pi$  = Constant - 3.14159

$\rho$  = Resistivity - ohms/ft.

$\rho_0$  = Zero order resistivity term - ohms/ft.

Special Symbols

$\nabla$  = Nabla operator

## BIBLIOGRAPHY

1. Bird, R. B., Stewart, W. E. Lightfoot, E. N., "Transport Phenomena," John Wiley, New York, (1960).
2. Bland, D. R., Proceedings of the Royal Society of London, 221, pp. 1-28, (1954).
3. Boucher, D. F., Alves, G. E., Chemical Engineering Progress, 55, No. 9, pp. 55-64, (1959).
4. Brown, G. G. and Associates, "Unit Operations," John Wiley, New York, (1950).
5. Brownell, L. E., and Katz, D. L., Chemical Engineering Progress, 43, No. 10, pp. 537-545, (1947).
6. Burgess, E., "Rocket Propulsion," Chapman and Hall, London, (1954).
7. Bussard, R. W., and DeLauer, R. D., "Nuclear Rocket Propulsion," McGraw-Hill, New York, (1958).
8. Cheung, H., "A Critical Reveiw of Heat Pipe Theory and Applications," UCRL-50453, University of California, Livermore, California, (1968).
9. Eastman, G. Y., Scientific American, 218, Number 5, pp. 38-46, (1968).
10. Farber, J., Chemical Reaction in an Electrically Heated Porous Medium, Ph.D. Thesis, The Pennsylvania State University, 1966.
11. Gelperin, J. J., and Kagan, A. M., Proceedings of the Third International Heat Transfer Conference, Chicago, Illinois, August 7-12, Volume IV, pp. 308-321, (1966).
12. Green, L. Jr., ASME-AIChE Heat Transfer Conference, University Park, Pa., August 11-15, 1957.
13. Green, L. Jr., Journal of Applied Mechanics, Trans. ASME, 19, pp. 173-178, (1952).
14. Grootenhuis, P. and Moore, N. P. W., Special Report of the Iron and Steel Institute, London, Number 43, p. 281, (1951).
15. Grootenhuis, P., Proceedings of General Discussion on Heat Transfer, Institution of Mechanical Engineers, pp. 363-366, (1951).
16. Grootenhuis, P., Powell, R. W., and Tye, R. P., Proceedings of the Physical Society, B, London, 65, p. 502, (1952).
17. Grootenhuis, P., Journal of The Royal Aeronautical Society, 63, No. 578, pp. 73-89, (1959).

18. Jakob, M., "Heat Transfer," Volume II, John Wiley, New York, (1957).
19. Keyser, C. A., "Basic Engineering Metallurgy," Prentice-Hall, New York, (1952).
20. Knudsen, J. G., Katz, D. L., "Fluid Dynamics and Heat Transfer," McGraw-Hill, New York, (1958).
21. Koh, J. C. Y., and del Casal, E., Proceedings of the 1965 Heat Transfer and Fluid Mechanics Institute, Los Angeles, California, June 21-23, pp. 263-281, (1965).
22. Kroll, C. L., Thesis in Chemical Engineering, Massachusetts Institute of Technology, (1951).
23. Ley, W., "Rockets, Missiles, and Space Travel," Viking, New York, (1951).
24. McAdams, W. H., "Heat Transmission," McGraw-Hill, New York, (1954).
25. Mickley, H. S., Sherwood, T. K., and Reed, C. E., "Applied Mathematics in Chemical Engineering," McGraw-Hill, New York, (1957).
26. Muskat, M., "The Flow of Homogeneous Fluids Through Porous Media," J. W. Edwards, Inc., Ann Arbor, Michigan, (1946).
27. Perry, J. H., Editor, "Chemical Engineers' Handbook," McGraw-Hill, New York, (1950).
28. Schneider, P. J., "Conduction Heat Transfer," Addison-Wesley, Cambridge, Mass., (1955).
29. Simmons, J. T., "The Physical and Thermodynamic Properties of Helium," Technical Report D-9027, Wm. R. Whittaker Co., Los Angeles, (1957).
30. Sutton, G. P., "Rocket Propulsion Elements," John Wiley, New York, (1949).
31. Tungsten Data Sheet, Sylvania Electrical Products, Towanda, Pennsylvania.
32. Walas, S. M., "Reaction Kinetics for Chemical Engineers," McGraw-Hill, New York, (1959).
33. Weber, R. L., "Heat and Temperature Measurement," Prentice-Hall, New York, (1950).
34. Weinbaum, S., and Wheller, H. L. Jr., Journal of Applied Physics, 20, pp. 113-122, (1949).
35. Weiner, M. M., and Edwards, D. K., Proceedings of the 1963 Heat Transfer and Fluid Mechanics Institute, Pasadena, California, June 12-14, pp. 236-250, (1963).

## INTERNAL DISTRIBUTION

- |                                     |                       |
|-------------------------------------|-----------------------|
| 1-3. Central Research Library       | 67. H. W. Hoffman     |
| 4. ORNL -- Y-12 Technical Library   | 68. F. J. Homan       |
| Document Reference Section          | 69. W. H. Jordan      |
| 5-24. Laboratory Records Department | 70. A. F. Joseph      |
| 25. R. G. Alsmiller                 | 71. L. Jung           |
| 26. D. E. Arnurius                  | 72. F. B. Kam         |
| 27. S. J. Ball                      | 73. P. R. Kasten      |
| 28. M. Bender                       | 74. R. J. Kedl        |
| 29. C. E. Bettis                    | 75. J. J. Keyes       |
| 30. A. A. Brooks                    | 76. O. H. Klepper     |
| 31. W. E. Browning                  | 77. B. B. Klima       |
| 32. V. R. Cain                      | 78. T. S. Kress       |
| 33. T. D. Calton                    | 79. M. E. Laverne     |
| 34. D. W. Cardwell                  | 80. J. Lewin          |
| 35. R. S. Carlsmith                 | 81. G. H. Llewellyn   |
| 36. H. P. Carter                    | 82. J. L. Lucius      |
| 37. W. L. Carter                    | 83. R. N. Lyon        |
| 38. R. D. Cheverton                 | 84. J. H. Marable     |
| 39. H. C. Claiborne                 | 85. B. F. Maskewitz   |
| 40. F. H. Clark                     | 86. R. D. McCulloch   |
| 41. W. B. Cottrell                  | 87. H. A. McLain      |
| 42. J. S. Crowell                   | 88. S. E. Moore       |
| 43. F. L. Culler                    | 89. F. R. Mynatt      |
| 44. W. Davis                        | 90. F. H. Neill       |
| 45. J. G. Delene                    | 91. D. B. Nelson      |
| 46. L. Dresner                      | 92. C. W. Nestor      |
| 47. R. C. Durfee                    | 93. J. P. Nichols     |
| 48. J. R. Engel                     | 94. C. E. Parker      |
| 49. C. H. Gabbard                   | 95. L. F. Parsly      |
| 50. R. B. Gallaher                  | 96. M. R. Patterson   |
| 51. W. R. Gambill                   | 97. S. K. Penny       |
| 52. W. F. Gauster                   | 98. R. B. Perez       |
| 53. F. G. Goff                      | 99. A. M. Perry       |
| 54. N. B. Gove                      | 100. L. M. Petrie     |
| 55. N. M. Greene                    | 101. H. B. Piper      |
| 56. G. E. Guest                     | 102. B. E. Prince     |
| 57. M. Feliciano                    | 103-152. R. P. Rannie |
| 58. M. H. Fontana                   | 153. M. Reeves        |
| 59. T. B. Fowler                    | 154. M. W. Rosenthal  |
| 60. A. P. Fraas                     | 155. R. Salmon        |
| 61. R. E. Funderlic                 | 156. J. P. Sanders    |
| 62. T. P. Hamrick                   | 157. W. K. Sartory    |
| 63. P. N. Haubenreich               | 158. L. B. Shappert   |
| 64. R. W. Hendricks                 | 159. J. D. Sheppard   |
| 65. R. F. Hibbs                     | 160. M. Siman-Tov     |
| 66. E. C. Hise                      | 161. T. M. Sims       |

- |                       |                                       |
|-----------------------|---------------------------------------|
| 162. A. H. Snell      | 171. J. L. Wantland                   |
| 163. W. C. Stoddart   | 172. C. C. Webster                    |
| 164. J. G. Sullivan   | 173. A. M. Weinberg                   |
| 165. J. R. Tallackson | 174. T. A. Welton                     |
| 166. D. G. Thomas     | 175. G. E. Whitesides                 |
| 167. M. L. Tobias     | 176. R. P. Wichner                    |
| 168. T. C. Tucker     | 177. R. E. Worsham                    |
| 169. W. D. Turner     | 178. M. M. Yarosh                     |
| 170. D. R. Vondy      | 179-193. Mathematics Division Library |

## EXTERNAL DISTRIBUTION

194. L. C. Eagleton, Chemical Engineering Department, Pennsylvania State University, University Park, Pennsylvania
195. A. J. Engel, Chemical Engineering Department, Pennsylvania State University, University Park, Pennsylvania
196. W. A. Jester, Nuclear Engineering Department, Pennsylvania State University, University Park, Pennsylvania
197. J. H. Jones, Chemical Engineering Department, Pennsylvania State University, University Park, Pennsylvania
198. E. E. Klaus, Chemical Engineering Department, Pennsylvania State University, University Park, Pennsylvania
199. W. A. Lloyd, Cannon Instrument Company, Boalsburg, Pennsylvania
200. N. J. Palladino, Dean, College of Engineering, Pennsylvania State University, University Park, Pennsylvania
201. A. W. Rose, Applied Science Laboratories, State College, Pennsylvania
202. M. E. Rose, Computers and Mathematics Branch, U.S. Atomic Energy Commission, Washington, D.C.
203. R. B. Sumantri, Applied Science Laboratories, State College, Pennsylvania
204. J. A. Swartout, Union Carbide Corporation, New York, N.Y.
205. Research and Technical Support Division, AEC, ORO
206. Patent Office, AEC, ORO
- 207-365. Given distribution as shown in TID-4500 under Engineering and Equipment category (25 copies - NTIS)